DUPLICATE

METEOROLOGICAL OFFICE

Forecasting Research

Forecasting Research Division
Technical Report No. 162

A review of systematic errors in the global Unified Model used for NWP 1994-95

by

S F Milton, C A Wilson and A Van der Wal

May 1995

Meteorological Office
London Road
Bracknell
Berkshire
RG12 2SZ
United Kingdom

ORGS UKMO F
National Meteorological Library
FitzRoy Road, Exeter, Devon. EX1 3PB

Forecasting Research
Technical Report No. 162

A review of systematic errors in the global Unified Model used for NWP 1994-95

by

S F Milton, C A Wilson and A Van der Wal

May 1995

Forecasting Research
Meteorological Office
London Road
Bracknell
Berkshire
RG12 2SZ
United Kingdom

© Crown Copyright 1995

This document has not been published. Permission to quote from it must be obtained from the Director of Forecasting Research at the above address.

CONTENTS

1. Introduction *Page* 3
2. Changes to the operational global model (92-95) *Page* 3
3. Systematic errors
    - 3.1 Zonally averaged systematic errors. *Page* 4
    - 3.2 Geographical distribution of systematic errors. *Page* 7
    - 3.3 Model hydrological cycle *Page* 10
    - 3.4 Clouds and radiation-comparison with ERBE *Page* 10
    - 3.5 Surface Fluxes *Page* 13
4. Two-timestep budget diagnostics.
    - 4.1 Thermal budget *Page* 15
    - 4.2 Discussion of tropopause cooling. *Page* 18
    - 4.3 Momentum budget *Page* 20
5. Summary *Page* 21
6. References. *Page* 23

Appendix A - Model Problems- suggested CFO priorities.
Appendix B - Outstanding problems in the operational suite (compiled by CF Division)

1. INTRODUCTION

This paper is a review of the of the systematic errors (SE) in the global Unified Model (UM) as formulated for operational Numerical weather Prediction (NWP), and is an update of results given in Milton and Wilson (1994). Most of the results presented are for the periods June-August 1994 and January-March 1995. Particular emphasis is given to ascribing possible sources for the SE and the discussions include;

(i) Time evolution of SE in the global UM since its introduction in June 1991.
(ii) Recent reductions in the model SE.
(iii) Comparisons with the ECMWF model.

An important perspective in assessing the SE in the global model is the relative importance of the different SE for operational NWP. With this in mind Appendix A and B give a list of errors compiled by the Central Forecast Office (CFO) and Central Forecast (CF) Division respectively together with rankings of their relative importance. In particular the list composed by CF Division represents an integrated response of 3 major users of the global model: Production and Services Provision (PSP), Defense Services (DS), and CFO. Many of the errors discussed in this paper are also known problems for climate simulations, although the relative importance of each SE may be different for climate applications.

The aim of this paper is to produce a comprehensive set of diagnostics of model problems against which to assess the impact of future changes to model formulation. In addition the diagnostics/errors can also be contrasted against those identified in the first (Mitchell and Senior, 1993) and second (Gallani, 1994) climate versions of the global Unified Model.

2. CHANGES TO OPERATIONAL GLOBAL MODEL (91-95)

To assess the impact of model changes on the SE we give here a list of the major changes to the operational global model and data assimilation since 1991.

12 November 1991	Horizontal diffusion of humidity changed from 4th to 2nd order.
24 March 1992	Implement vertical diffusion in the tropics.
7 April 1992	Introduce ECMWF-like LW transmissivities.
9 March 1993	1) Horizontal diffusion of humidity changed from 2nd to 4th order. 2) Correct error in position of orographic standard deviation for gravity wave drag calculation. 3) Correct 2nd order term in vertical advection calculation.
3 August 1993	Introduction of ERS-1 scatterometer winds into the assimilation. (Bell, 1994a)

11 January 1994	2nd Climate Version Physics introduced into the global model (Hammon and Wilson, 1993) (1) Include downdraughts in convection scheme. (2) Introduce rapidly mixing boundary layer. (3) Layer clouds in 3 layers for SW (4) Random overlap replaced by Max/Random overlap in LW (5) Revision of evaporation rates for snow. (6) Threshold for precipitation over sea reduced.
12 April 1994	Change global assimilation to balance surface pressure and temperature increments using wind increments (WINDBAL)
29 November 1994	Humidity fix to radisondes in LAM and global models (Bell, 1994b) (1) Revised processing of radiosonde humidity (replacing vertical by interpolation to midpoint and introducing a boost near saturation) (2) Revised humidity assimilation (to conserve RH during T update)
13 December 1994	(1) Long physics timesteps for both global and LAM models- global model has 3 physics timesteps per hour compared with 6 for the dynamics. (2) Also include code in both models to prevent superadiabatic profiles from being generated. (Wilson et al, 1994)
10 January 1995	New Gravity wave drag and orographic roughness in LAM and global models (Milton et al., 1994)

3. SYSTEMATIC ERRORS.

3.1 Zonally Averaged Systematic Errors

Zonal wind

In January 1995 the zonally averaged zonal wind errors at T+72 (Fig 1(b)) are largest in the northern hemisphere. Westerly errors occur in mid-latitudes poleward of the analysed subtropical jet (Fig 1(a)) and extend throughout the troposphere. The westerly errors are flanked by easterly errors of similar magnitude. In the tropics the easterlies in the upper troposphere are too intense by 1m/s as are the westerlies on the equatorward side of the subtropical jets. Easterlies are too intense in the tropical boundary layer. In the southern hemisphere the dominant error is the increased easterly flow over Antarctica, with smaller westerly errors in the mid-latitudes. There is considerable symmetry between the zonal wind errors in the two hemispheres, despite the differing amounts of land mass.

The errors in the zonal wind are reflected in the kinetic energy (total) of the flow (Fig. 3). The northern hemisphere shows a reduction of kinetic energy at the jet core and an increase on the poleward and equatorward flanks. This pattern is robust and can be seen in other northern hemisphere winter months. In the southern hemisphere there is a general increase in

kinetic energy at the jet core.

The model change to include orographic roughness and update the gravity wave drag scheme was made on 10 January 1995 so the results for January 1995 contain the response from two different model formulations. Figure 4 shows the zonally averaged zonal wind errors for February 1994 and February 1995 which compares model SE before and after the changes to gravity wave drag and orographic roughness. Clear reductions can be seen in the westerly bias in northern hemisphere mid-latitudes and the easterly bias in the stratosphere at 40N.

In July 1994 (Fig 2) some of the largest errors appear in the tropics. These errors are baroclinic in nature with an upper tropospheric westerly bias of 2 m/s at 300hPa and an easterly bias in the boundary layer between 0S and 20S. Similar errors of opposite sign can be seen between 0N and 20N. This quadrupole pattern is similar to the response of the tropical atmosphere to an anomalous heating asymmetric about the equator as modelled by Gill (1980 - fig. 2(c)) using a linear Sverdrup balance. This may suggest that the tropical diabatic heating in the UM global model is too intense. In the extratropics we see a similar picture to that in January, with increased westerlies in mid-latitudes of both hemispheres and easterly biases over both poles. The errors in the kinetic energy are largest in the southern hemisphere, with increases poleward of the subtropical jet core at 50S and equatorward of the jet core at 20S (Fig 3).

Temperature

The zonally averaged T+72 temperature bias has a similar structure in both January (Fig. 1(d)) and July (Fig 2(d)) consisting of a cold bias at the tropopause stretching from pole-to-pole with a maximum in the tropics of order -1K. Maxima in the cold bias can also be seen in the northern and southern hemisphere below 600mb in subtropics and mid-latitudes. These lower tropospheric errors are particularly large in the southern hemisphere. There is a small warm bias (<0.2K) in the tropical mid-troposphere and in the stratosphere. The tropical warm bias does not appear in long climate simulations. There is some seasonal variability in the errors with the northern hemisphere cold bias largest in July at both the tropopause and in the lower troposphere.

There is a high degree of correlation between the pattern of zonally averaged layer cloud (Fig. 5) and the temperature biases at the tropopause and in the southern hemisphere boundary layer. The southern hemisphere cooling maximum is located equatorward of the main layer cloud maxima. These points are discussed further in section 4. The role the temperature biases play in other aspects of the model is not well known. However the cooling at the tropopause implies a destabilization of the upper troposphere which could potentially affect the growth rate of baroclinic waves and hence alter synoptic developments in mid-latitudes. Errors in the zonally averaged temperatures and zonal wind are consistent with each other via the thermal wind relation raising the possibility that some of the wind biases may be thermally forced.

Meridional Wind

The pattern of errors in the meridional wind is similar for both January (Fig. 1(f)) and July (Fig. 2(f)) with increases in the Hadley circulation of order 30%-40% between T+00 and T+72. Errors are largest in July and take the form of a counter-clockwise circulation in the upper troposphere. Increases in the Hadley circulation may indicate excessive tropical diabatic heating in the global UM. However, care must be taken as errors in the frictional dissipation,

and eddy heat and momentum fluxes can also contribute to errors in the mean meridional circulation.

Time Evolution of Systematic Errors

Figure 6 shows a time latitude plot of the zonally and monthly averaged mean sea level pressure (MSLP) errors at T+72 from June 1991 to May 1995. This clearly shows a distinct dependence of the error upon latitude. Pressures are too low in the extratropical stormtrack belts from 50N-80N and 50S-80S and to a lesser extent in the tropical belt. Pressures are too high in the subtropics of both hemispheres. There is a considerable seasonal cycle in the northern hemisphere with the largest negative errors in DJF. The introduction of the new gravity wave drag scheme and orographic roughness has considerably reduced the northern hemisphere wintertime biases in the extratropics and subtropics. This can be seen by comparing the errors in February 1995 with those in previous Februaries. Changes to the model prior to January 1995 had little impact upon these errors. Similar errors and improvements can also be seen in the 500hPa geopotential height (not shown).

Figure 7 shows a similar plot to fig. 6 but for the T+72 zonal wind error at 850hPa. Again we see the problem of the extratropical westerly bias in both hemispheres. This has been reduced in the northern hemisphere since January 1995. The other systematic features are the large tropical errors during JJA, which are associated with an excessive Indian monsoon circulation (see section 3.2). No obvious improvements can be seen in this error.

The time-latitude plot of the T+72 zonal wind error at 250hPa (Fig 8) exhibits more intermonthly variability than the 850hPa field. The general pattern is for westerly bias in mid-latitudes (50N and 50S) and in the subtropics (20N and 20S) and easterly bias in the tropics. Since the introduction of the fourth order moisture diffusion in March 1993 the tropical easterly bias has become worse during June-October.

The tendency for too strong a Hadley circulation in the model (Fig 8B) appears to have reduced since 1992. The large errors in January-February 1992 (Fig. 8B(c)) were much reduced by January-February 1993 following the introduction of vertical diffusion in the tropics in March 1992. The large errors in JJA were reduced in 1994 following the introduction of the 2nd climate physics (2CV) in January 1994. In particular there is reduction of the positive bias in meridional wind below 800hPa and the negative bias at 200hPa. This is due to the inclusion of downdraughts in the convection scheme.

Finally we consider the time evolution of the T+72 temperature bias from October 1992 to February 1995. At 850hPa (Fig 8C(a)) there are cold biases in the northern and southern hemisphere extratropics with maxima in the summer months for each hemisphere. The seasonal cycle in the errors are larger in the northern hemisphere suggesting a link with the land mass. In the tropics the model suffered from a warm bias until January 1994 when the introduction of downdraughts in convection (2nd Climate physics) removed this. At 300hPa (Fig. 8C(b)) the cold bias dominates with maxima in the extratropics. There was a large overall reduction in the cold bias with the introduction of fourth order moisture diffusion in March 1993. We also note that the northern hemisphere cold bias shows a distinct seasonal cycle with the largest errors from May to September. The tropical cold bias at 200hPa (not shown) shows little improvement with time.

3.2 Geographical Distribution of Systematic Errors

Temperature

In January 1995 the cooling bias in the southern hemisphere extratropics at 850hPa covers most longitudes, whilst in the northern hemisphere the largest biases are in the ocean basins (Fig. 9(a)). Regions of significant local warm bias can be seen over the North Africa/Sahel, Himalayas, Andes and off the western coasts of South America, Africa and Australia (regions of extensive stratocumulus cloud). Although the 850hPa level is below high orography such as the Himalayas and Andes the warm biases are also evident on model levels (see Fig 36(c)). At 250hPa the cooling is largest over the oceanic sectors with maxima in the North Atlantic and tropical east Pacific amongst other regions. This level is not ideal for studying the temperature bias as it is above the maximum bias in the extratropics but below that in the tropics (Fig. 1(d)).

In July the southern hemisphere 850hPa cold bias is similar to that in January but located further north (Fig 9(c)). In the northern hemisphere the zonally averaged cold bias is larger than in January (Fig. 8C(a)) and fig. 9(c) shows that this cold bias is located mainly over the land regions, with maxima over the Rockies, Europe, and northern Asia. The areas of warm bias are identical to those in January, although the warm bias off the western coast of South America is considerably smaller in July. At 250hPa the cooling is largest over the oceans (Fig 9(d)).

Mean Sea Level Pressure (MSLP)

For MSLP we show February 1995 as this is the first whole month after the introduction of the new gravity wave drag scheme and orographic roughness. In both February and July there is a strong correlation between the areas of warming at 850mb (Fig. 9) and areas of negative MSLP error (Fig. 10(a) and 10(b)). Examples are the Himalayas, Andes, and North Africa (care must be taken interpreting MSLP over the orography). Pressures are too high in the Atlantic and Pacific midlatitude ocean sectors in both months. In the southern hemisphere the subtropical highs are too intense and the circumpolar trough is too deep leading to increased westerly wind errors in the southern hemisphere stormtrack region at 50S.

Figure 11(a) shows the T+72 error in MSLP for February 1994, before the gravity wave drag and orographic roughness changes. Comparing with February 1995 (Fig. 10(b)) the negative errors are much larger in February 1994 over the northern hemisphere continents, particularly northeast Asia. The contribution the systematic error component makes to the total mean square error is given by the following ratio

$$\frac{\left[\frac{1}{N}\,\Sigma E\right]^2}{\frac{1}{N}\,\Sigma E^2}$$

Where E is the error (forecast - analysis) at a given day and the summation is over a whole month. In February 1994 (Fig. 11(b)) the systematic error in MSLP over Asia accounts for between 60% and 80% of the total mean square error whereas in February 1995 (Fig 11(c))

this has been reduced to ~20%. Similar reductions can be seen over North America, and in the subtropical Pacific where errors in the subtropical high have been reduced. The systematic errors remain a large fraction (>80%) of the total mean square error in the tropical regions.

Divergent and Rotational wind

A useful way to look at wind errors is to split the wind vector into its divergent ($v(\chi)$) and rotational ($v(\psi)$) components. These can be further expressed in terms of the scalar functions, velocity potential (X) and streamfunction (Ψ)

$$\mathbf{V} = \mathbf{V}(\chi) + \mathbf{V}(\psi) = \nabla\mathbf{X} + \mathbf{k} \times \nabla\Psi$$

The velocity potential shows the planetary scale divergent circulation and is related to the divergence (D) by $D=\nabla^2\mathbf{X}$. The divergent wind is proportional to the gradients in **X** and flows perpendicular to the contours from negative (areas of divergence) to positive (areas of convergence) values. The streamfunction is related to the relative vorticity (ξ) by $\xi=\nabla^2\Psi$.

Figure 12 shows the velocity potential at 850hPa and 250hPa for January 1995. For the analysis at 850hPa (Fig. 12(a)) areas of convergence occur over the main tropical convective regions of Indonesia/Australasia, Southern Africa and South America, with areas of compensating divergence over North Africa, tropical east Pacific, and tropical Atlantic. At 250hPa we have the opposite with divergence over the main tropical convective regions (Fig. 12(d)). The T+72 errors in velocity potential show a marked increase in the tropical divergent circulation (Fig. 12(c) and 12(f)). There is increased convergence at 850hPa over South America, North Africa, east of the Himalayas and Indian Ocean, and a clear increase in the Walker circulation between the Pacific and Indian Oceans. These errors are also consistent with the lower troposphere warm biases noted in Fig. 9(a) and suggest too strong tropical diabatic heating in the model. Errors of the opposite sign appear at 250hPa (Fig 12(f))

Similar errors in the divergent circulation occur in July 1994, with an increased Walker circulation between Pacific and Indian Oceans and increased convergence at 850hPa over North Africa and South America (Fig. 13 (c)). The errors at 250hPa show a very strong projection onto the Hadley circulation with enhanced north to south flow over Africa, the Indian Ocean, and South America (Fig. 13(f))

Finally we consider the rotational errors for January 1995. At 850hPa the analysed (Fig 14(a)) and T+72 forecast (Fig. 14(b)) streamfunction fields show the subtropical anticyclones with westerly flow in midlatitudes and easterlies in the tropics. The T+72 error (Fig 14(c)) is dominated by a pair of anticyclones straddling the equator in the west and central Pacific, with intense easterly errors along the equator. Over Africa we see the reverse, with a pair of erroneous cyclones and westerly flow along the equator. The errors in the equatorial winds are consistent with the area of erroneous convergence in the Indian Ocean (Fig. 12(c)) and with Gill's (1980) model of the response of the tropical circulation to anomalous diabatic heating. At 250hPa (Fig. 14(f)) we see rotational errors of the opposite sign to those at 850hPa, with a pair of cyclonic centres downstream of the region of enhanced divergence in the Indian Ocean (Fig 12(f)) leading to westerly errors consistent with those noted in the zonally averaged wind at 20N and 20S (Fig 1(b)). A pair of erroneous anticyclones occur over Africa, upstream of the divergence error in the Indian Ocean.

In summary, a large proportion of the tropical/subtropical wind errors appear to be associated with increased divergent circulation over the Indian Ocean, South America, and Africa. Sardesmukh and Hoskins (1988) have used the upper tropospheric vorticity balance to demonstrate that the divergent circulation generated by tropical convective heating plays an important role in the generating rotational flow in the subtropics and mid-latitudes, More diagnostic work is required to investigate the role that errors in the tropical divergent circulation may be having upon mid-latitude forecasts. A recent change to prevent horizontal diffusion occurring over steep orography appears to have a beneficial imapct upon errors in the divergent circulation, most noteably over the South America and the Himalayas (Wilson et al. ,1995).

The Subtropical Jets

Accurate forecasts of the position and intensity of the jetstreams is of prime importance for customers in Civil Aviation. Tenenbaum (1991) has documented the tendency of operational model analyses to underestimate the strength of the jets compared to independent aircraft reports. The global UM is no exception and a constant scaling of 1.04 is currently applied the model winds at upper levels.

We consider here the errors in the forecast jets as compared to the UM analyses. Figure 15 shows the January 1995 monthly-mean zonal wind at 250mb for the analysis, T+72 forecast, and the T+72 mean error. On the whole the T+72 forecast is an accurate representation of the analysed zonal wind. However, the mean error shows that there is a systematic increase in westerlies on the equatorward side and systematic decrease in the westerlies on the poleward side of the East Asian and Atlantic subtropical jets. Similar errors can be seen in the southern hemisphere at the same longitudes. This is consistent with the cyclonic circulations noted in the 250hPa streamfunction and implies an equatorward shift in the zonally averaged jetstreams. It is possible that these errors may be linked in part to the excessive divergent circulation in the Indian Ocean noted in the previous section. If this proves correct then improving the Hadley/divergent circulation should be given high priority to reflect the high priority given to reducing errors in the jets (see appendices A and B). Another possibility is that the errors arise from the interaction of the large scale flow with the orography of the Himalayas and Rockies which are both located upstream of the jets. Further diagnostic studies of the role of diabatic and orographic forcing in the global UM are required to progress further in identifying the source of these errors.

Asian Summer Monsoon flow - July 1994

Figure 16 shows the analysed winds and T+72 wind errors at 850hPa over the Indian Ocean during July 1994. The analysis (Fig. 16(a)) show the Monsoon circulation with easterly flow at 10S curving northwards and forming a Somali jet of 25m/s and westerly flow at 10N extending beyond the Phillipines. The Hovmoller plot of 850hPa wind errors (Fig 7) showed the signature of an over intense Monsoon circulation and this can clearly be seen in the T+72 errors (Fig. 16(b)), with excessive easterlies at 10S and excessive westerlies between 10N and 20N. Also evident is a very strong cyclonic circulation over North Africa which is consistent with the increased low level convergence in this region. At 250hPa (Fig. 17) the errors show an increase in the divergent circulation in the central Indian Ocean consistent with the velocity potential errors. Westerly errors occur at 20S on the equatorward side of the subtropical jet. Over North Africa we have an erroneous upper level anticyclone due to the enhanced divergent flow at upper levels. The most likely source of the overactive Monsoon circulation

is excessive tropical diabatic heating.

3.3 Model Hydrological Cycle.

Global precipitation and evaporation.
The globally averaged precipitation minus evaporation (P-E) provides a useful measure of the model's hydrological balance, and should equal zero for long time means. This is shown for the global model at various forecast ranges in Figure 18(a). On its introduction in June 1991 the global UM suffered from a clear spin up in P-E, with a deficit in global precipitation compared to evaporation during the assimilation and balance only being achieved beyond day 3. This spin up was reduced with the introduction of fourth order moisture diffusion in March 1993 and has been largely removed with the changes to the assimilation of moisture in November 1994.

The time series of globally averaged precipitation (Fig. 18(b)) shows the deficit in precipitation during the assimilation in early model versions with model precipitation only equalling the Jaeger (1976) precipitation climatology by day 3. The current model formulation (February 1995) shows that the precipitation during the assimilation is equivalent to the Jaeger climatology and undergoes a small spinup in later forecast ranges with values approaching 3 mm/day by day 3. In the tropics (Fig. 18(c)) the model now suffers a small spin down with time since the change to moisture assimilation in November 1994. The geographical distributions of precipitation are given in Milton and Van der Wal (1994).

The change in zonally averaged evaporation between T+00 and T+72 is shown in figure 19 as a time latitude diagram. In the northern hemisphere summer (JJA) the model shows a considerable decrease in surface evaporation between T+00 and T+72. This occurs mainly over the continents and is a manifestation of the well known summer drying problem which is linked to deficiencies in cloud cover. Initially there is too little cloud cover leading to a large downward flux of shortwave radiation which drives excessive evaporation over land in the early stages of the forecast. This moistens the lower atmosphere, increases low cloud cover, cuts off the solar radiation and reduces the surface evaporation at later forecast ranges. There are corresponding increases in the relative humidity and low cloud in the lower troposphere (not shown). The change to the moisture assimilation in November 1994 does increase the cloud cover at T+00 which may have partially alleviated this problem. There is also a possible link between these changes in the moisture and low cloud fields and the 850hPa temperature errors which show the same seasonal behaviour with largest errors over land in JJA (Fig. 8C(a) and fig. 9(c)).

More work is required to validate the model's moisture fields against independent measures such as vertically integrated water vapour available from SSM/I satellite data.

3.4 Clouds and Radiation - Comparisons with ERBE

Cloud is a key component in modelling of present day climate and climate change scenarios. However cloud is also crucial in an NWP context for the accurate prediction of surface temperatures and precipitation. There are many issues to be addressed in parametrizing cloud

in a model, including cloud-radiation interactions and the role of clouds in the hydrological cycle. The problem is made worse by the fact that there are few datasets against which to validate clouds or cloud properties. This section contrasts cloud amounts with those from ECMWF and compares the top of the atmosphere (TOA) radiative fluxes from the model in August 1994 with those measured in August 1988 during the Earth's Radiation Budget Experiment (ERBE-Barkstrom, 1988). We concentrate on zonally averaged measures as this minimizes any interannual differences in comparing TOA radiative fluxes from 1988 and 1994. Of course zonal averages mask important regional detail and a more detailed description of the comparisons is given elsewhere.

Cloud Amounts.

In August 1994 there is a spinup in cloud amounts of all 4 types between T+00 and T+72 (Fig. 20) . The largest spin-up occurs in the extratropics, whilst in the tropics there is virtually no change in the small (~10%) medium and low cloud amounts. The spin-up is most marked for the low cloud in the northern hemisphere and is associated with the feedback which leads to the drying of the summer continents discussed in the previous section. Bell (1994b) showed that the impact of the change to moisture assimilation introduced in November 1994 is to reduce cloud spin-up by increasing cloud amounts at T+00. The cloud amounts for January 1995 (Fig. 21) show the spin-up is reduced compared to January 1994 (Fig. 22), in fact for low cloud there is a small spin down. In general the overall cloud distributions have not changed. The globally averaged total cloud amount for January at T+00 is ~49% which is less than the 63% given by the International Satellite Cloud Climatology Project (ISCCP) data (Rossow et. al, 1993). A major contribution to this difference may come from the small amounts of medium and low cloud in the tropics, which are less than those in the ground based obervational climatology of Warren et. al. (1985). Slingo et al. (1993) have also compared vertically integrated liquid water paths with those derived from SSM/I and found values in the tropics to be underestimated in the UM.

The introduction of fourth order moisture diffusion in March 1993 lead to increases in tropical high cloud (Fig. 23) and convective cloud (not shown) during JJA at T+00 suggesting more active tropical convection in the model since this change (see also thermal budget studies (Milton, 1993)). This coincides with increased easterly errors in the 250hPa wind in the tropics (Fig. 7). The introduction of fourth order moisture diffusion has reduced the spin-up in the model hydrological cycle but has had a detrimental impact on other aspects of the tropical circulation.

Finally we contrast the cloud amounts at T+24 from the UM and ECMWF model. The ECMWF model uses the diagnostic cloud scheme originally devised by Slingo (1987) during the periods considered here, but a new prognostic cloud scheme has been developed and recently implemented at ECMWF (Tiedtke, 1993). In DJF 1993 (Fig. 24) ECMWF has much larger high cloud amounts in the tropics and southern hemisphere. For medium cloud both models are comparable in the extratropics but between 30N and 30S the UM has cloud amounts of ~5% compared to ~15% in the ECMWF model. For low cloud the UM has very large cloud amounts in the southern hemisphere stormtrack region compared to ECMWF whilst north of 60N the reverse is true. In the tropics the low cloud amounts are less in the UM. Convective cloud amounts are very similar, reflecting the similarity of the diagnostic relationships used to derive convective cloud amounts in both models. Similar conclusions can be drawn for JJA 1993 (Fig. 25), although there are seasonal variations in both models, such

as the large increase in low cloud in the UM over the northern hemiphere pole in JJA. In general ECMWF has layer cloud distributions which have a smaller dependence upon latitude, giving them more layer cloud in the tropics but less in the extratropics than the UM. In the new ECMWF prognostic cloud scheme the high cloud amounts have decreased compared to the diagnostic scheme whilst the medium and low cloud amounts have increased (Tiedtke, 1993).

It should be noted that cloud amount is an ill defined quantity. More work is required to validate the cloud in the NWP analyses and forecasts against data such as cloud water paths derived from data sources such as the the International Satellite Cloud Climatology Project (ISCCP, Rossow and Schiffer, 1988)) and SSM/I (Lin and Rossow, 1994).

Outgoing Longwave Radiation (OLR)

Figure (26(a)) shows the zonally averaged OLR from ERBE for August 1988 and the UM for August 1994. The UM measurements are a daily mean from T-06 to T+18 of forecasts from 00Z. The shape of the OLR as a function of latitude is accurate in the UM with a clear minimum in the ITCZ and maxima in the subtropics. However, the magnitude is systematically overestimated by 15-20 Wm^2 between 60N and 50S with smaller errors at the poles. In the global mean the model OLR is too large by 15 W/m^2. In general the OLR is affected most by the presence of high cold cloud, hence the minimum in the tropics. These OLR errors may suggest either

(i) Insufficient cloud cover during the early stages of the forecasts,
(ii) Incorrect parametrization of high (?) cloud longwave emissivities.
(iii) Incorrect clear-sky OLR.

Cloud amounts for August 1994 (Fig. 20) at T+00 are less than those in later forecast ranges and also less than those in the ECMWF model (Fig. 25). It would be useful to compare the UM TOA radiation budget with ERBE at T+72 after cloud has spun up.

The model clear-sky OLR (Fig. 26(d)) is around $10W/m^2$ too large compared to ERBE, and as such accounts for ~50% of the errors in the zonally averaged total OLR field. Largest differences are located over the tropical land areas (not shown) of the Sahara, Arabian Peninsula (40-60 W/m^2) and South America (20-40 W/m^2). This warming of the land may be due to too insufficient optically thick cloud in the tropics.

Planetary Albedo

The planetary albedo is defined as the ratio of the outgoing to the incoming SW radiative flux. It is generally dominated by the presence of optically thick cloud which occurs in the lower troposphere. The UM albedo agrees reasonably well with ERBE (Fig. 27(a)), but is an overestimate by 10% north of 60N and 5% between 20S and 60S (Fig 27(b)). This latter error coincides with the excessive low cloud amounts in the southern hemisphere stormtrack regions.

In contrast the clear-sky albedo (Figure 27(c)) shows that at most latitudes the model *underestimates* the albedo. The largest local errors in clear-sky albedo occur over the Sahara where the model has an albedo of 20%-30% and ERBE shows 30%-40% (not shown). This underestimation of the Saharan albedo has been pointed out in earlier versions of the UM, and

may be a contributing factor in the excessive heating of the North African regions (Fig. 9). At 80N the clear sky albedo is overestimated in the UM and hence a large proportion of the overestimate in total planetary albedo north of 60N noted in the previous paragraph appears related to the clear sky component, apart from directly at the pole where it is due to the excessive low cloud amounts (Fig 5(b)).

Longwave Cloud Forcing (LWCF)
The LWCF is defined as the clear sky flux of OLR minus the total (cloudy+clear sky) flux of OLR and represents the LW radiative effects of clouds on the earth atmosphere system. The positive values imply a heating of the earth-atmosphere system at most latitudes (Fig 28(a)). In the ITCZ the LWCF is a maximum, and the UM is in good agreement with ERBE. Outside of the ITCZ the UM LWCF is everywhere less than the ERBE value and globally averaged is only 22.7 W/m^2 compared to 27.1 W/m^2 for ERBE. Again this is suggestive of either too little cloud or incorrect cloud emissivities.

Shortwave Cloud Forcing (SWCF)
This is defined in the same way as the LWCF. As discussed by Slingo and Slingo (1988) the SWCF is mainly felt at the surface as the atmosphere is relatively transparent to SW radiation. The fact that the UM clear sky albedo is less than ERBE but the total (cloudy + clear) albedo is higher than ERBE implies that the albedo of the model clouds is too high. This can be seen in the SWCF which is everywhere larger in magnitude than ERBE (Fig 28(c) and (d)). The errors in the SWCF of clouds is either a function of (i) excessive cloud amounts, or (ii) incorrect parametrization of cloud optical properties. For the southern hemisphere stormtrack region where the SWCF errors are largest the evidence points towards excessive cloud amounts. Elsewhere it is uncertain what is the cause of the errors.

Total Cloud Forcing
The net cloud radiative forcing is the sum of LWCF and SWCF. For ERBE the globally averaged value is -19.3 W/m^2 compared to -31.3 W/m^2 for the UM. Hence clouds act to cool the present day climate. This process is too efficient in the UM for the cloud distributions present in the model at ~T+00.

Summary
- Low and medium cloud amounts too low in the tropics?.
- Southern hemisphere low cloud amounts too high.
- OLR too large - insufficient cloud/incorrect cloud emissivities?
- Longwave cloud forcing too small - insufficient cloud/incorrect cloud emissivities?.
- Shortwave cloud forcing too large - excessive low cloud amounts in extratropics?.
- Clear sky albedos too small - Incorrect prescribed land surface albedos?.
- Clear Sky OLR is too large - excessive heating of land (Tropics)?

3.5 Surface Fluxes - Comparisons with ECMWF.

Accurate modelling of the surface energy balance is crucial for the prediction of surface temperatures over land. In this section we consider the surface turbulent and radiative fluxes in the UM and ECMWF. Unlike the TOA fluxes we do not have a comparable climatology with global coverage, hence we can only infer possible errors in the surface fluxes from other known deficiencies in the models.

Globally Averaged Surface Energy Balance.
Figure 29 shows the annual mean values for 1993 of the latent heat flux, sensible heat flux, net SW radiative flux and net LW radiative flux at the surface from the UM and ECMWF models. The values given are daily means. These are calculated in the UM by averaging together the 12 hour fluxes from T-06 to T+06 of the 00Z and 12Z forecasts. The ECMWF fluxes are calculated from the first 24 hours of the 12Z forecasts. Also shown are global estimates compiled by Ramanathan et. al (1989) from a variety of observational sources. The fluxes are all depicted as positive quantities but the sign of the fluxes is given on the diagrams, where (-) denotes an upward flux. The net flux can be either positive (downwards) or negative (upwards). There are a number of systematic differences between the UM and ECMWF;

- The UM latent heat flux is less than ECMWF which in turn is less than the climatology.
- The UM sensible heat flux is greater than ECMWF. The ECMWF value compares well with the climatology.
- The UM SW radiative flux is larger than ECMWF and closer to climatology.
- The LW radiative fluxes in both models and the climatology are comparable.

The global and annual averages mask a lot of detail in the fluxes. Figure 30 and 31 show the zonally averaged surface fluxes for DJF 1992/1993 and JJA 1993. In the following discussion the turbulent fluxes are defined as positive upwards and the radiative fluxes as negative upwards.

Latent Heat Flux
The ECMWF latent heat flux is higher than the UM in both DJF and JJA particularly between 30N and 30S. Only in JJA between 30N and 60N is the ECMWF latent heat flux less than the UM and this is associated with the excessive evaporation in the UM over NH summer continents during the early stages of the forecasts.

Sensible Heat Flux.
The sensible heat flux is in good agreement between the two models from 80N to 30N but between 30N and 60S the sensible heat of the UM is consistently larger than ECMWF in both DJF and JJA. This is linked to the excess heating of the land masses, which is largest in the tropics.

Net Shortwave Radiation at Surface
The largest differences between the two models occurs in the southern hemisphere stormtrack in DJF where the UM has less downward SW radiation than ECMWF. This is a consequence of the greater cloud cover in the UM (see Fig. 24). It is also worth noting that the ECMWF net SW flux in southern hemisphere mid-latitudes exceeds that in the tropics. This has been discussed by Foreman et al. (1994) and implies an unrealistic requirement for a net transport of heat from midlatitudes to the equator in the ocean in a coupled ocean-atmosphere system. This suggests insufficient extratropical low cloud cover in the ECMWF model in DJF. The two models are in better agreement in JJA in the southern hemisphere, although the amount of incoming solar radiation at high latitudes is small. In the northern hemisphere there is a

greater net downward SW flux in the ECMWF model, again consistent with the UM having larger cloud amounts in the extratropics. In the tropics the UM has larger net downward SW radiation at the surface in both DJF and JJA reflecting the smaller amounts of cloud in the UM.

Net Longwave Radiation at Surface
The biggest differences are associated with low cloud in the southern hemisphere with UM having smaller net LW flux due to the increased LW emissions to surface from the extra low cloud. In a similar manner the ECMWF net LW flux is smaller in the subtropics where the ECMWF cloud amounts are larger than those in the UM.

More effort is required to validate the model surface fluxes against any existing or future observational datasets. The results also need to be re-assessed in light of the changes to the UM moisture assimilation introduced in November 1994 and recent changes to the ECMWF cloud scheme.

4. TWO-TIMESTEP BUDGET DIAGNOSTICS.

In this section we consider diagnostics of the global UM thermal and momentum balance by employing the technique of Klinker and Sardesmukh (1992). This involves running very short-range forecasts (in our case 2 timesteps) from the four operational analyses available per day for a whole month and determining the contribution from each model routine to the monthly mean thermal and momentum balance. In theory there should be a balance between the parametrised and dynamical tendencies when averaged over a long enough period. However for a model with significant SE growth there will be a residual initial "tendency". Klinker and Sardesmukh demonstrated that this residual bears a strong resemblance to the model SE at later forecast ranges. This allows one to look at contributions to the residual from individual model routines and form hypotheses on *possible* error sources. For the purposes of the discussion we have concentrated upon the two-timestep budgets from 12/1/95 to 6/3/95 comprising 210 two timestep forecasts. Similar results are found for July 1994.

4.1 Thermal budget

Zonally averaged
Figure 32(a) shows the sum of all the parametrized terms in the zonally averaged thermal budget. This is the diabatic heating applied to the model and consists of terms due to radiation, convection, boundary layer turbulent mixing, and large scale condensational heating (evaporation of precipitation and formation/dissipation of layer cloud). Heating occurs in the tropical troposphere associated with latent heat release in tropical convection, in the boundary layer from 60N to 60S, and in the extratropical mid-troposphere due to diabatic heating in the stormtracks. Significant cooling occurs in the subtropics above 900mb, at the tropopause and over the poles. Figure 32(b) shows the dynamical heating terms with their sign reversed. This represents an "implied" diabatic heating which would be required in order to balance the dynamical terms. In general there is a great deal of similarity between the parametrized and (-)dynamical tendencies. If the Unified Model is in thermal balance at T+00 then these two terms should be identical. The degree of imbalance is given by the total tendency (Fig. 32(c)) which is the sum of the parametrized and dynamical terms. The total tendency bears a

remarkable resemblance to the zonally averaged T+72 temperature error (Fig. 1(d)), with a tropopause cooling, cooling in mid-latitudes (particularly large in the southern hemisphere), warming in the tropical mid-troposphere, and near surface cooling between 50N and 80N. Also evident in the total tendency is a warming of the near surface layers in the tropics.

We can split the thermal balance further by considering the contribution to the parametrized diabatic heating from the individual model routines (Fig. 33). These results suggest that the cold bias/cooling tendency at the tropopause and in the southern hemisphere boundary layer may be associated with excessive radiative cooling (Fig 33(c)) which leads to a net diabatic cooling (Fig. 32(a)) which is not balanced by the dynamics (Fig. 32(b)). The warming tendency/error in the tropical mid-troposphere is coincident with the maximum in convective heating. This suggests that convective heating may be too large at these levels early in the forecasts. Gregory and Rowntree (1990) have shown in single column tests that the convection scheme tends to produce a shallower heating profile when run from observed profiles than when initialised with typical model profiles. This is consistent with the results found here.

Summarizing, the main zonally averaged temperature errors are listed below together with their possible sources as inferred from the thermal balance.

- Tropopause cooling - Radiative cooling too large (Cloud?)
- Southern hemisphere boundary layer cooling - Radiative cooling too large/excessive low cloud
- Tropical mid-troposphere too warm - Convective heating too large/profile too shallow.
- Extratropical mid-tropospheric cooling - insufficient parametrized heating in stormtracks
- Near surface cooling (50N-80N) ?
- Near surface warming 10N-30S - Too much sensible heating in boundary layer.

Tropical Thermal Balance.

In order to explore the geographical variations in the thermal balance/systematic errors in more detail we have plotted height (model level) vs longitude plots of the thermal balance averaged over the tropical belt from 20N to 20S (Fig. 34).

Concentrating on the tropopause cooling, the total temperature tendency (Fig. 34(a)) shows this is a maximum between 40E and 150W. Again the cooling is due an imbalance between the dynamics (Fig. 34(b)) which requires a diabatic warming at these longitudes and the parametrized tendencies (Fig. 34(c)) which give a diabatic cooling. We note that this is a region where both the high layer cloud (Fig. 34(d)) and convective activity (Fig. 34(g)) are a maximum. The diabatic cooling at this level is dominated by the LW radiative terms (Fig. 34(e)) associated either with layer or convective cloud. Some compensating heating occurs due to SW radiation (Fig 34(f)) but none from convection which has negligible heating rates at this level (<1 K/day). Heating from large scale condensation is negligible over the tropical belt and is not shown.

The total tendency also shows areas of excess warming at model level 10 associated with convection (Fig 34(g)) and in the lowest model layers over Africa (0E-30E), Indonesia (90E-150E) and South America (80W-50W) due to sensible heating from the boundary layer scheme (Fig. 34(h)).

Northern Hemisphere Extratropical Thermal Balance.
Figure 35 shows a similar height-longitude plot for the thermal balance in mid-latitudes between 40N-60N for the troposphere (model levels 1 to 14)

The parametrized diabatic cooling at the tropopause is larger than that in the tropics and covers all longitudes (Fig 35(c)). This is not balanced by the dynamics (Fig 35(b)) leading to the familiar cooling in the total tendency. The largest contribution to the diabatic cooling comes from LW radiation (Fig 35 (e)), with maxima where there is extensive high cloud cover over the oceans (Fig. 35 (d)). SW heating is negiligble and not shown. Convective heating is shallow in the extratropics (Fig 35(g)) and the latent heating due to large scale condensation (Fig. 35 (f)) peaks at around 600-700hPa in the stormtracks. It is worth noting that the dynamical cooling at 60W, 150E, 90E and 40E in the upper troposphere/stratosphere (Fig 35(b)) implies a need for substantial diabatic heating at these locations. Some of these dynamical increments may be due to short timescale adjustments in the dynamics which have no projection on the longer term systematic errors of the model.

Another major feature in the total tendency is the residual cooling at model layers 1 and 2 over the continental land masses (70E-150E and 75W-120W). The LW radiation scheme (Fig 35(e) provides the largest contribution to this residual cooling which is linked to the systematic near-surface cooling in the T+72 zonally averaged temperature error (Fig 1(d)).

Lower Tropospheric Thermal balance - Geographical Distribution
Finally we briefly consider the thermal balance at model level 4 ~ 870hPa in more detail. Figure 36(a) shows the "implied" diabatic heating given by the (-) dynamical increments. The major features are a requirement for strong diabatic heating off the eastern seaboard of the U.S and Asia and in the ITCZ, and areas of strong diabatic cooling off the western coasts of North and South America, Australia, and Africa associated with the regions of extensive stratus/stratocumulus. The parametrized diabatic heating (Fig 36(b)) is very similar to that implied from the dynamics but there are important differences. These are shown in the "residual" total temperature tendency (Fig. 36(c)), which bears a strong resemblance to the T+72 850hPa temperature errors (Fig 9).

We list below the major features in the total temperature tendency (Fig 34(c)) and their possible sources

- The cooling at 40S comes from excessive parametrized diabatic cooling (Fig. 34(b)) due to LW radiative cooling caused by excessive low cloud. As discussed earlier the cooling is largest on the equatorward side of the main cloud belt where the shallower clouds occur (Fig 5) and large cloud top cooling is taking place.

- The largest total tendency in the northern hemisphere is off the eastern seaboard of the U.S. where the parametrised diabatic heating does not balance the dynamical cooling- Insufficient latent heating from convection or LS condensation?.

- The warming over the Andes, north Africa, northern India, and eastern Australia comes from too large a parametrized diabatic heating (Fig 35(b)) which has its origin

in excessive sensible heating of the lowest few layers by the boundary layer scheme

- The warming over the oceans off the western coast of South America and South Africa has its largest contribution from the dynamics. This is due to excessive local subsidence, and probably linked to the errors in the divergent circulation over South America and South Africa (see fig.12(c)). This is borne out by the fact that the warming tendency is largest off South America where the divergent circulation errors are particularly large

- The large warming tendency over the Himalayas arises because the dynamics and parametrized terms have the opposite sign and do not balance. The parametrised terms suggest a diabatic warming of the Tibetan Plateau of 2 K/day whilst the dynamics terms also warm by up to 3K/day presumably due to subsidence.

- The large cooling over Ethiopia comes from the dynamical terms and suggests excessive ascent over the East African Highlands

4.2 Discussion of the tropopause cooling

The parametrized radiative heating appears to be the most likely source of the large cooling bias at the tropopause, possibly associated with the properties of high cloud in the model. A number of possible scenarios exist for generating such erroneous cloud-radiation interactions and several have been discussed in the recent literature. However the role of other diabatic processes (i.e. convection) cannot be discounted. Possible scenarios for the cold bias include;

a. Incorrect High cloud amounts.

The local impact of high clouds on temperatures is difficult to anticipate, being a complex function of cloud amount, radiative properties of clouds in both the LW and SW, and their vertical distribution (Ramanathan et. al (1983);Slingo and Slingo (1988)). It is difficult to validate the high cloud amount as it is not a well defined quantity. More observational and modelling work is required to validate quantities such as the Ice Water Paths (IWP) in high clouds in both tropics and midlatitudes. These issues have been addressed in recent observational and modelling studies (Francis et. al, 1994).

b. Incorrect Cloud geometry and Vertical Distribution

Large uncertainties exist in modelling the vertical profile of cloud radiative forcing. Sensitivity studies with the NCAR CCM (Slingo and Slingo (1988)) have shown that the LW radiative impact of high cloud is to warm the tropical upper troposphere but cool the extratropics, whilst Randall et al. (1989) using the UCLA GCM found a different LW radiative impact with cooling at the tropical tropopause and warming below due to their high ('anvil') clouds. The radiative heating profile is sensitive to whether cloud is located in the cold tropical tropopause or in mid-latitudes (Slingo and Slingo,1988) and as shown by the above experiments is also a strong function of the cloud geometry/cloud vertical distribution present in a given model.

c. Incorrect LW emissivities of high cloud

Too low LW emissivities are consistent with the OLR being too large. The emissivities themselves are determined in the model by the following relationship (Ingram, 1993)

$$\varepsilon = 1 - \exp [-K \, . \, CWP]$$

Where CWP is the cloud water path (Liquid Water Path (LWP) and/or Ice Water Path(IWP)) and K is a tuneable constant set to 130 $m^2 \, kg^{-1}$ for water clouds and 65 $m^2 \, kg^{-1}$ for ice cloud. If emissivities are too low it is possible that this may be due to the IWP being too low or the the value of K being too small.

d. SW radiative heating of high cloud is too low.

Ramaswamy and Ramanathan (1989) have considered the role of SW heating by cirrus clouds on the maintenance of the tropical upper troposphere thermal balance and show that this term may be a significant component in the diabatic heating of the upper troposphere. SW radiative properties are determined by the optical depth (τ), the single scattering albedo (ω), and the asymmetry factor (g), which are functions of the spectral interval, IWP and the cloud particle size distribution characterized by the effective radius (r_e). The tunings are thought to be physically realistic for water clouds (Slingo, 1989) but less certain for ice clouds. Again we do not know how realistic the IWP is for the model high clouds. More SW radiative heating could be introduced by retuning the cloud optical properties. If the SW radiative heating of high clouds was deficient we might expect to see a larger cold bias in the summer hemispheres where solar insolation is largest. There is some evidence of such an effect in the northern hemisphere (Fig 8C(b)).

e. Role of latent heating due to convection in the tropics.

Recent comparison of the thermal balance in the UM and ECMWF models for July 1994 has shown that the ECMWF model has a small cooling tendency at the tropical tropopause (E.Klinker, personal communication). The radiative cooling of the UM and ECMWF are similar at the tropical tropopause, and the major difference is that the heating associated with convection (Fig. 33(d)) penetrates higher in the ECMWF model and acts to balance the radiative cooling. This may suggest that the convective heating in the UM does not penetrate high enough.

f. Convective cloud-radiation interaction in the tropics - Anvil clouds.

Recent work at the Hadley centre (Webb and Senior, personal communication) has suggested that the tropical high layer cloud in climate simulations is optically thin and exerts a small radiative influence. At least half of the radiative cooling at the tropical tropopause comes from the convective towers. The convective cloud amounts are currently determined from an empirical relationship that attempts to include the coverage due to anvil clouds whilst modelling the cloud as a convective tower. The suggestion is that the vertical geometry of the convective clouds is incorrect, and that the tower should be replaced by a 'thinner' tower plus an anvil in order to correctly model the radiative heating profile. In the real atmosphere anvil clouds may have a significant radiative influence and can locally warm in the tropics by 20K/Day (Ackerman et al., 1988) depending on the value of the ice water content. Anvil clouds are not explicitly modelled in the UM at present.

To summarise, the cooling at the tropopause in the UM remains one of the outstanding biases. More sensitivity experiments are required to ascertain the role high cloud plays in determining this error. In addition more work is required to determine if the tropical tropopause cooling has the same error source as the mid-latitude tropopause cooling.

4.3 Momentum budget

Since the introduction of a new gravity wave drag scheme and orographic roughness the imbalance in the initial zonal momentum budget has been reduced. Figure 37 shows the zonal momentum balance for Jan/Feb/Mar 95. The total tendency (Fig 37(c)) is now much smaller than that in December 1993 (Fig. 38(c)), particularly in the boundary layer. This suggests that remaining errors in the zonal wind (Fig 1 and 2) may be related to the temperature bias through the thermal wind relation. There are still problems over Antarctica with a large easterly momentum tendency (Fig 37(c)) which matches the T+72 zonal wind error at this location (Fig 1(b)). It is hoped that ongoing collaboration with the British Antarctic Survey will shed light on mechanisms behind this error.

Although the stratospheric gravity wave drag has been reduced it is possible that this may still be overdone. Evidence for this comes from the dynamics tendencies (shown with sign reversed) at 40N and jet level. These show westerly tendencies at the site of the applied gravity wave drag and easterly tendencies below (Fig. 37(b)). This pattern is consistent with zonal wind tendencies that would be generated by a thermally direct (counterclockwise) meridional circulation in the upper troposphere. The hypothesis is that such a meridional circulation will be generated in order to maintain geostrophic and hydrostatic balance in the presence of an excessive drag in the stratosphere (see Milton et al. 1994 for more discussion.). The impact of these dynamical adjustments is to cause a residual momentum tendency at 200hPa which *decelerates* the subtropical jet (Fig. 37(c)). A height-longitude section of the zonal momentum balance for the latitude band 30N-50N and the free troposphere (model level 6-19) supports this hypothesis (Fig 39). The largest dynamical tendencies (Fig. 39(b)-shown with sign reversed) are coincident with those longitudes where the gravity wave drag is applied in the stratosphere (Fig. 39(d)), namely over the Himalayas and Rockies. Over the Himalayas the dynamical tendencies lead to a residual total tendency (Fig (39(b)) which causes a deceleration of 12 m/s/day in the entrance of the Pacific subtropical jet (Fig. 39(a)). This is also the longitude where there are large reductions in the 250hPa zonal wind in the T+72 forecasts compared to analyses (Fig 15(c)). A similar but smaller deceleration occurs in the Atlantic jet entrance region. Further sensitivity tests are required to confirm a link between reductions in forecast jet strength and excessive gravity wave drag.

5. SUMMARY

The following list summarises the outstanding systematic errors in the global UM and their possible sources;

Tropopause cooling
Radiative cooling too large - Radiative properties of high cloud (SW+LW)?
- Radiative properties of convective cloud (Tropics)?
- High cloud amounts and Ice Water Paths (IWP)?

Convective heating does not penetrate high enough in the Tropics?
Cold bias in northern hemisphere winter oceanic stormtracks.
Too little parametrized diabatic heating - Convection? LS Condensation?
Cold bias over northern hemisphere winter continents in model layer 1.
Excessive LW cooling?
Cold bias at 850hPa over northern hemisphere continents in summer.
Linked to excessive low cloud/evaporation over summer continents.
Southern hemisphere stormtrack cooling
Excessive low cloud - Radiative cooling too large.
Warming in the tropical mid troposphere.
Convection too intense in early stages of forecasts/heating profile too shallow?
Overactive tropical divergent circulation (Hadley cell) /Monsoon circulation too intense
Excess diabatic heating in model - Warming of tropical land masses-insufficient cloud?
- Convection too intense in early stages of forecasts?

Equatorward shift of Subtropical jets.
Linked to errors in the tropical divergent circulation?
Reduction in zonal wind speed in jet entrance regions
Dynamical response to excessive stratospheric gravity wave drag?
Easterlies too intense in upper tropical troposphere.
Error has worsened with introduction of fourth order moisture diffusion.
Extratropical westerly bias
Linked to cold bias via thermal wind relation?
Easterly bias over Antarctica in DJF
Dynamical adjustment of model - Incorrect orographic/diabatic forcing over Antarctica
Drying out of northern hemisphere summer continents
Excess evaporation due to insufficient cloud cover at T+00.
Planetary Albedo too large / SWCF too large.
Excessive low cloud in mid-latitudes.
OLR too large./LWCF too small.
Insufficient high cloud in early stages of forecasts.
LW emissivities of high cloud too small (Ice water paths too small?).
Clear sky OLR too large.
Warming of tropical land masses - too little tropical cloud?
Clear sky albedos too small
Prescribed land surface albedos too small - Sahara?

Of the high priority items in appendix A, more work is required to understand the systematic nature of the development errors and the role such errors as the tropopause cooling play in

their formation. Similarly more diagnostic studies are required to assess the nature of the systematic errors in surface temperatures. A number of problems which directly affect surface temperatures have been discussed, such as the deficiencies in cloud cover and possible errors in the surface energy balance. It is believed that attacking these problems will yield improvements in surface temperature forecasts.

A further point is that two of the major errors, the excessive Hadley circulation and the cold bias in the troposphere, have been given a low priority by most of the model users. These errors are fundamental measures of the global general circulation and point to serious deficiencies in model formulation. We argue that correcting these errors is of primary importance for improving model forecasts.

The time-latitude plots have revealed that the global UM has steadily improved since its introduction in June 1991.

The diagnostics used in this study can only suggest possible error sources. Further modelling sensitivity studies are required to test out some of the hypotheses on error sources given in the summary list.

6. REFERENCES

Ackerman,T.P.,K-N Liou, F.P.J.Valero and L.Pfister, 1988: Heating rates in tropical anvils. *JAS, 45,1606-1623.*

Barkstrom, B.R.,1988: The Earth Radiation Budget Experiment (ERBE). *Bull.Am. Meteor.Soc.,65,1170-1185*

Bell, R.S. 1994a: The assimilation of ERS-1 scatterometer winds. *Forecasting Research Tecnical Note No. 89.*

Bell, R.S. 1994b: Revised moisture assimilation - Results of a parallel trial. *Forecasting Research Tecnical Note No. 132.*

Foreman, S.J., J.O.S. Alves,and N.P.J. Brookes ,1994: Assessment of surface fluxes from numerical weather prediction systems. *Forecasting Research Tecnical Note No. 104.*

Francis, P.N., A.Jones, R.W. Saunders, K.P. Shine, A.Slingo, and Zhian Sun, 1994: An observational and theoretical study of the radiative properties of cirrus: Some results from ICE'89.*Quart. J. Roy. Metoer. Soc., 120, 809-848.*

Gallani, M.L., 1994: Comparisons between 1st and 2nd versions of the climate model. *Hadley centre Internal Note No. 58.*

Gill, A.E., 1980: Some simple solutions for heat induced tropical circulation.*Quart. J. Roy. Metoer. Soc., 106, 447-462.*

Gregory, D., and P.R. Rowntree, 1990: A mass flux convection scheme with representation of cloud ensemble characteristics and stability dependent closure. *Mon. Weath. Rev., 118, 1483-1506*

Hammon, O.M and C.A. Wilson, 1993: Global forecast model trials of revised "Frozen" physics. *Forecasting Research Tecnical Note No. 76.*

Ingram, W.J., 1993: Radiation. *Unified Model Documentation Paper no. 23.*

Jaeger,L., 1976 : Monthly precipitation maps for the entire earth. *Bericht Deutscher Wetterdienst 18 Nr 139, 38pp*

Klinker, E. and P.D.Sardesmukh, 1992: The diagnosis of mechanichal dissipation in the atmosphere from large scale balance requirements. *JAS, 49,608-627.*

Lin, B. and W.B. Rossow, 1994: Observations of cloud liquid water path over the oceans:Optical and microwave remote sensing methods. *Journ. Geophys. Res., 99, 20,907-20,927.*

Lorenc, A.,D.Barker,R.S.Bell,B.Macpherson,and A.J.Maycock, 1994: On the use of radiosonde

humidity observations in mid-latitude NWP. *Forecasting Research Division Scientific Paper No. 28.*

Milton, S.F. 1993: Diagnosing the source of systematic errors in the global unified model. I- The thermal budget. *Forecasting Research Tecnical Note No. 64.*

Milton, S.F. and A.Van Der Wal, 1994: The spin-up precipitation and evaporation of global and LAM Unified model forecasts January 1992- May 1994. *Forecasting Research Tecnical Note No. 136.*

Milton,S.F., C.A.Wilson, O.M.Hammon, and F.Rawlins,1994: Impact of a new gravity wave drag scheme and orographic roughness in the unified model. III Revised schemes and second parallel suite trial for global and limited area models. *Forecasting Research Tecnical Note No. 139.*

Milton, S.F. and C.Wilson, 1994: Progress report on diagnosing the source of systematic errors in the global unified model: *Forecasting research working paper No. 167.*(Available from Forecasting Research Division, UKMO.)

Mitchell, J.F.B. and C.A. Senior, 1993: The Unified Model (Climate). Version 1:Atmosphere. *Hadley Centre Internal Note No. 33.*

Ramanathan, V., B.R. Barkstrom, and E.F. Harrison, 1989: Climate and the earths radiation budget. *Physics Today, 42,22-32.*

Ramanathan, V., E.J. Pitcher, R.C.Malone, and M.C. Blackmon, 1983: The response of a spectral general circulation model to refinements in radiative processes. *JAS, 40, 605-630.*

Ramaswamy,V. and V. Ramanathan, 1989: Solar absorption by cirrus clouds and the maintenance of the tropical upper troposphere thermal structure. *JAS, 46, 2293-2310.*

Rossow W.B., A.W. Walker and L.C. Gardner, 1993:Comparison of ISSCP and other cloud amounts. *Journal of Climate, 6, 2394-2418.*

Rossow,W.B. and R.A.Schiffer, 1991:ISCCP Cloud Data Products.*Bull.Am. Meteor.Soc.,72,2-20*

Sardesmukh, P.D. and B.J. Hoskins, 1988: The generation of global rotational flow by steady idealized tropical divergence. *JAS,45,1228-1251.*

Slingo,A. and J.M. and Slingo, 1988: The response of a general circulation model to cloud longwave radiative forcing. Part I- Introduction and intial experiment. *Quart. J. Roy. Metoer. Soc., 114, 1027-1062.*

Slingo,A., 1989: A GCM parametrization for the shortwave radiative properties of water clouds. *JAS,26,1419-1427.*

Slingo,A., A.Jones, and M.J. Webb, 1993: Satellite validation of unified model simualtions of clouds and related variables. *In proceedings of ECMWF seminar on " Developments in the use of satellite data in NWP" September 1993.*

Slingo,J.M, 1987: The development and verification of a cloud prediction scheme for the ECMWF model. *Quart. J. Roy. Metoer. Soc., 113, 899-927.*

Tenenbaum,J., 1991: Jet stream winds:Comparison of analyses with independent aircraft data over soutwest Asia. *Wea. and Forecasting, 6, 320-336.*

Tiedtke, M, 1993: Representation of clouds in large-scale models. *Mon. Wea. Rev., 121, 3040-3061.*

Van Der Wal, A.D. and S.F. Milton, 1995: A comparison of the surface fluxes in the UKMO and ECMWF global model analyses and forecasts - 1992 to 1994. *Forecasting Research Tecnical Note* (in preparation).

Warren, S.G., C.J.Hahn, and J.London, 1985: Simultaneous occurrence of different cloud types. *J.Climate Appl. Meteor., 24, 658-667.*

Wilson, C.A.,F.Rawlins and O.Hammon, 1994: Cause and cure of the superadiabatic lapse rate in the limited area and global models. *Forecasting Research Tecnical Note No. 125.*

Wilson, C.A.,O.Hammon, and S.F.Milton 1995: Trial of a local correction of negative humidity and modified horizontal diffusion near steep orography in the global and limited area model. *Forecasting Research Tecnical Note No 165.*

APPENDIX A

ANNEX
to Loose Minute M/AD(CF)/4/1/1
dated 30th January 1995

MODEL PROBLEMS: SUGGESTED CFO PRIORITIES

Item	Description	Priority	
1.b	Development errors	High	1
2.c	Low surface temperatures	High	1
2.e	Med-level instability	High	1
3.a	Jets mispositioned	High	1
3.b	Jets underestimated	High	1
1.c	Consistency between runs	Medium	2
2.b	Aviation temperature errors	Medium	2
2.d	Mesoscale model cooling	Medium	2
2.f	Incorrect temperatures in products	Medium	2
4.a	Light rain throughout forecast	Medium	2
4.c	Mistreatment of convection	Medium	2
4.d	Rain distribution in the LAM	Medium	2
4.e	Cloud	Medium	2
4.f	Temperature modifcation due to cloud	Medium	2
5.a	P and H fields: anomalies in PMSL over high ground	Medium	2
1.a	Excessive activity in the Hadley cell	Low	3
2.a	Cooling thro' troposphere	Low	3
3.c	Enstrophy	Low	3
4.b	Showers in LAM	Low	3

Notes:

The above listing is based on limited input. There are two considerations in listing priorities for items in that aviation products call for a high priority in view of the customer requirements, while the forecasters involved with model interpretation place a higher priority on the improvement of the model output.

The medium/low priority on some of the items (eg Showers in the LAM) is that problems of this kind can be accepted as characteristics by the forecasters and suitable adjustments made to the model output in the production of forecasts in knowledge of the problem. This is not so easy when dealing with development errors and medium-level instability.

Appendix B - Outstanding Problems in the Operational Suite (Compiled 3 March 1995)

Three user groups have assigned priorities (High Medium Low) to each item. Priorities are shown in order for PSP, DS, and Central Forecast Office (CFO). The priorities have been summarised as a single integer, where HHH=1 and LLL=7.

1 General.		Priority index
a) Excessive activity in the Hadley Cell.	(LLL)	7
b) Development Errors	(HHH)	1
c) Consistency between runs.	(HMM)	3
2. Temperature.		
a) Cooling in the troposphere.	(LLL)	7
b) Aviation temperatures in the stratosphere.	(LMM)	5
c) Low surface temperatures.	(HMH)	2
d) Medium level instability.	(MMH)	3
3. Winds		
a) Jets mispositioned.	(MHH)	2
b) Underestimation of jets for aviation users.	(MMH)	3
c) Loss of enstrophy.	(LML)	6
4. Moisture and precipitation.		
a) Spurious light rain.	(HHM)	2
b) Shower activity in the LAM	(MML)	5
c) Mistreatment of convective rain	(MHM)	3
d) Rainfall distribution in the LAM.	(HHM)	2
e) Cloud associated with low surface temp.	(MMM)	4

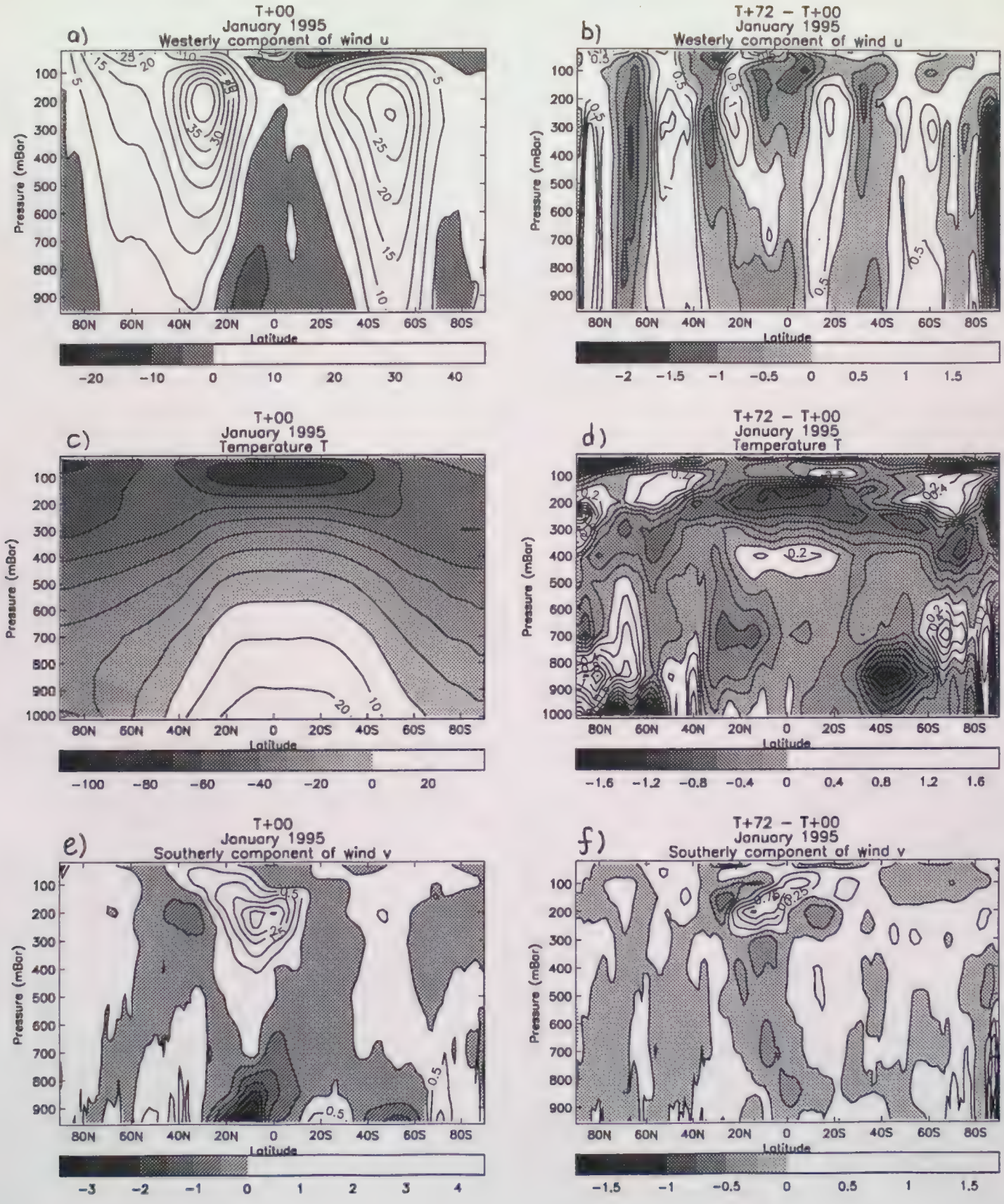

Figure 1: Zonally averaged height latitude cross sections for January 1995 of a) Analysed zonal wind, b) T+72 zonal wind error, c) Analysed temperature, d) T+72 temperature error, e) Analysed meridional wind, f) T+72 meridional wind error

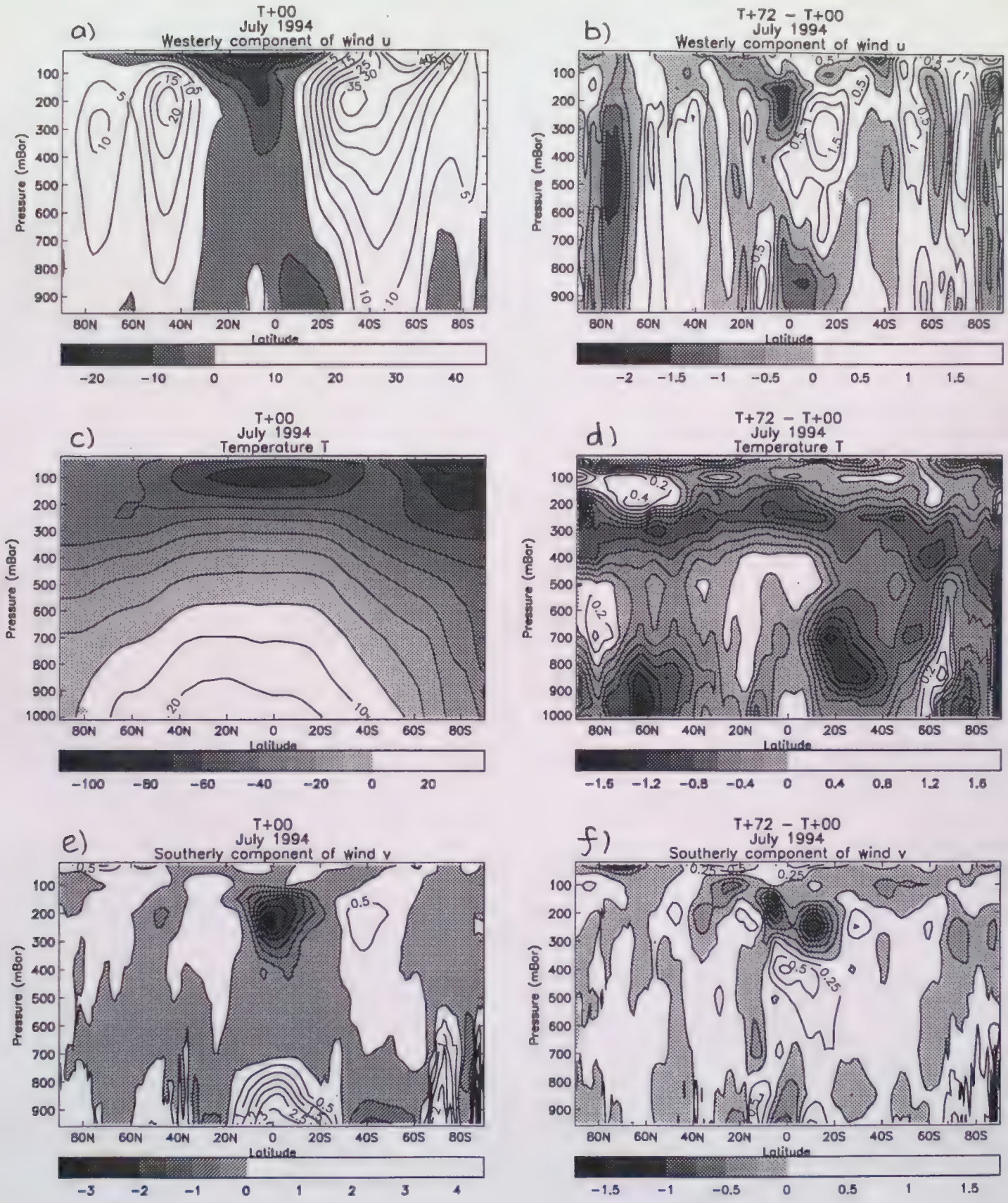

Figure 2 : Zonally averaged height latitude cross sections for July 1994 of a) Analysed zonal wind, b) T+72 zonal wind error, c) Analysed temperature, d) T+72 temperature error, e) Analysed meridional wind, f) T+72 meridional wind error

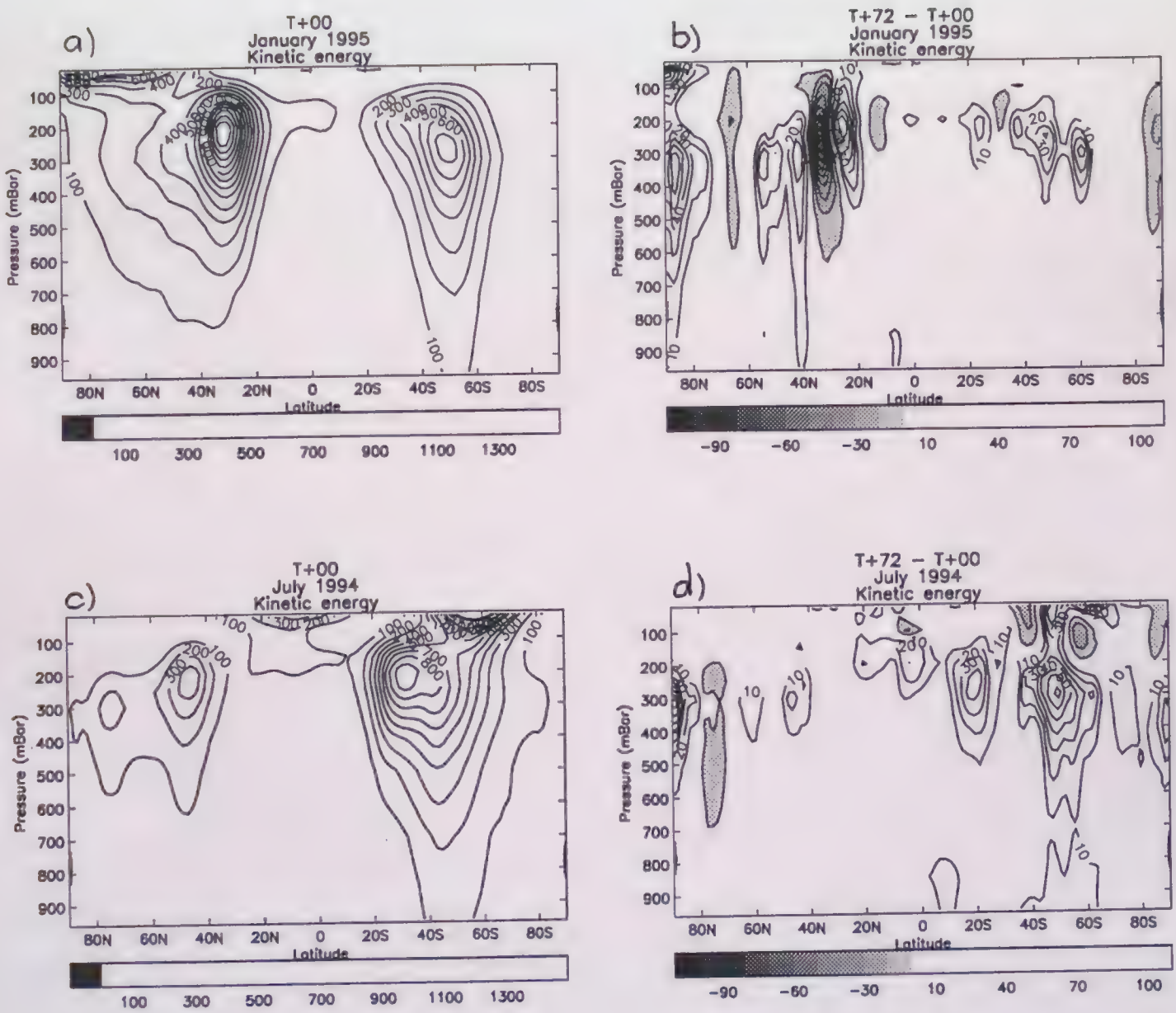

Figure 3 : Zonally averaged monthly-mean height-latitude cross sections of a) analysed kinetic energy, January 1995 b) T+72 kinetic energy error, January 1995, c) as a) but for July 1994, d) as b) but for July 1994

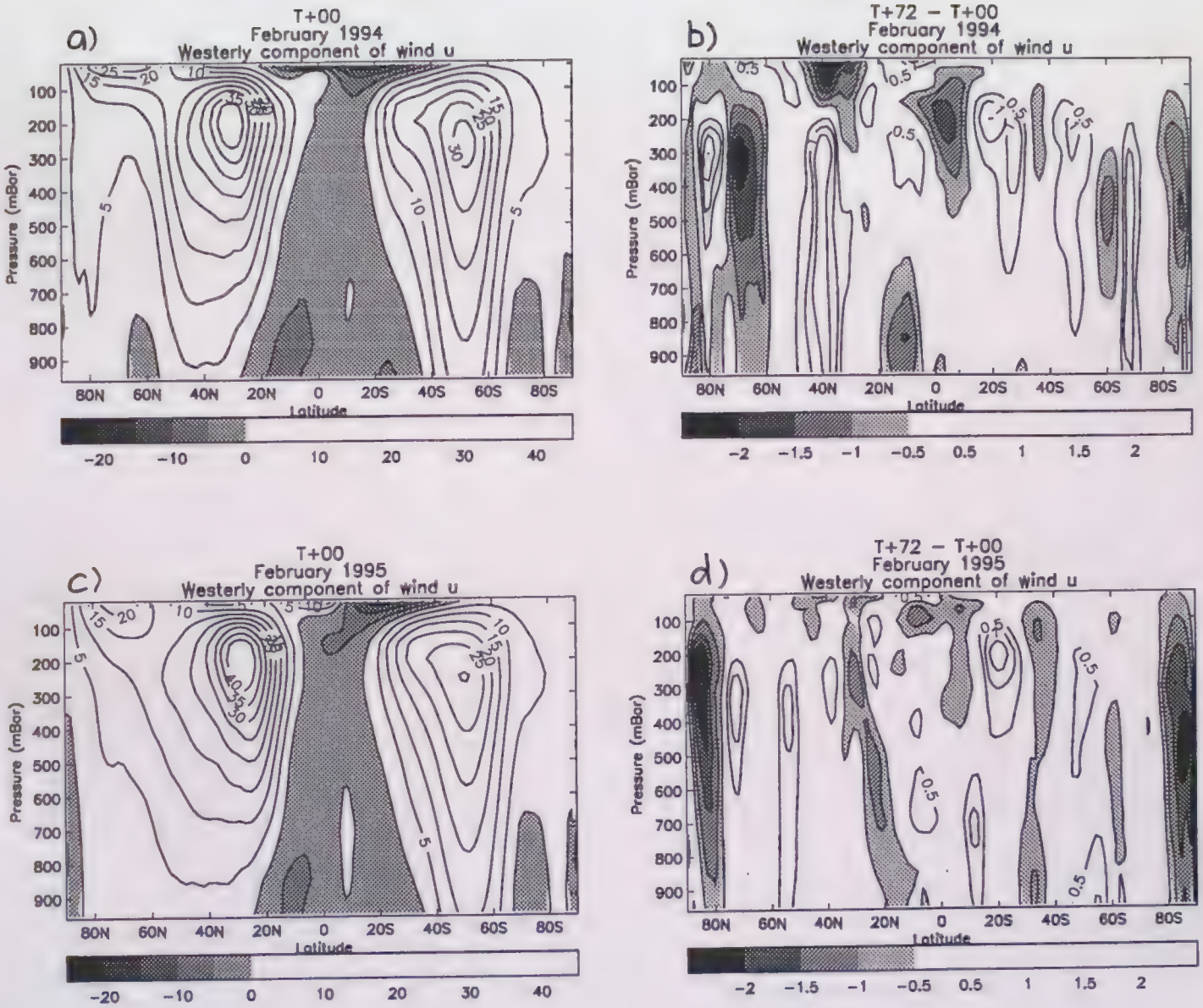

Figure 4 : Zonally averaged monthly-mean height-latitude cross sections for a) analysed zonal wind, February 1994, b) T+72 zonal wind error, February 1994, c) as a) but for February 1995, d) as b) but for February 1995. Zero contour omitted in

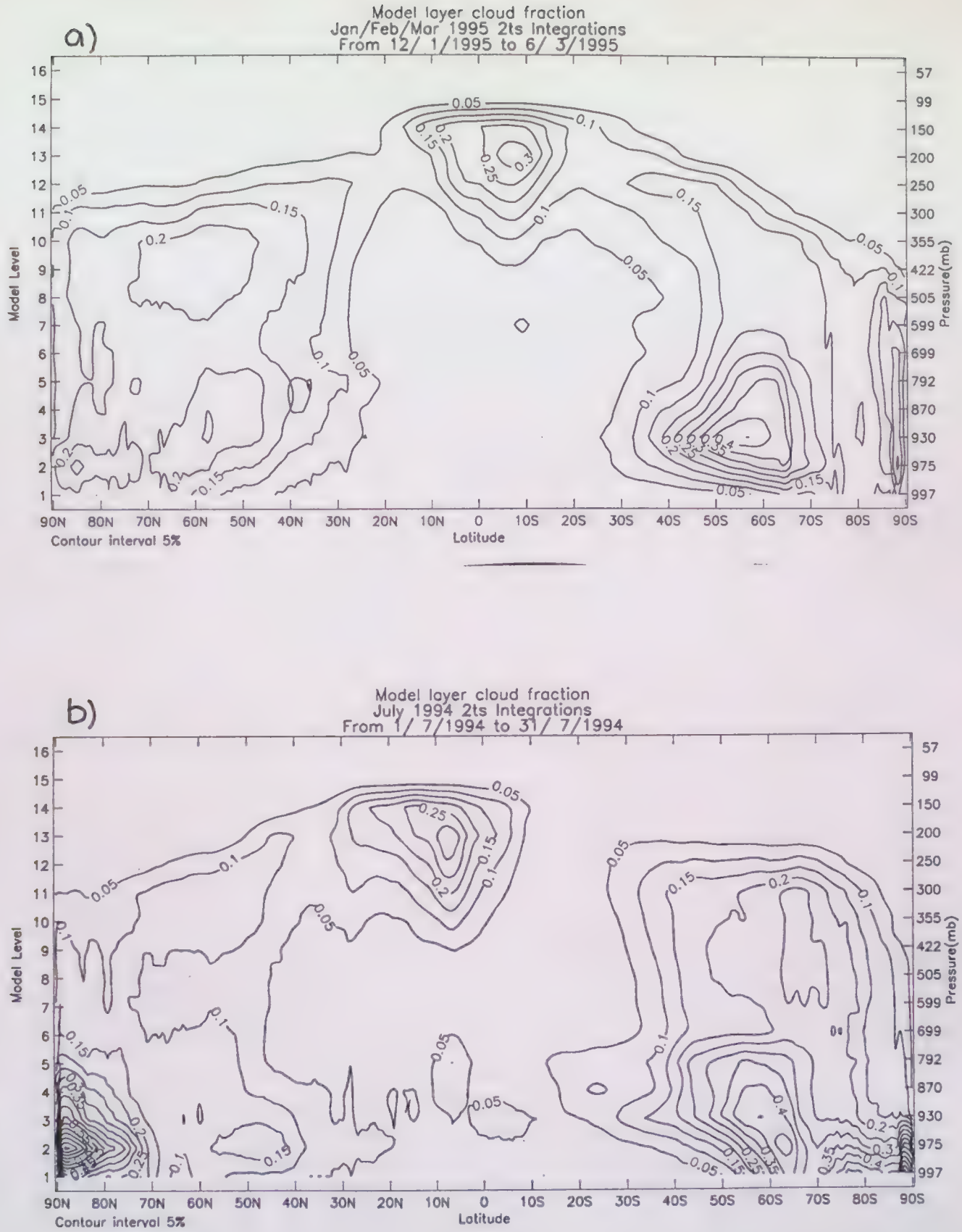

Figure 5 : Zonally averaged layer cloud fraction on model levels at T+00 for a) January-March 1995 b) July 1994.

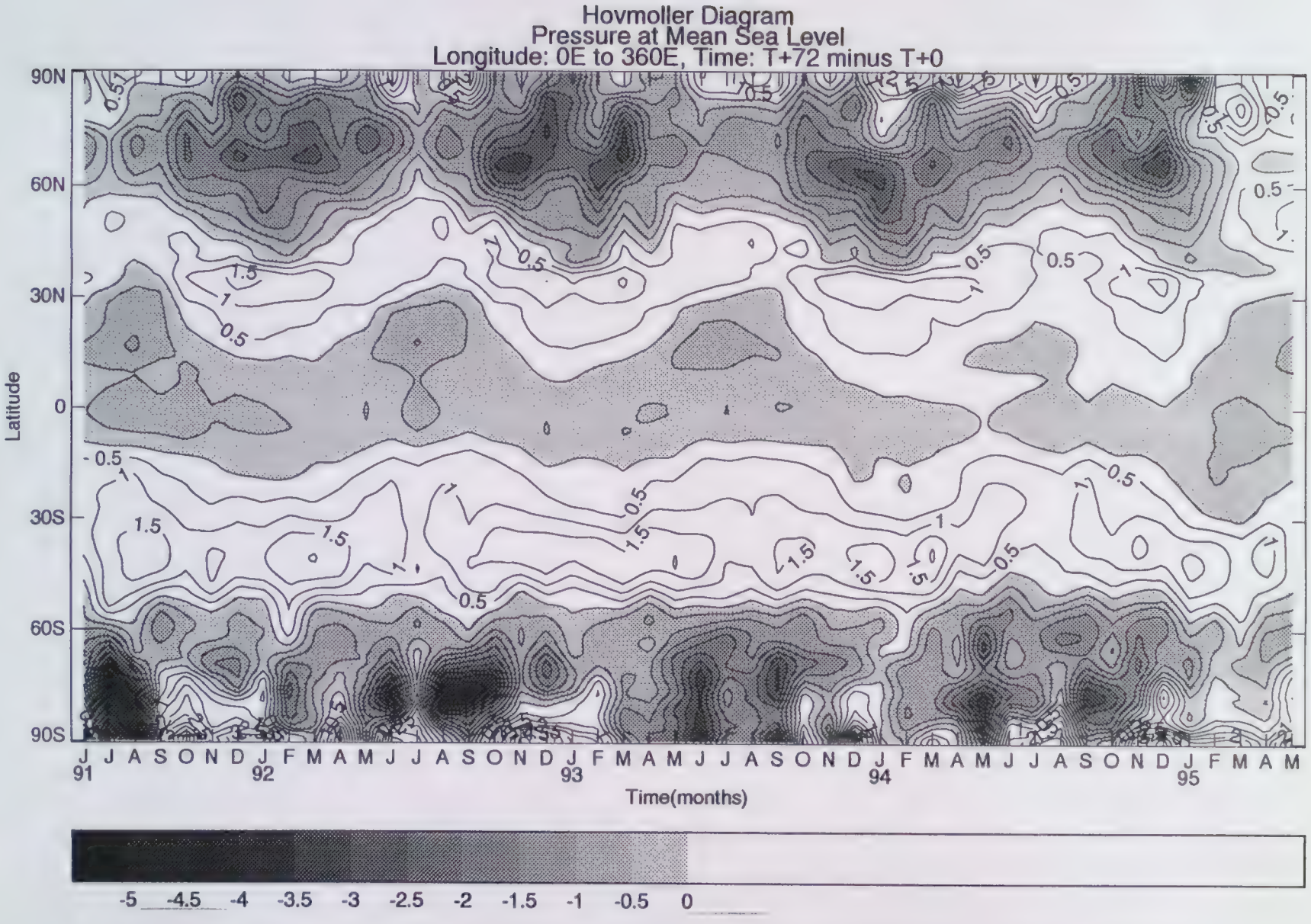

Figure 6 : Time latitude diagram of zonally averaged T+72 mean sea level pressure errors from June 1991 to May 1995.

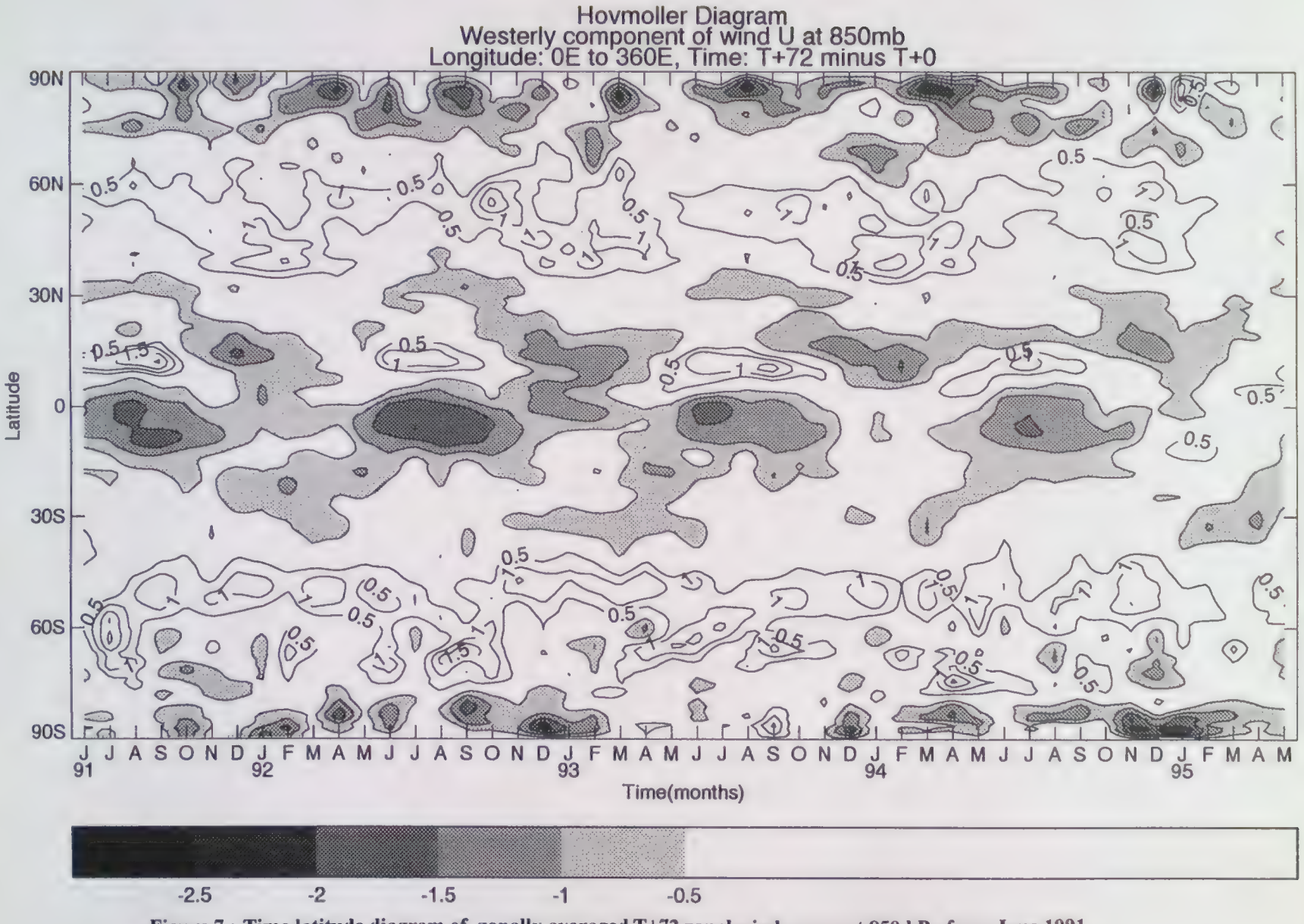

Figure 7 : Time latitude diagram of zonally averaged T+72 zonal wind errors at 850 hPa from June 1991 to May 1995.

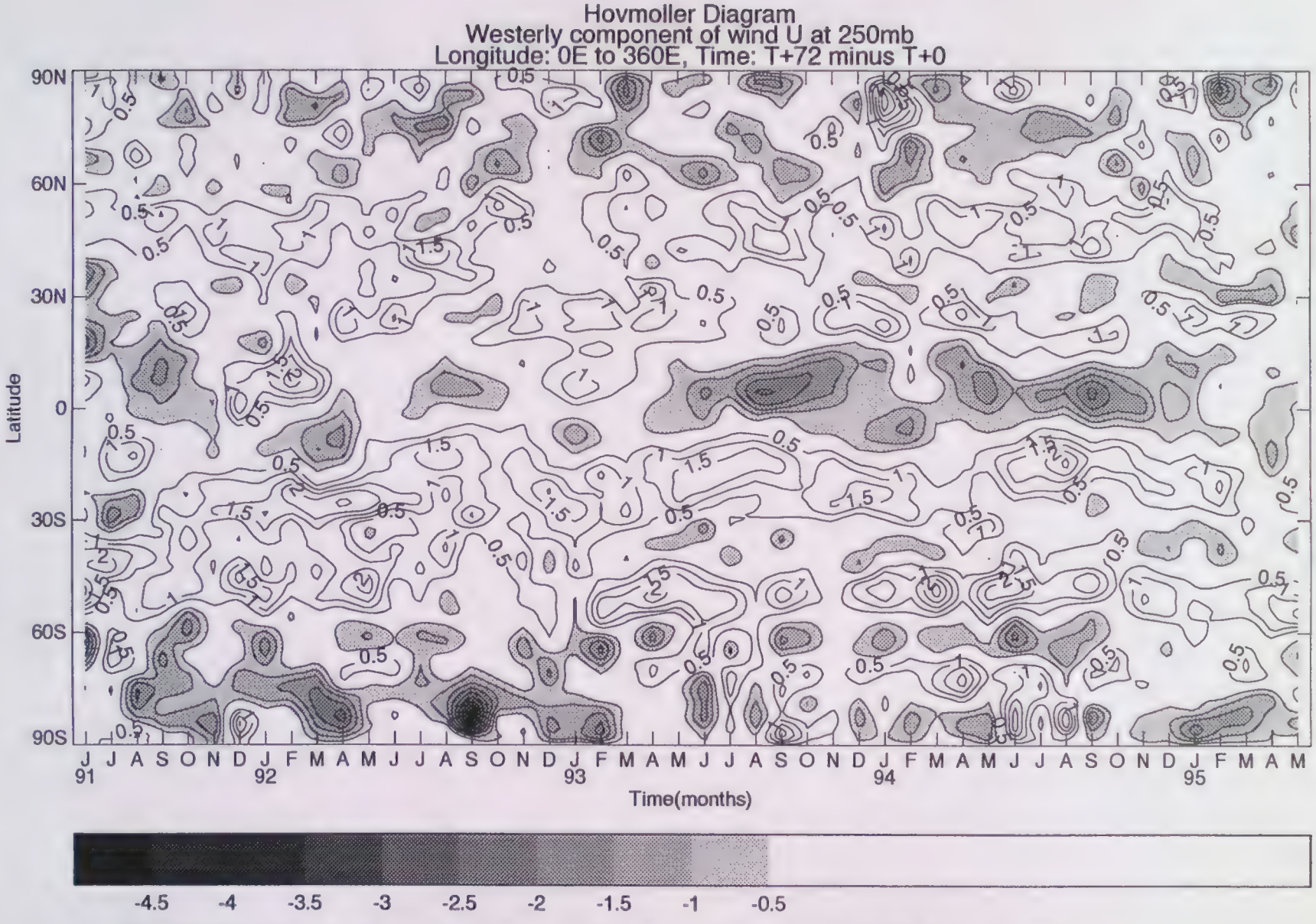

Figure 8 : Time latitude diagram of zonally averaged T+72 zonal wind errors at 250 hPa from June 1991 to May 1995.

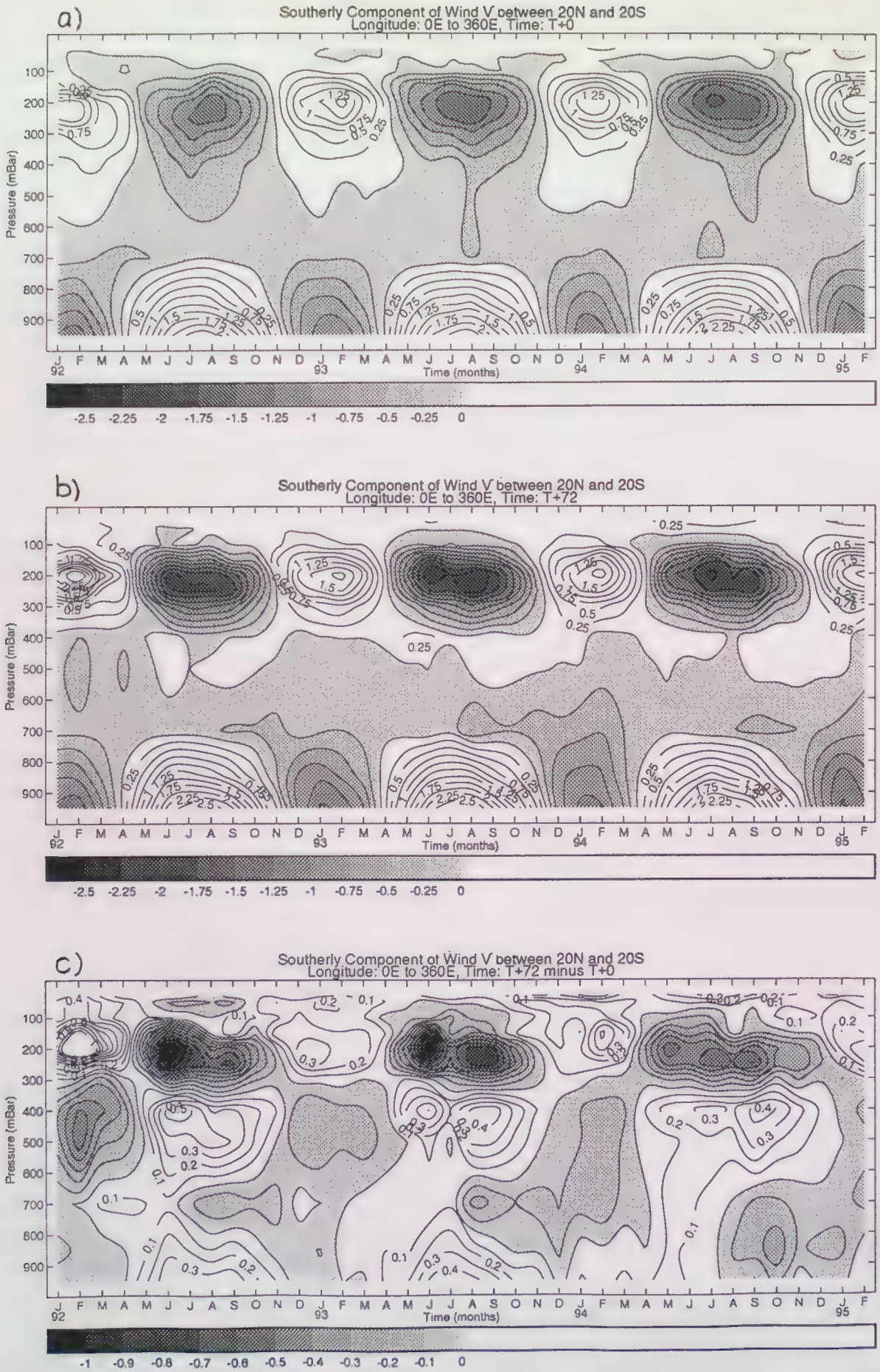

Figure 8B : Zonally averaged height - Time sections of monthly averaged, zonally averaged meridional wind averaged over the latiditude band 20N-20S and covering January 1992 to February 1995 for a) T+00, b) T+72 , c) T+72 - T+00.

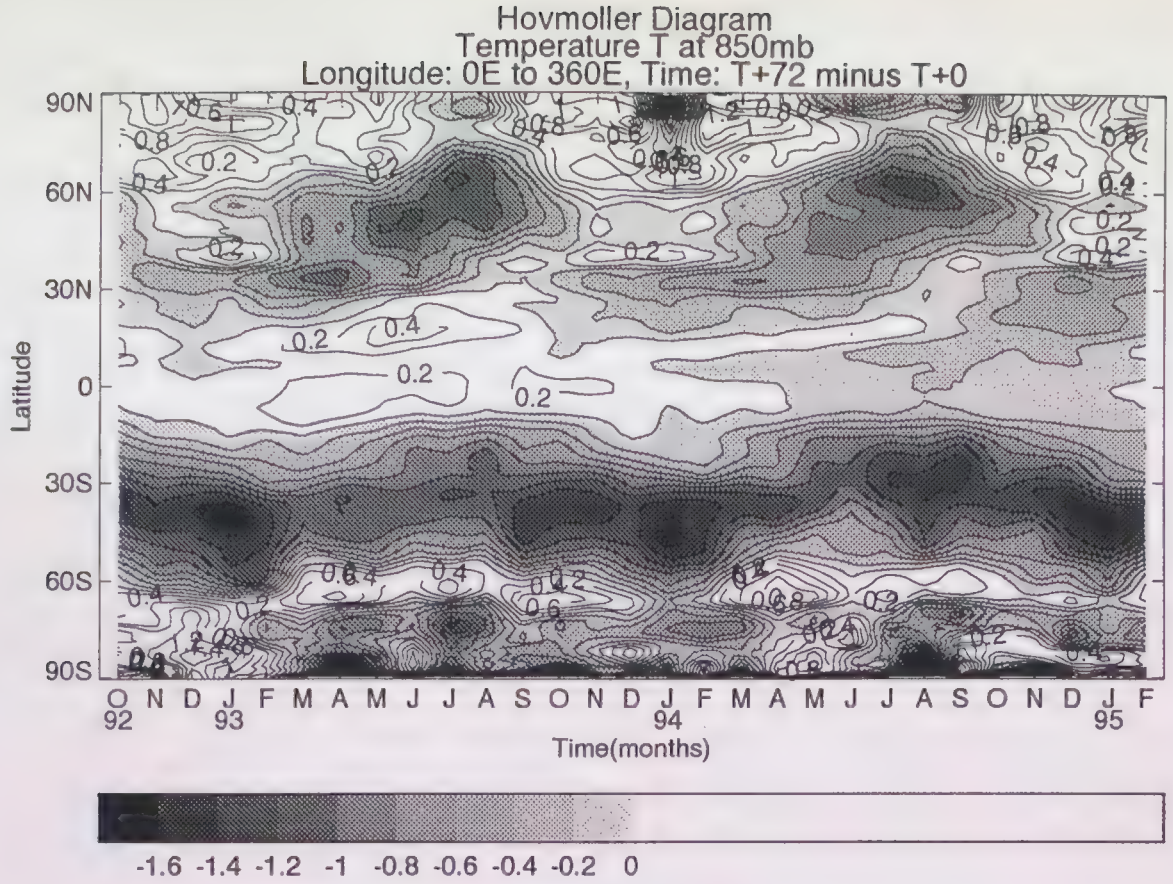

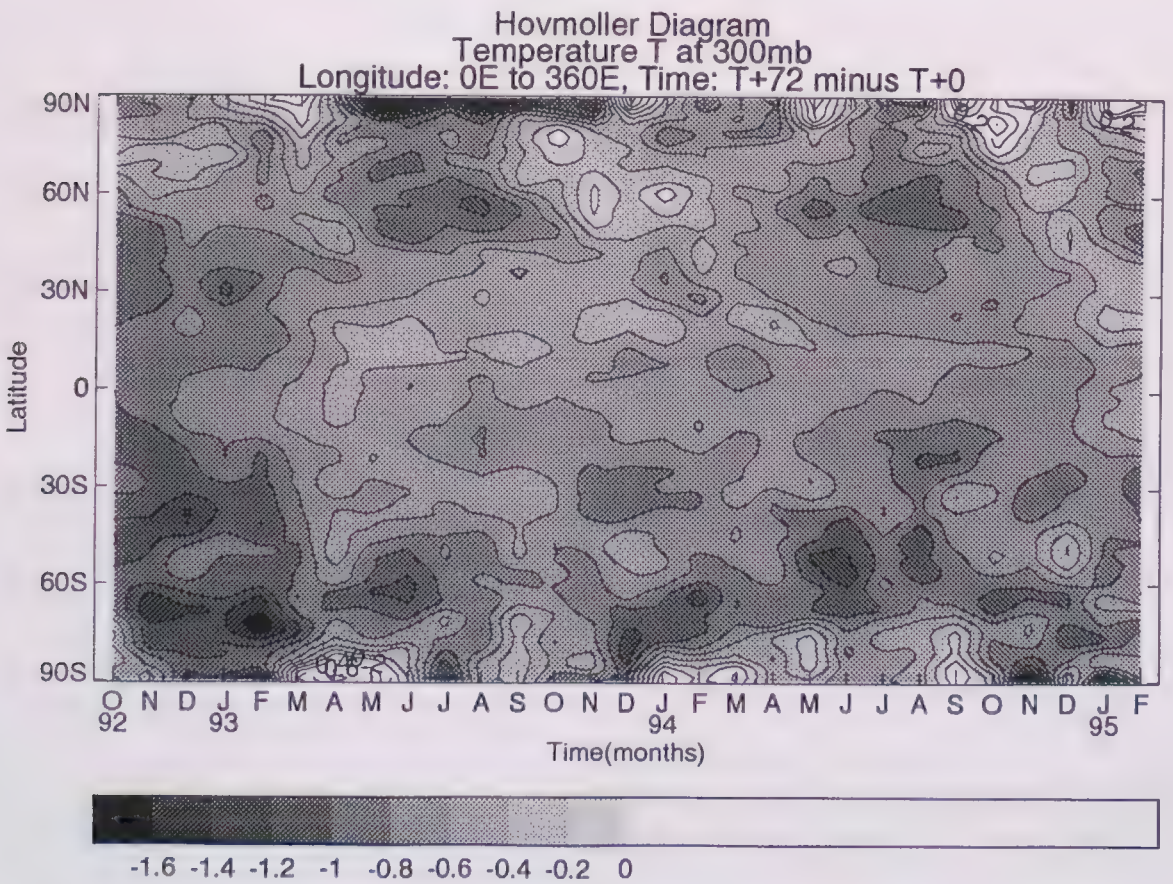

Figure 8C : Time latitude diagram of zonally averaged, monthly averaged T+72 temperature errors from October 1992 to February 1995. a) 850mb, b) 300mb.

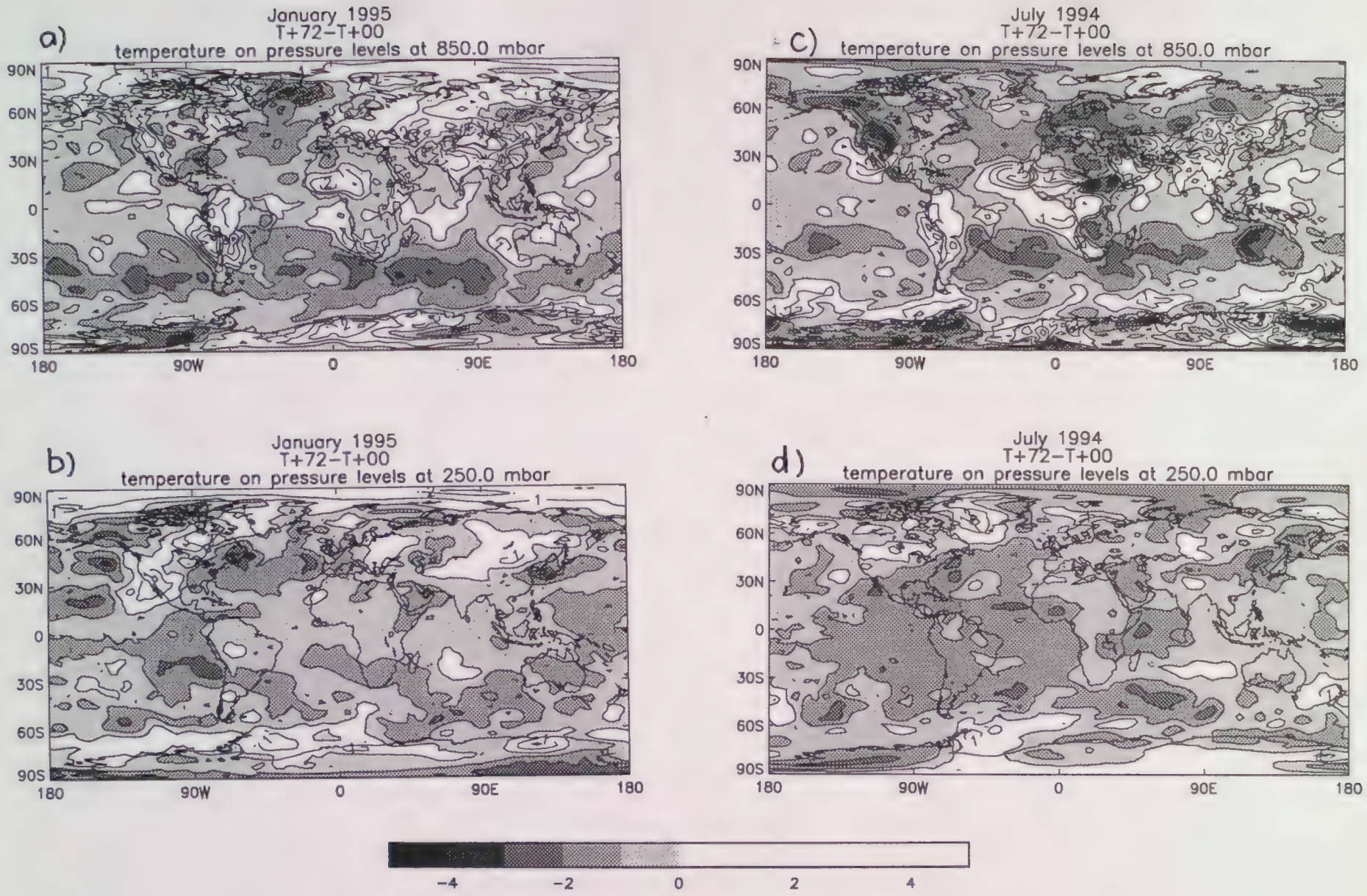

Figure 9 : T+72 mean temperature error a) 850mb for January 1995 ,b) 250mb for January 1995, c) 850mb for July 1994, d) 250mb for July 1994.

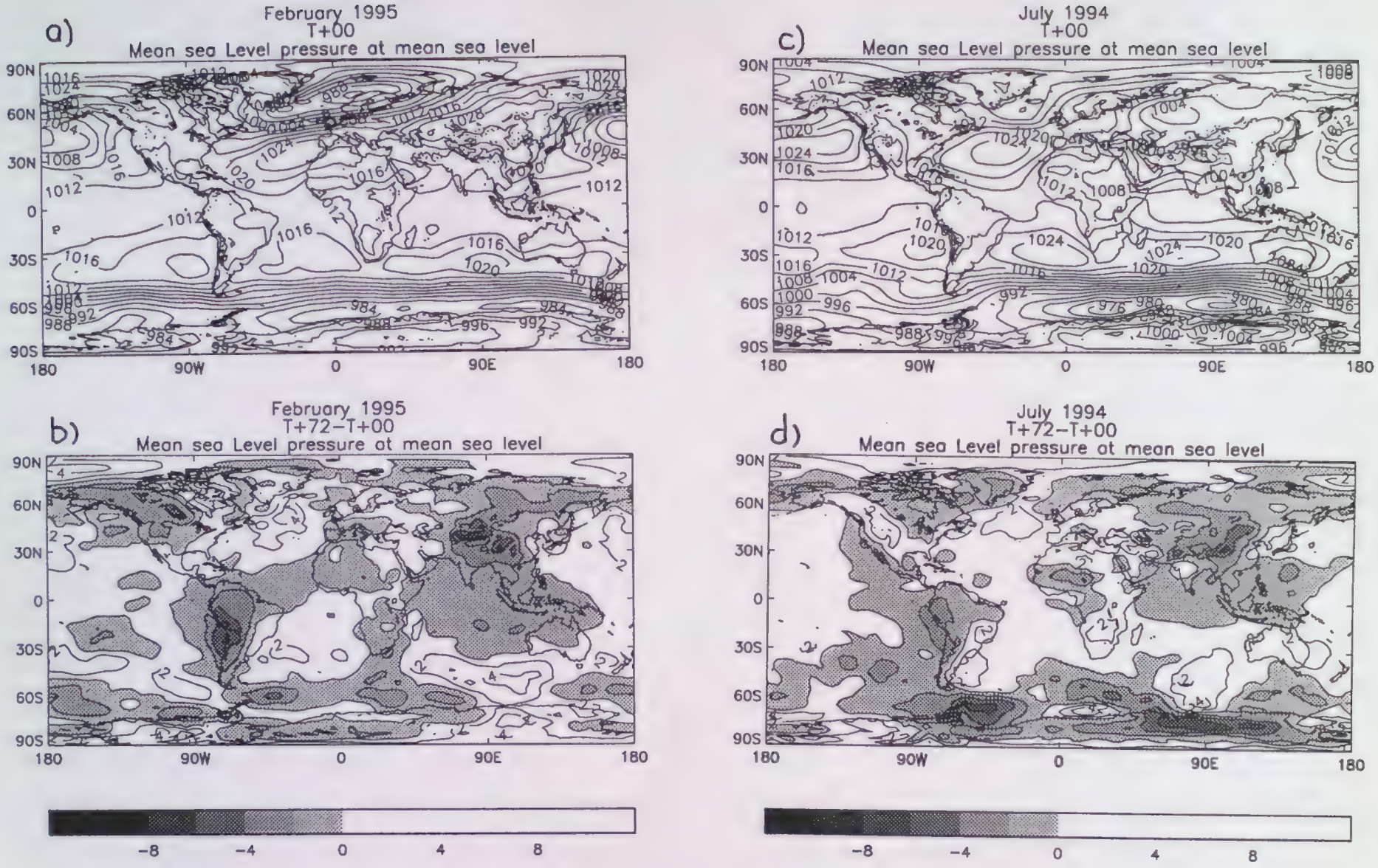

Figure 10: Mean sea level pressure a) Analysed at 00Z for February 1995 b) T+72 mean error for February 1995, c) Analysed at 00Z for July 1994, d) T+72 mean error for July 1994.

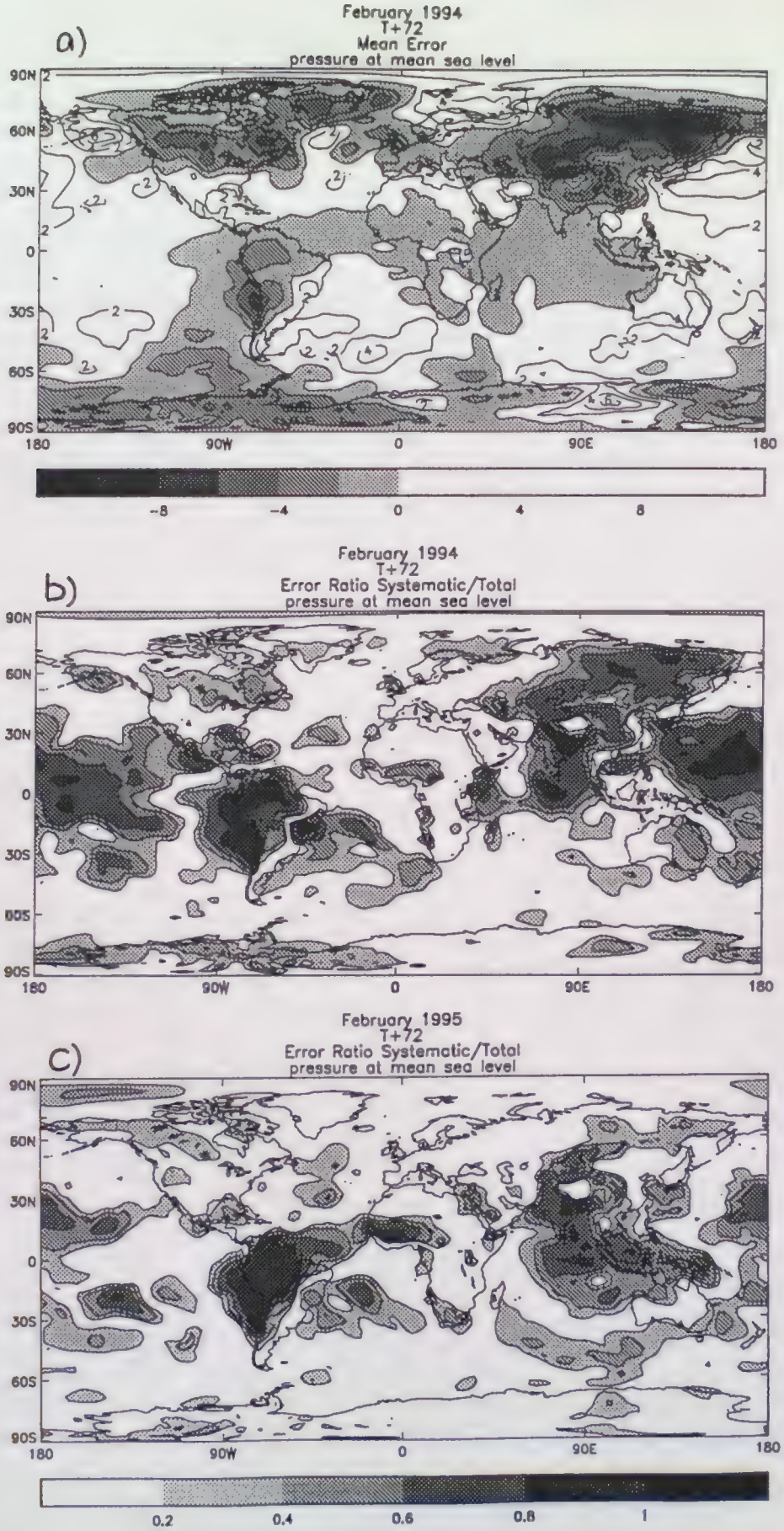

Figure 11: Mean sea level pressure a) T+72 mean error for February 1994, b) Ratio of mean error squared to mean square error (see text for discussion) at T+72 for February 1994, c) as b) but for February 1995.

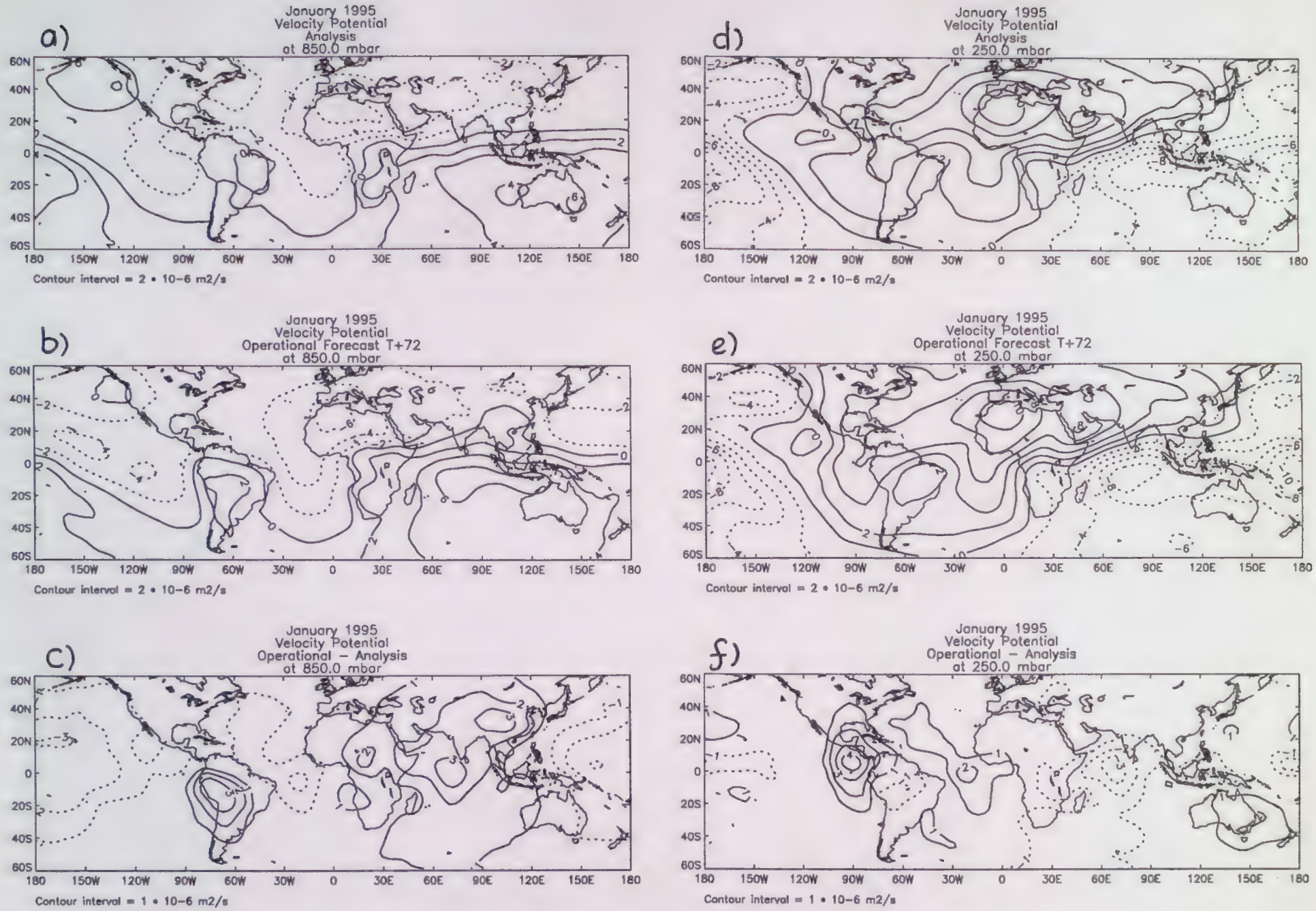

Figure 12 : Velocity potential fields for January 1995 for a) Analysis at 850mb ,b) T+72 forecast at 850mb, c) T+72 error at 850mb, d) Analysis at 250mb ,e) T+72 forecast at 250mb, f) T+72 error at 250mb.

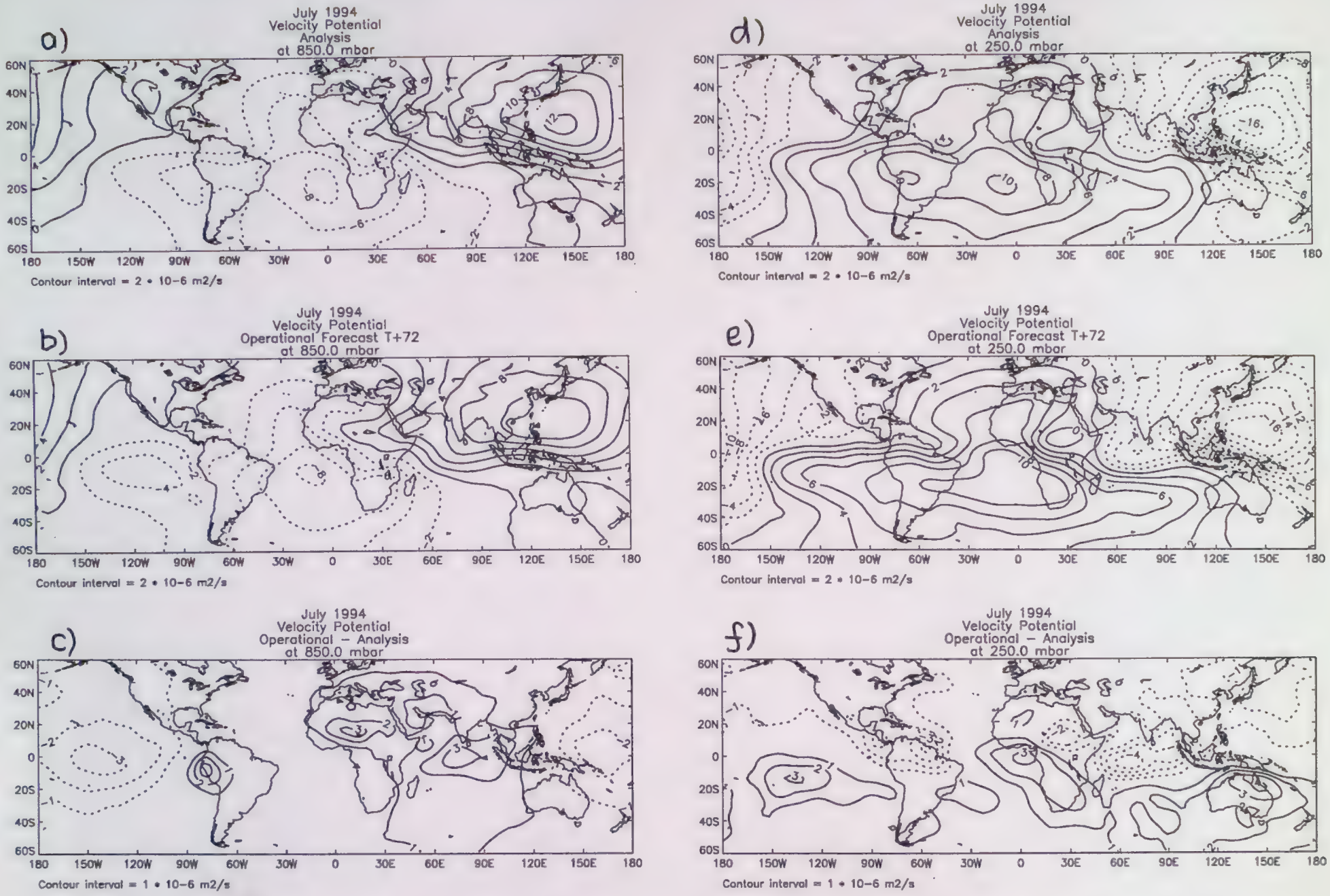

Figure 13 : Velocity potential fields for July 1994 for a) Analysis at 850mb ,b) T+72 forecast at 850mb, c) T+72 error at 850mb, d) Analysis at 250mb ,e) T+72 forecast at 250mb, f) T+72 error at 250mb.

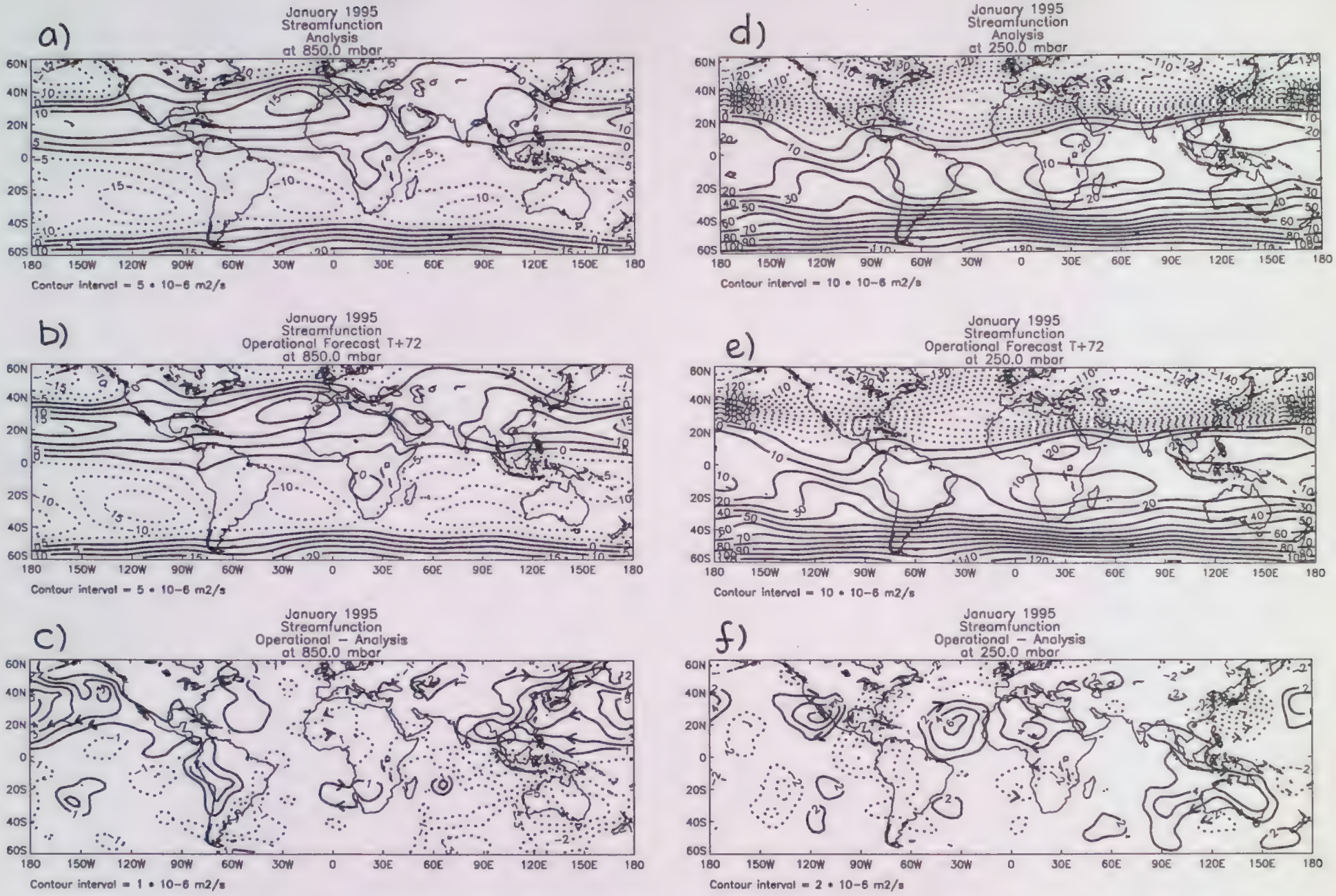

Figure 14 : Streamfunction fields for January 1994 for a) Analysis at 850mb ,b) T+72 forecast at 850mb, c) T+72 error at 850mb, d) Analysis at 250mb ,e) T+72 forecast at 250mb, f) T+72 error at 250mb.

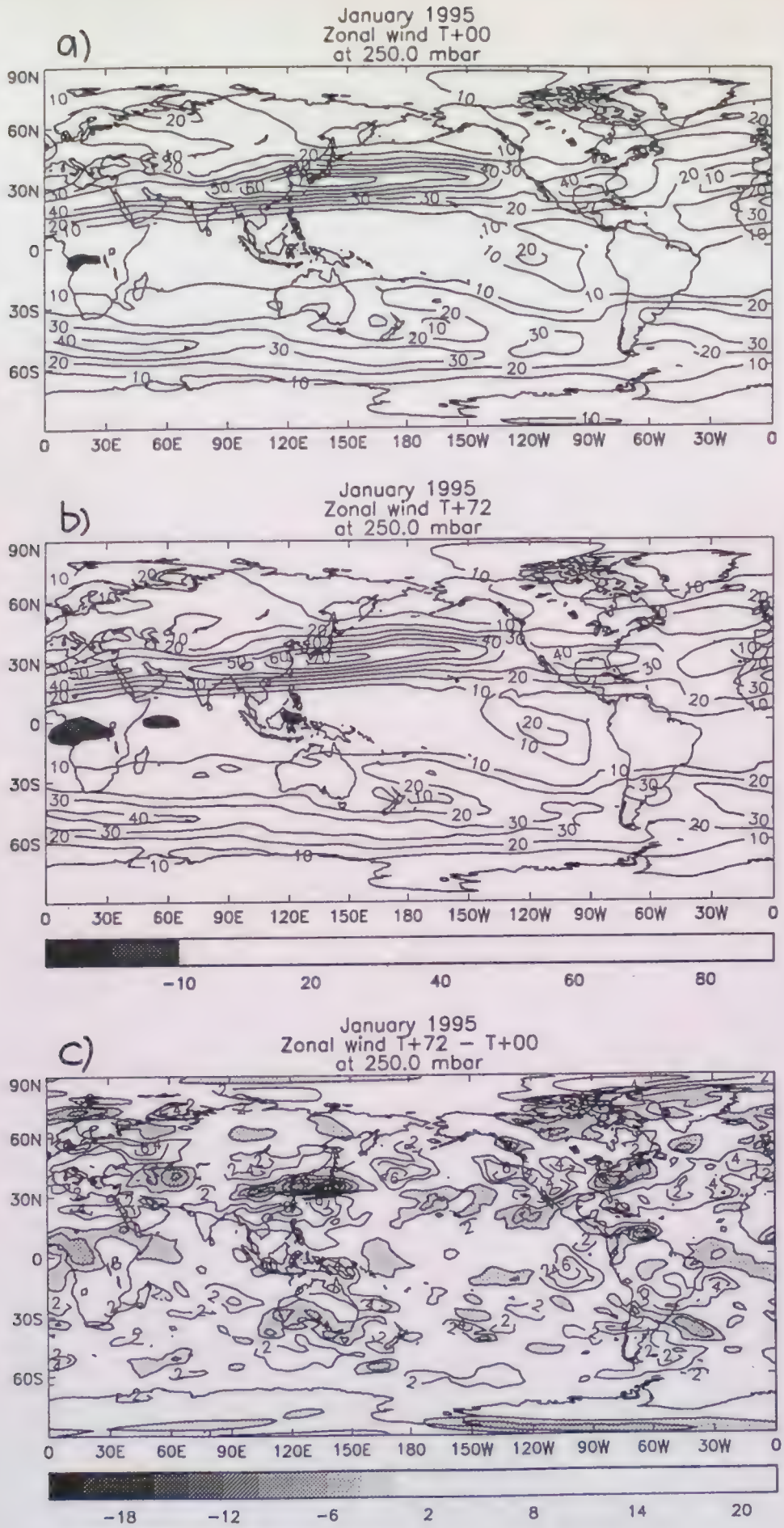

Figure 15: Zonal wind at 250hPa for January 1995 a) Analysis at 00Z, b) T+72 forecast, c) T+72 mean error.

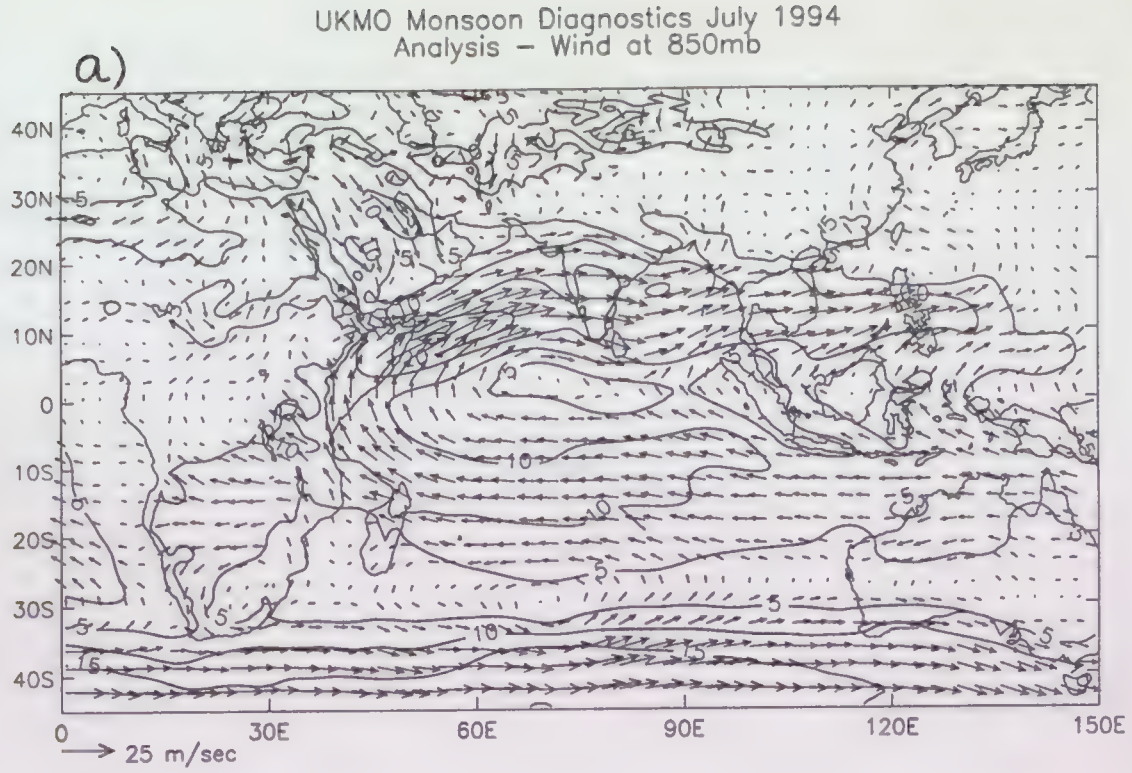

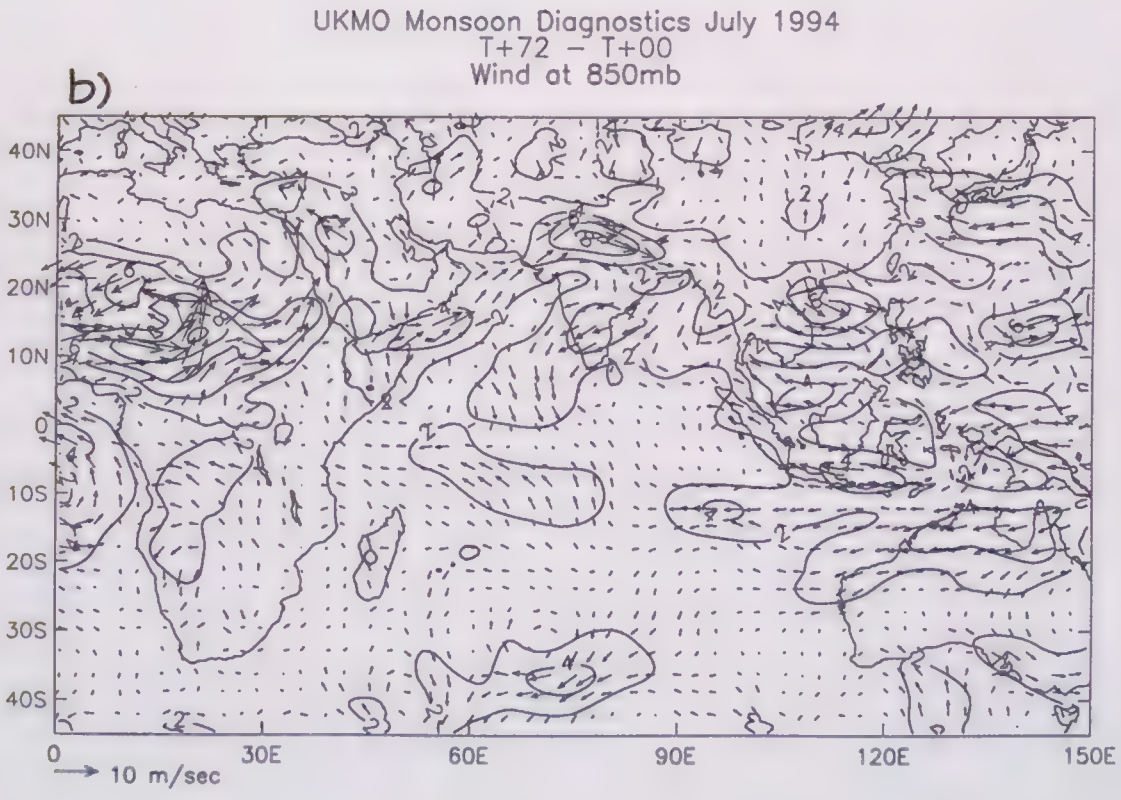

Figure 16: 850hPa wind over the Monsoon region during July 1994. a) Analysis, b) T+72 wind error.

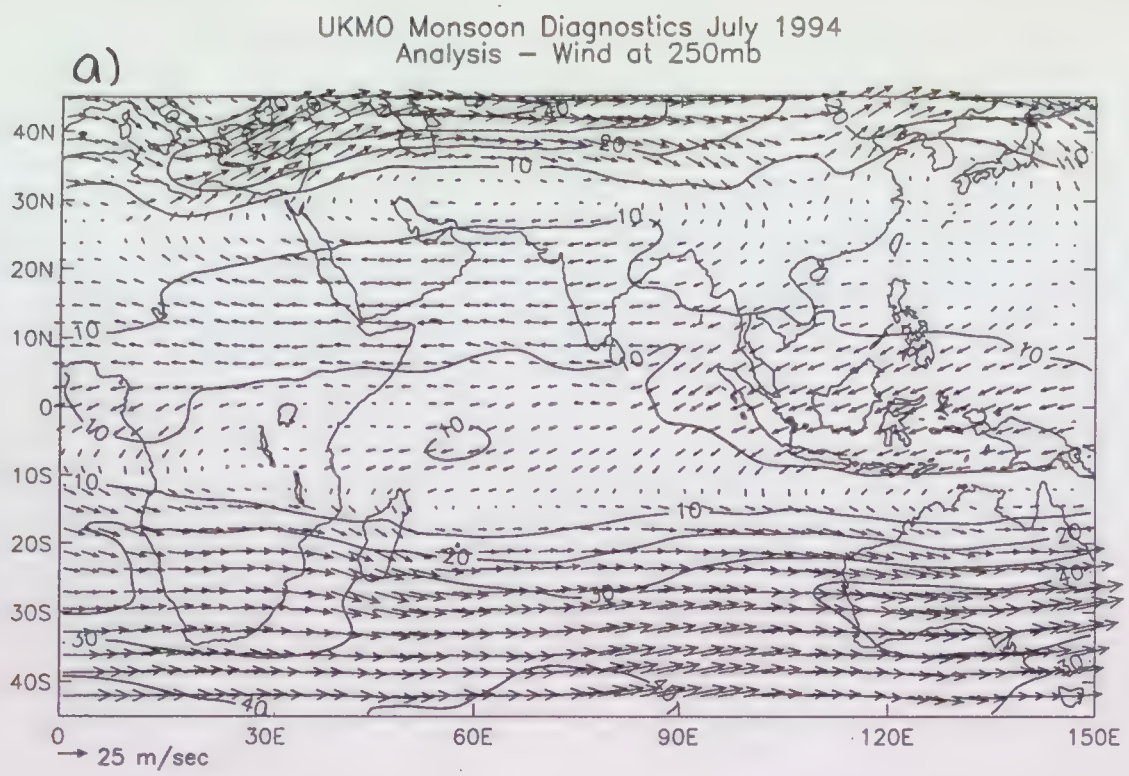

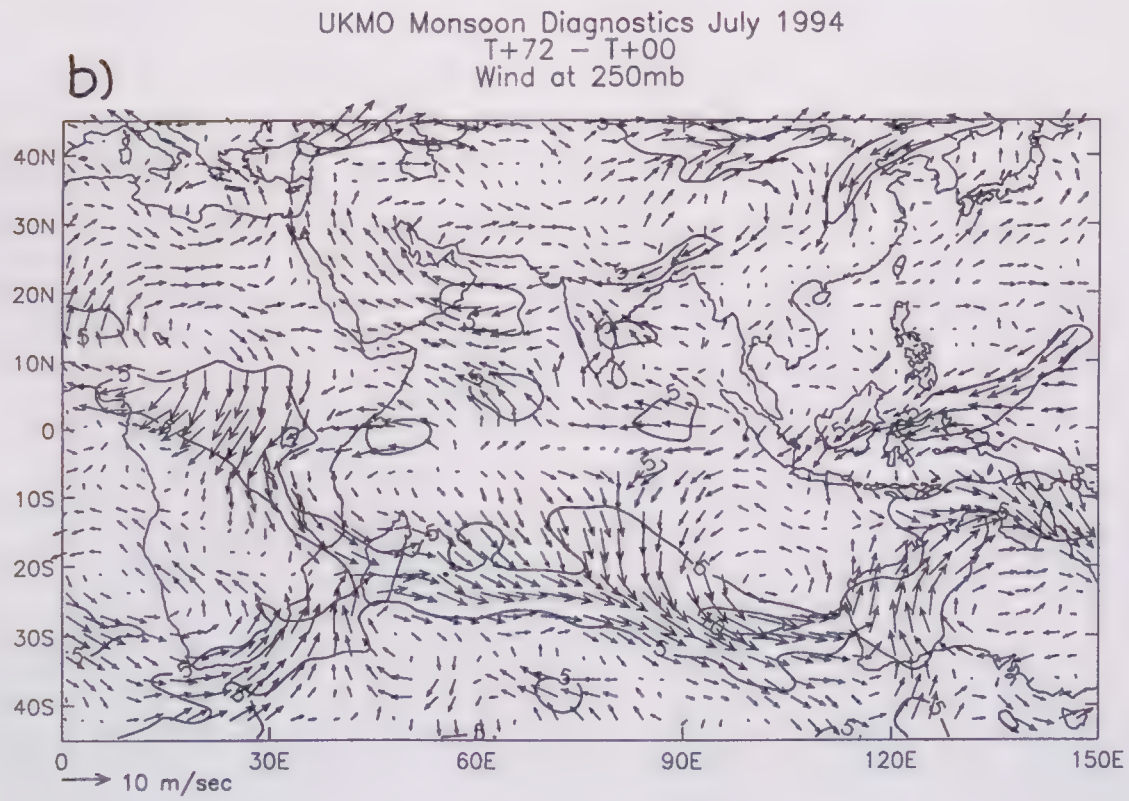

Figure 17: 250hPa wind over the Monsoon region during July 1994. a) Analysis, b) T+72 wind error.

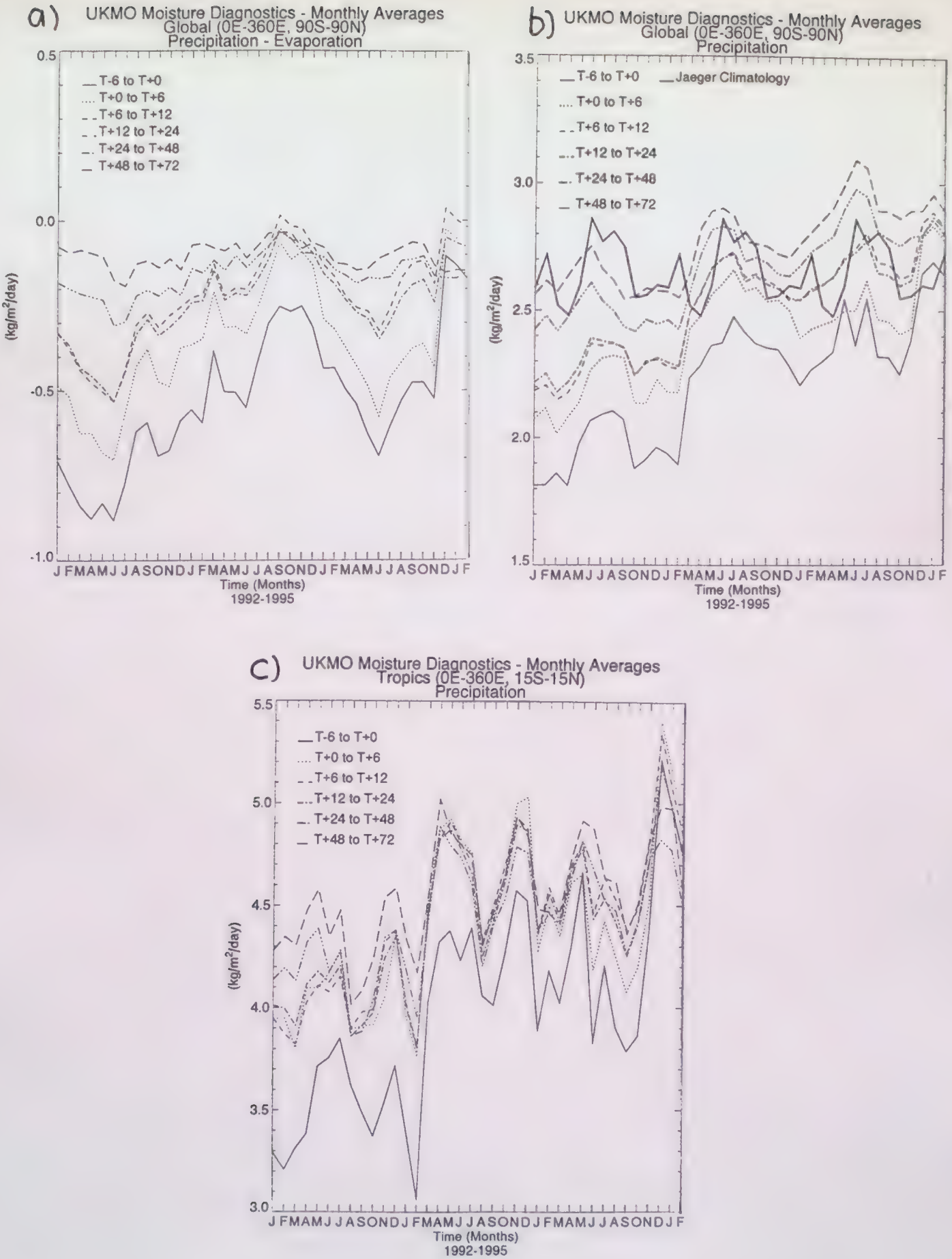

Figure 18: Time series (June 1991- Feb 1995) of monthly mean a) Precipitation -evaporation b) Global average precipitation. c) Tropical precipitation (15N-15S).

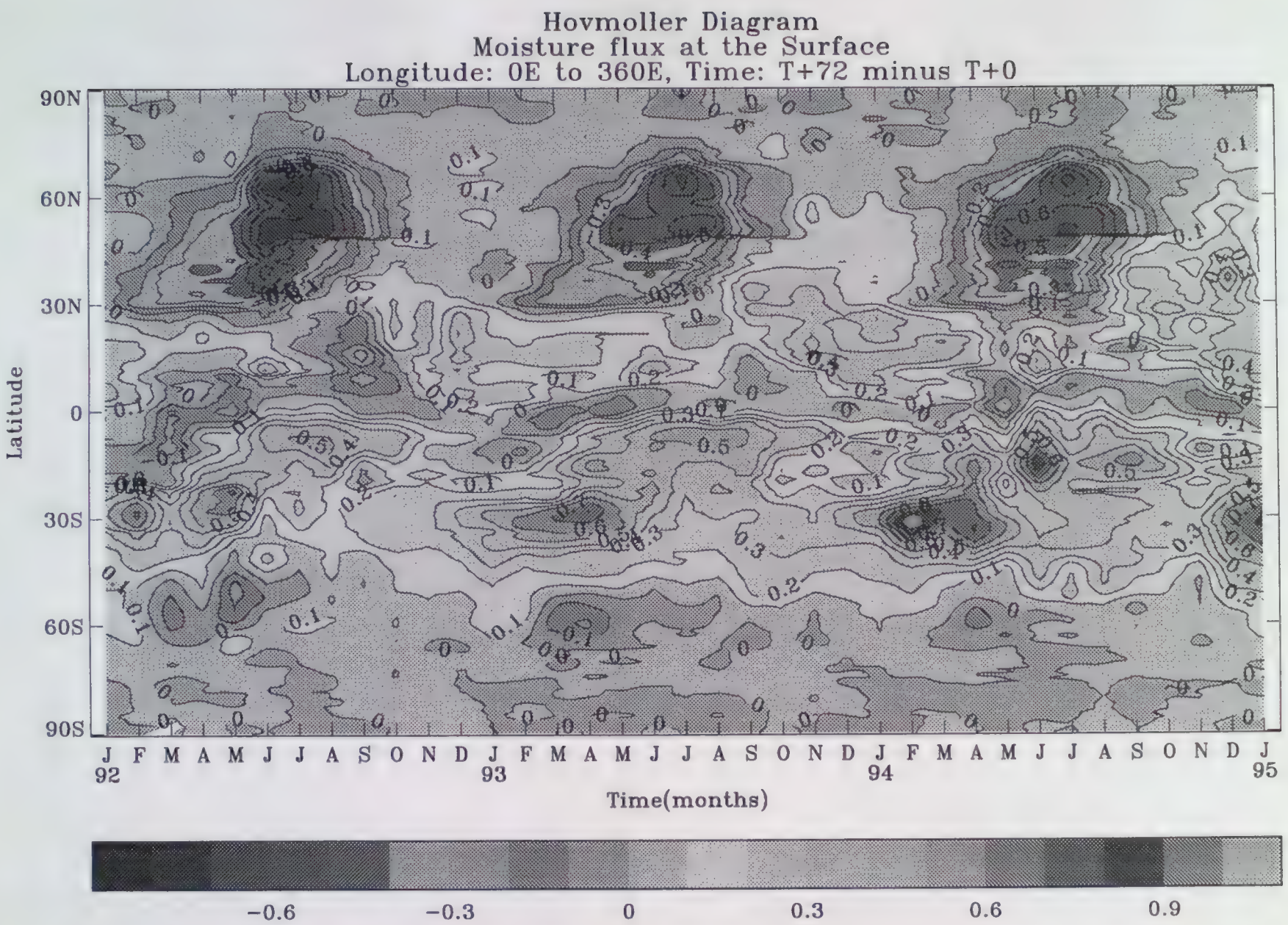

Figure 19: Time latitude diagram of zonally averaged change in surface evaporation between T+00 and T+72. Monthly means from June 1991 to February 1995.

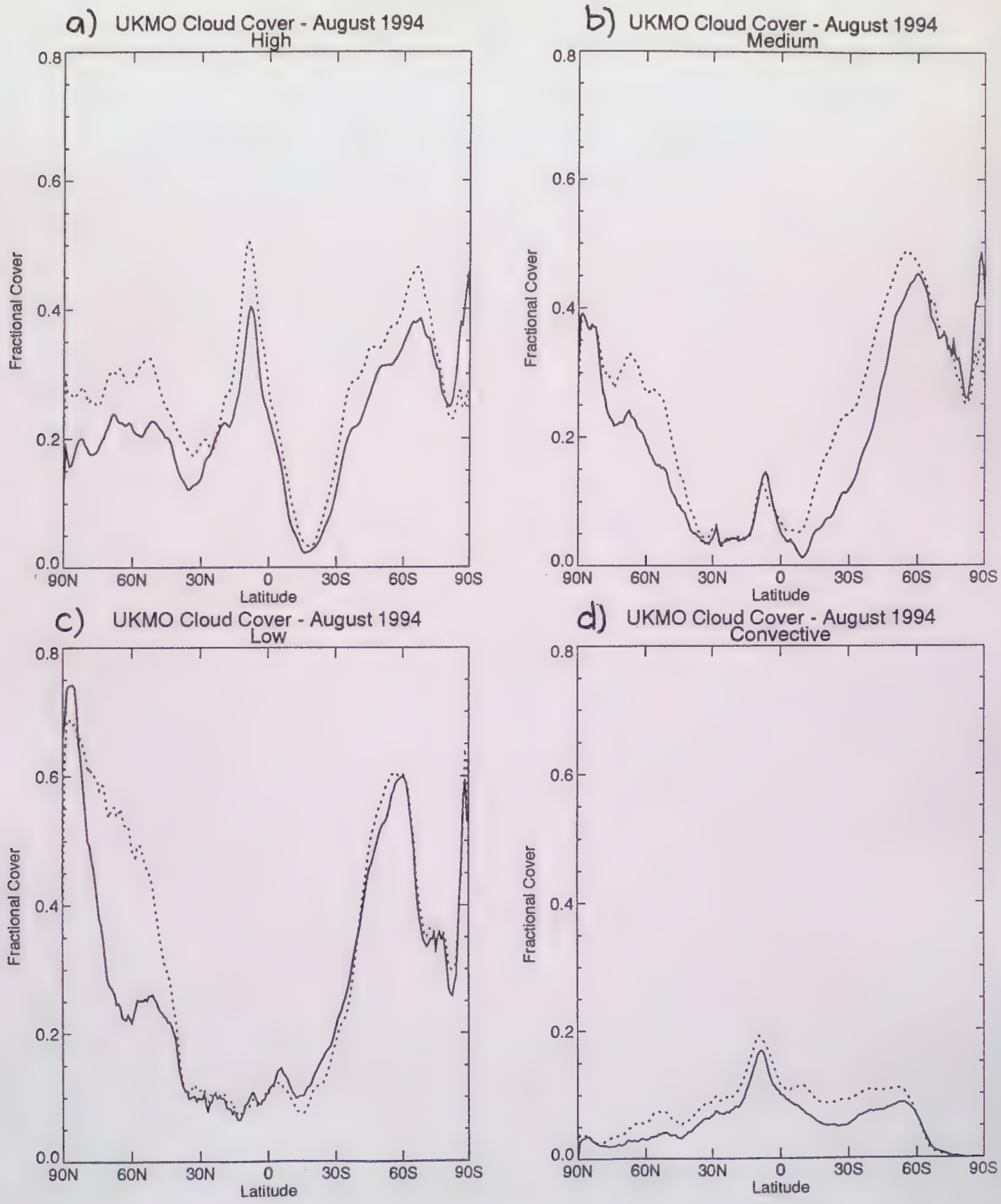

Figure 20: Monthly mean cloud amounts at T+00 (solid) and T+72 (dashed) for August 1994. a) High cloud, b) Medium cloud, c) Low cloud d) Convective cloud.

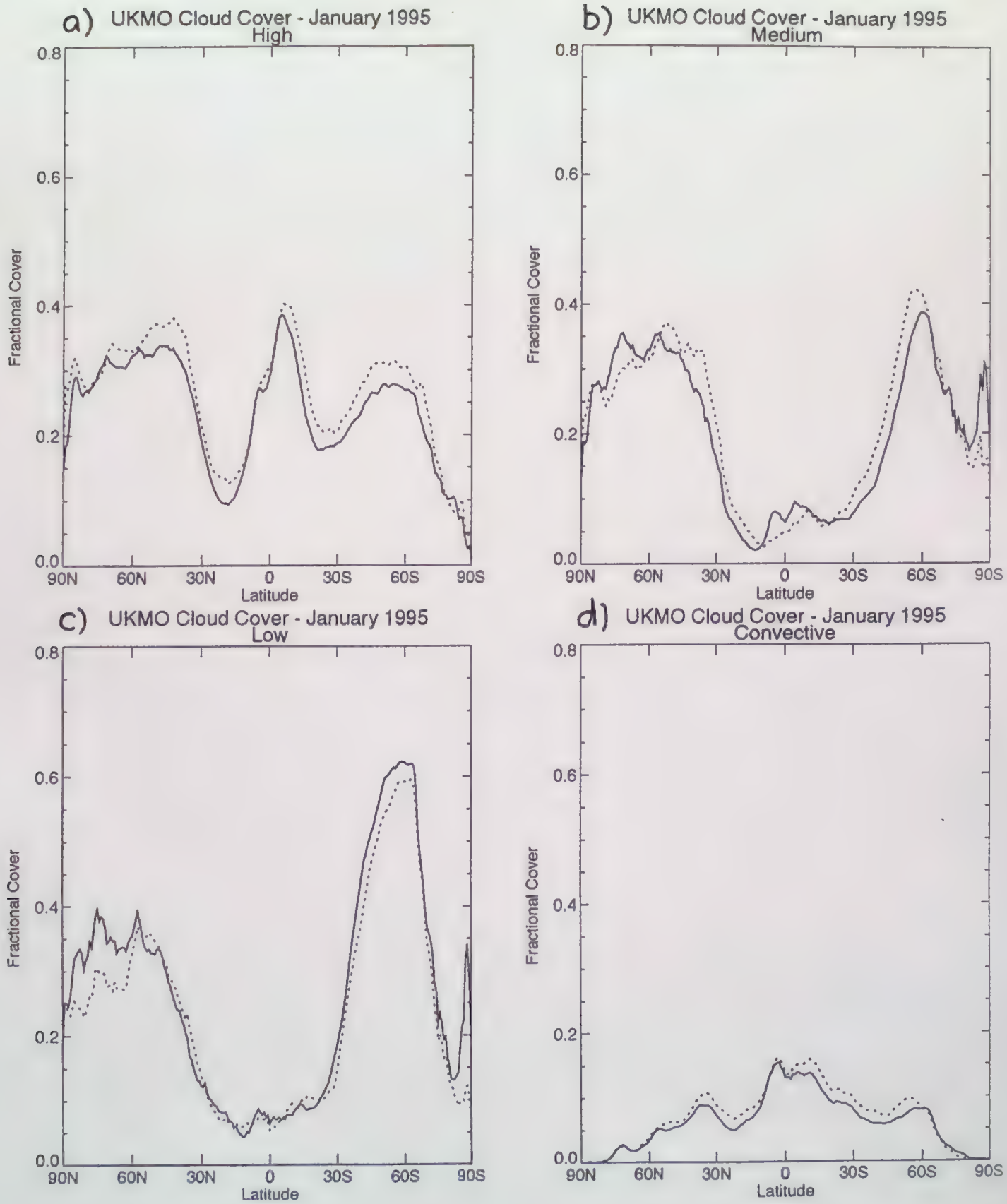

Figure 21: As figure 20 but for January 1995.

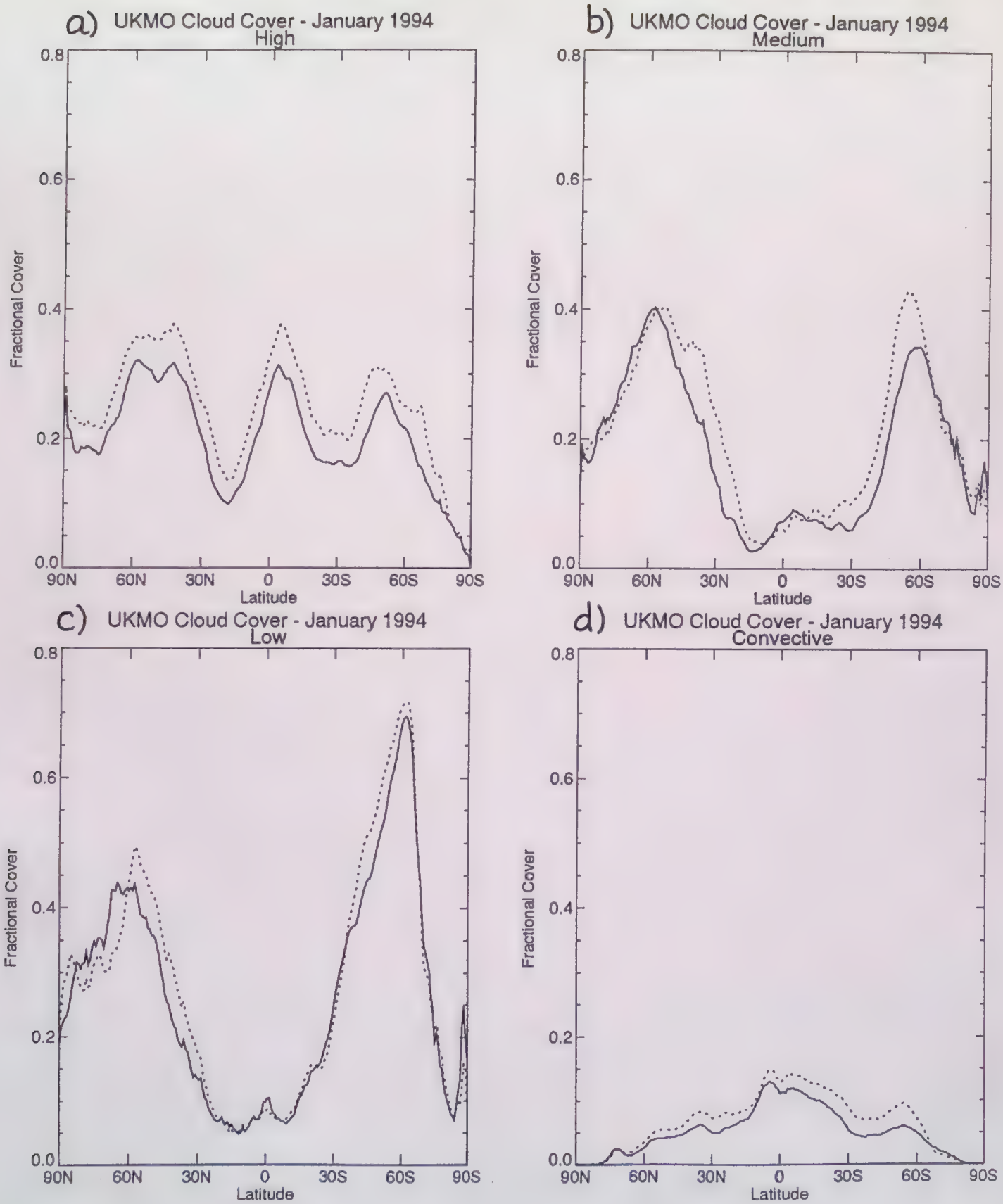

Figure 22: As figure 20 but for January 1994.

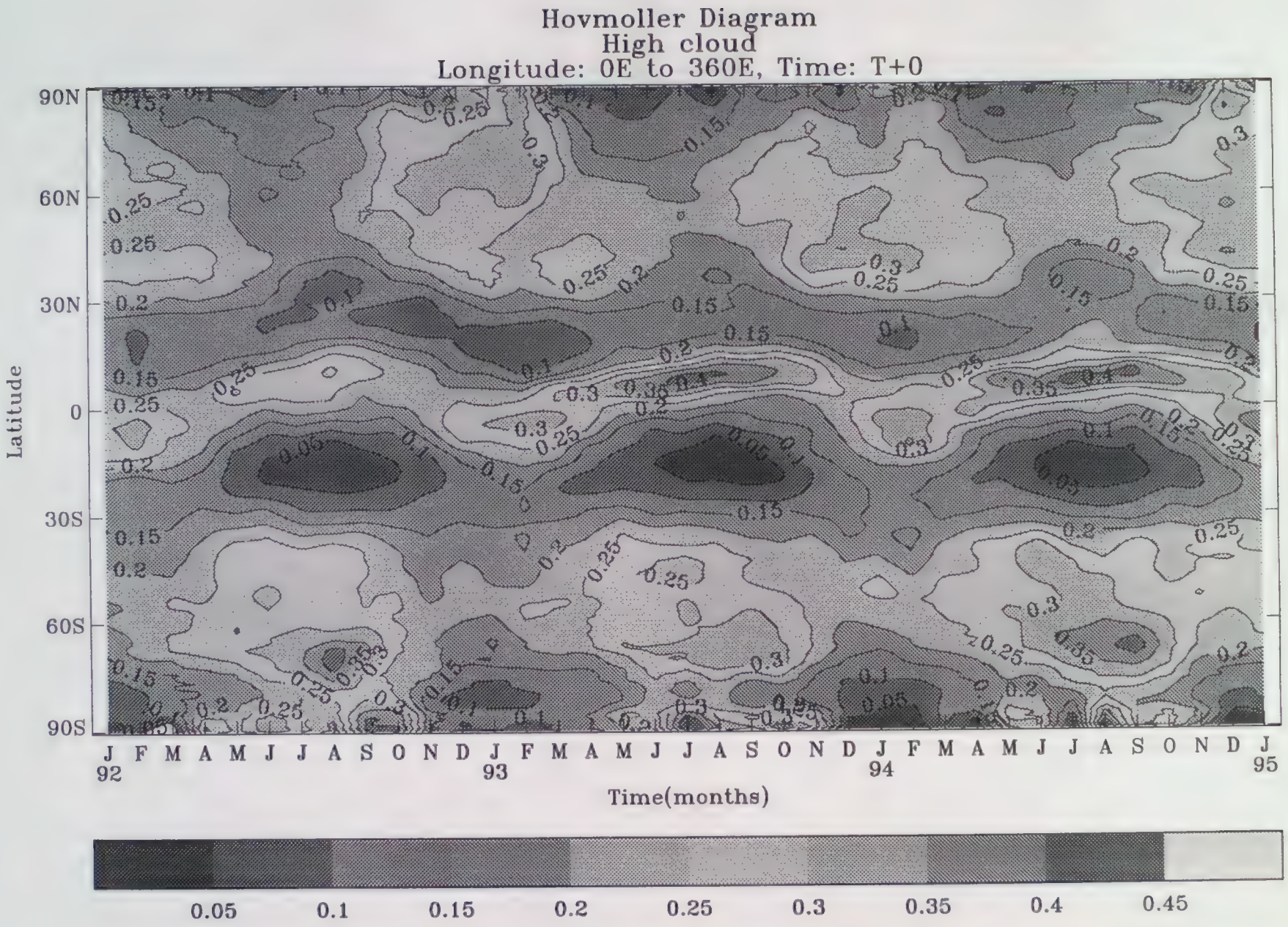

Figure 23: Time latitude diagram of zonally averaged high cloud amounts at T+00. Monthly means from June 1991 to February 1995.

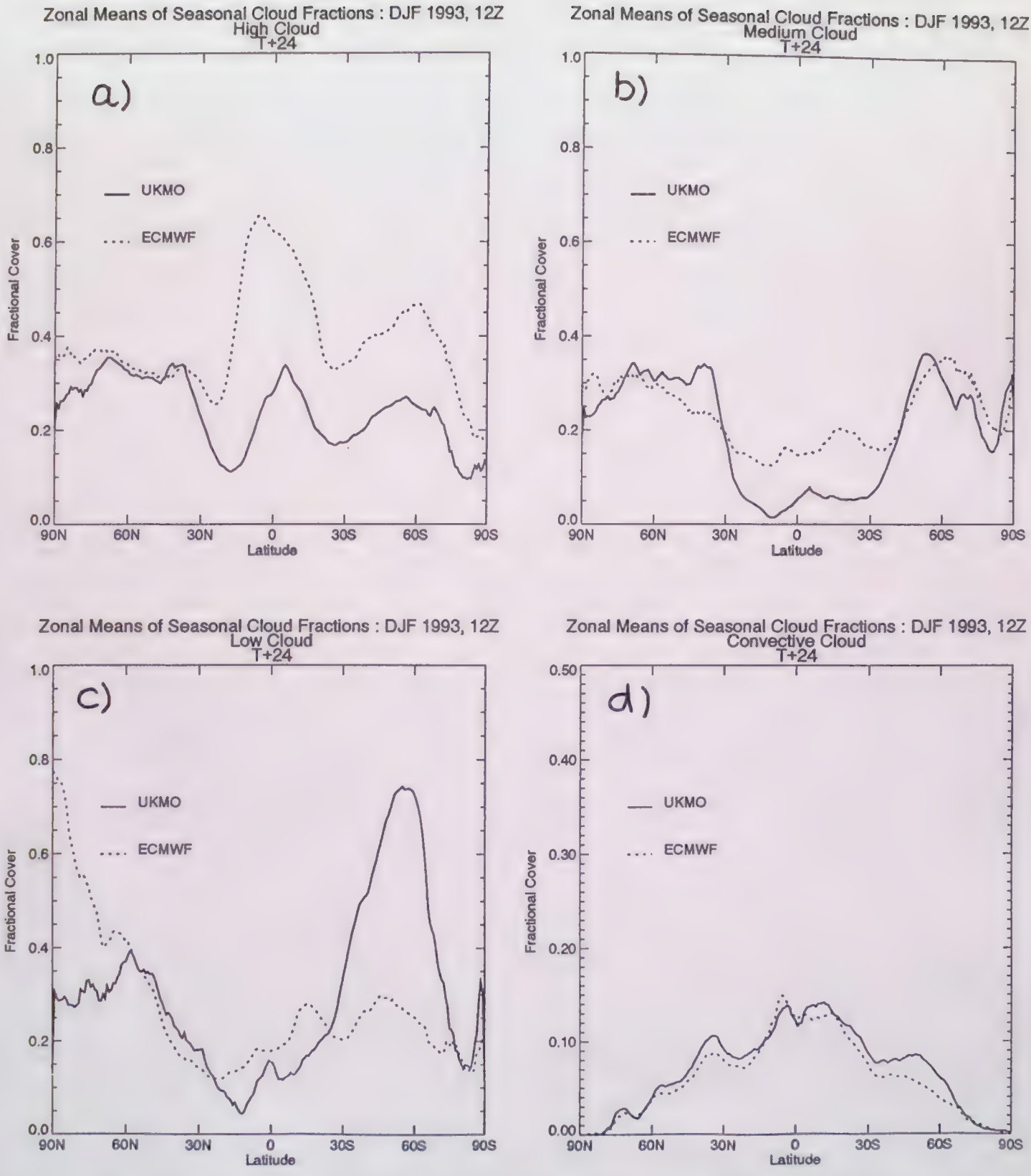

Figure 24: Monthly mean cloud amounts at T+24 for the Unified Model (solid) and ECMWF (dashed) for December,January, and February 1992/93. a) High cloud, b) Medium cloud, c) Low cloud d) Convective cloud.

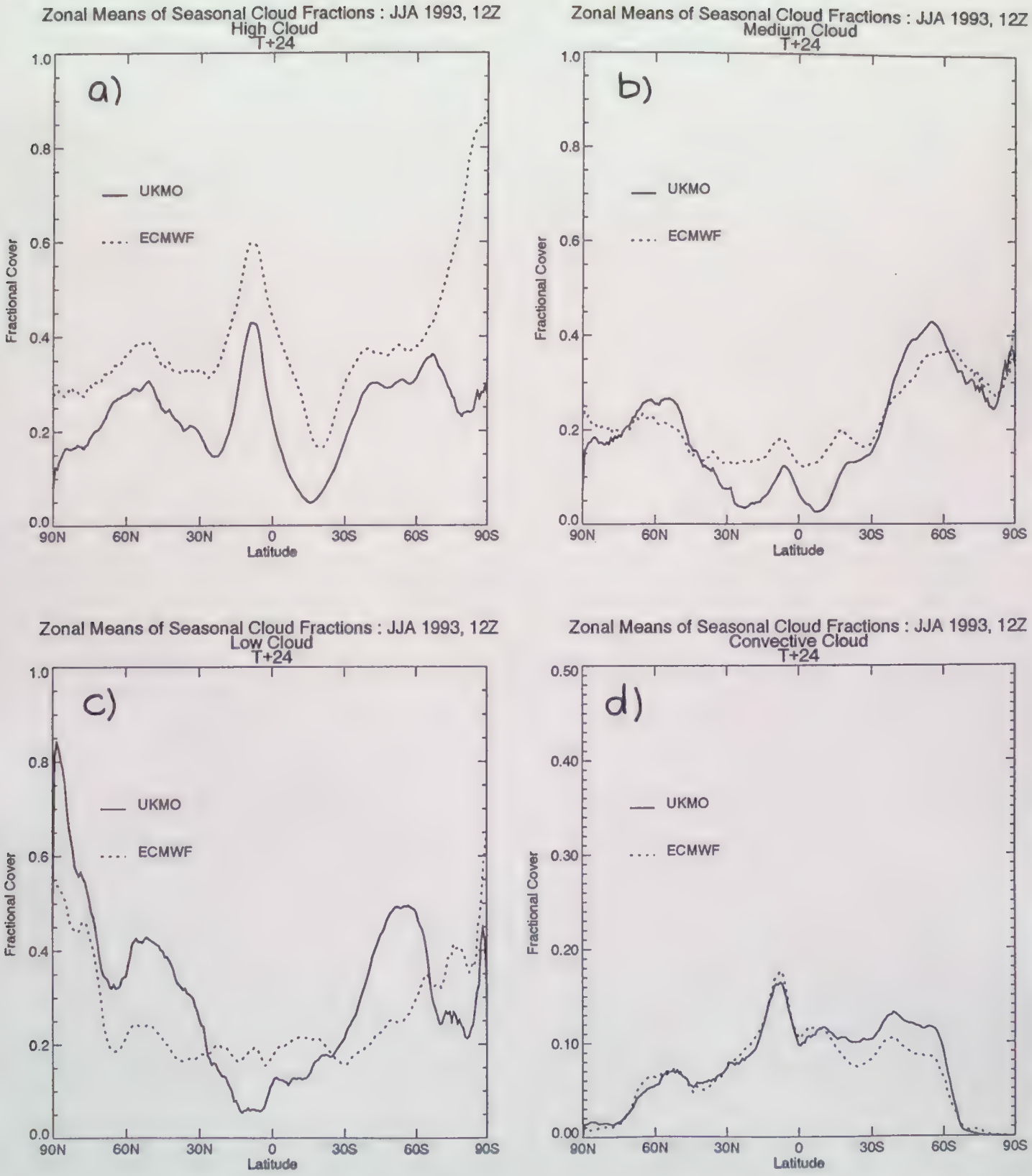

Figure 25: As figure 24 but for June,July, and August 1993.

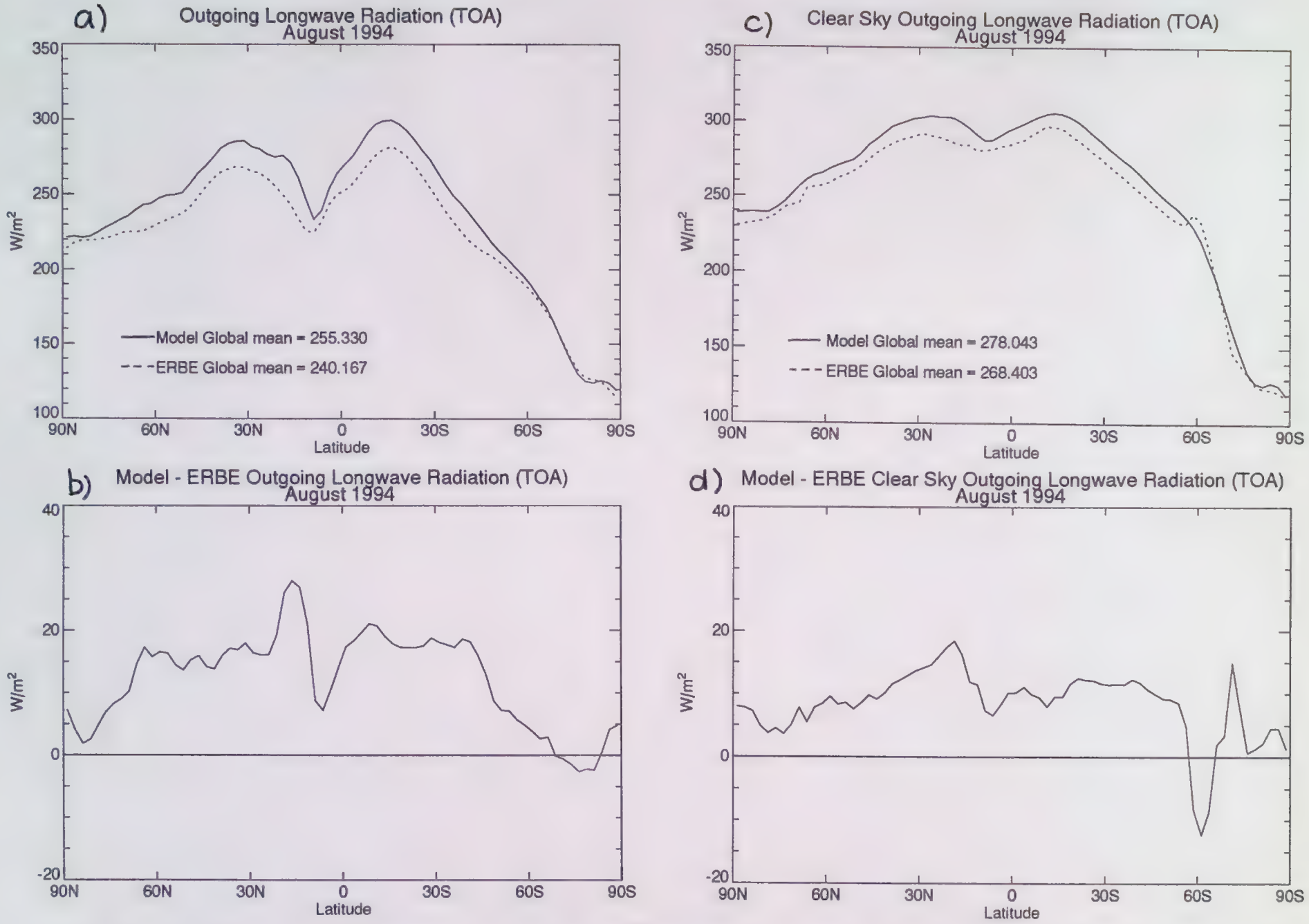

Figure 26: a) Outgoing longwave radiation (OLR) for UM (solid) during August 1994 and ERBE (dashed) during August 1988, b) UM-ERBE for OLR, c) as a) and d) as b) but for clear sky OLR.

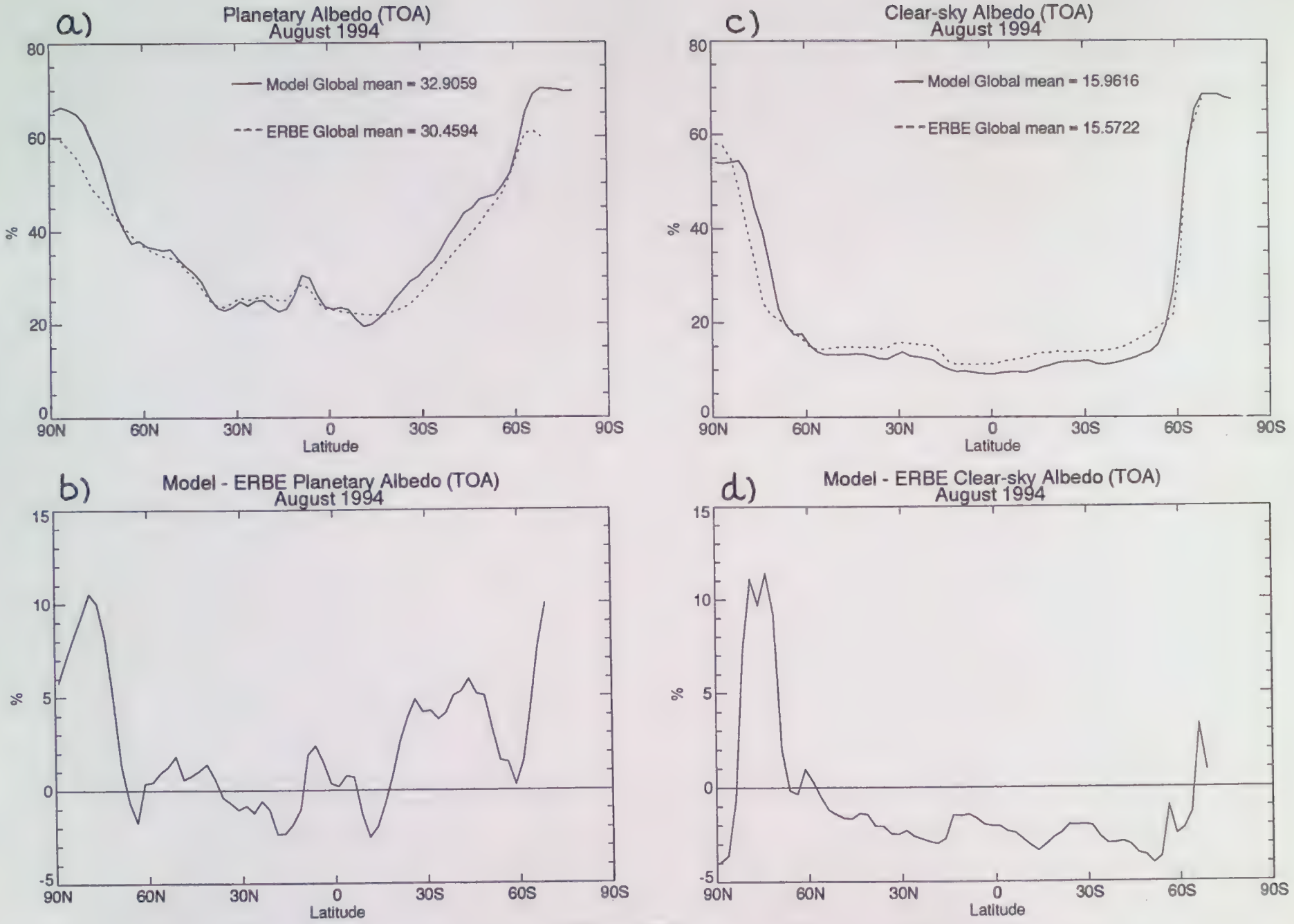

Figure 27: a) Planetary albedo (TOA) for UM (solid) during August 1994 and ERBE (dashed) during August 1988, b) UM-ERBE for planetary albedo, c) as a) and d) as b) but for clear sky albedo.

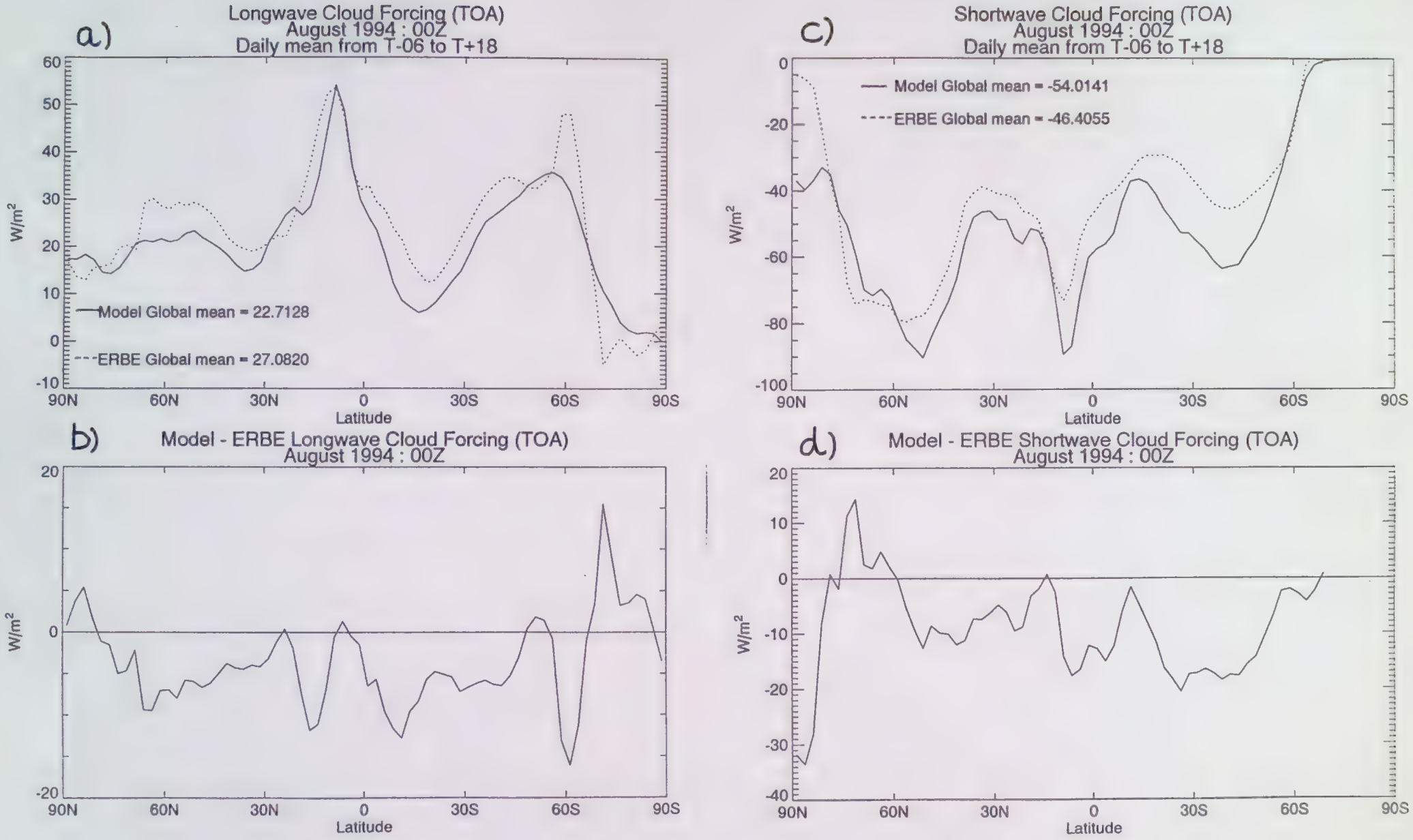

Figure 28: a) LW cloud forcing (TOA) for UM (solid) during August 1994 and ERBE (dashed) during August 1988, b) UM-ERBE for LW cloud forcing, c) as a) and d) as b) but for SW cloud forcing.

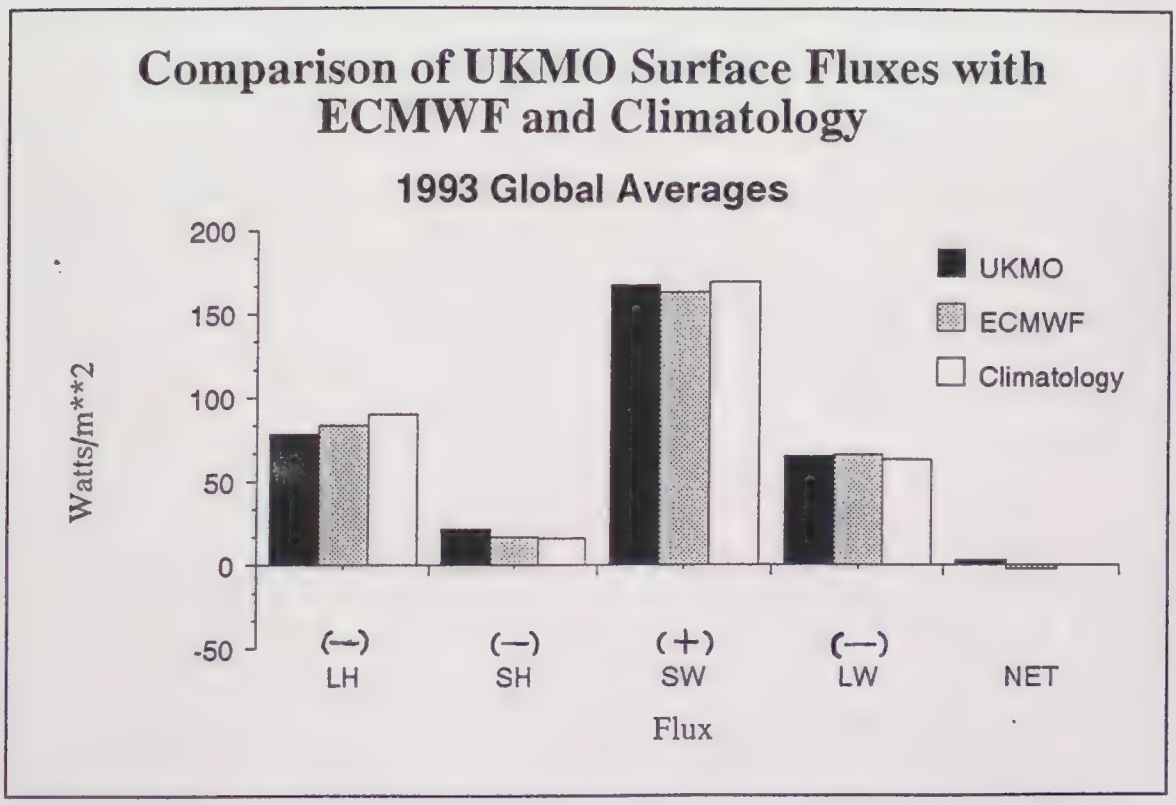

Figure 29: Annually and globally averaged surface fluxes for 1993 for Unified Model (UKMO), ECMWF, and climatological estimates from Ramanathan et al. (1989).

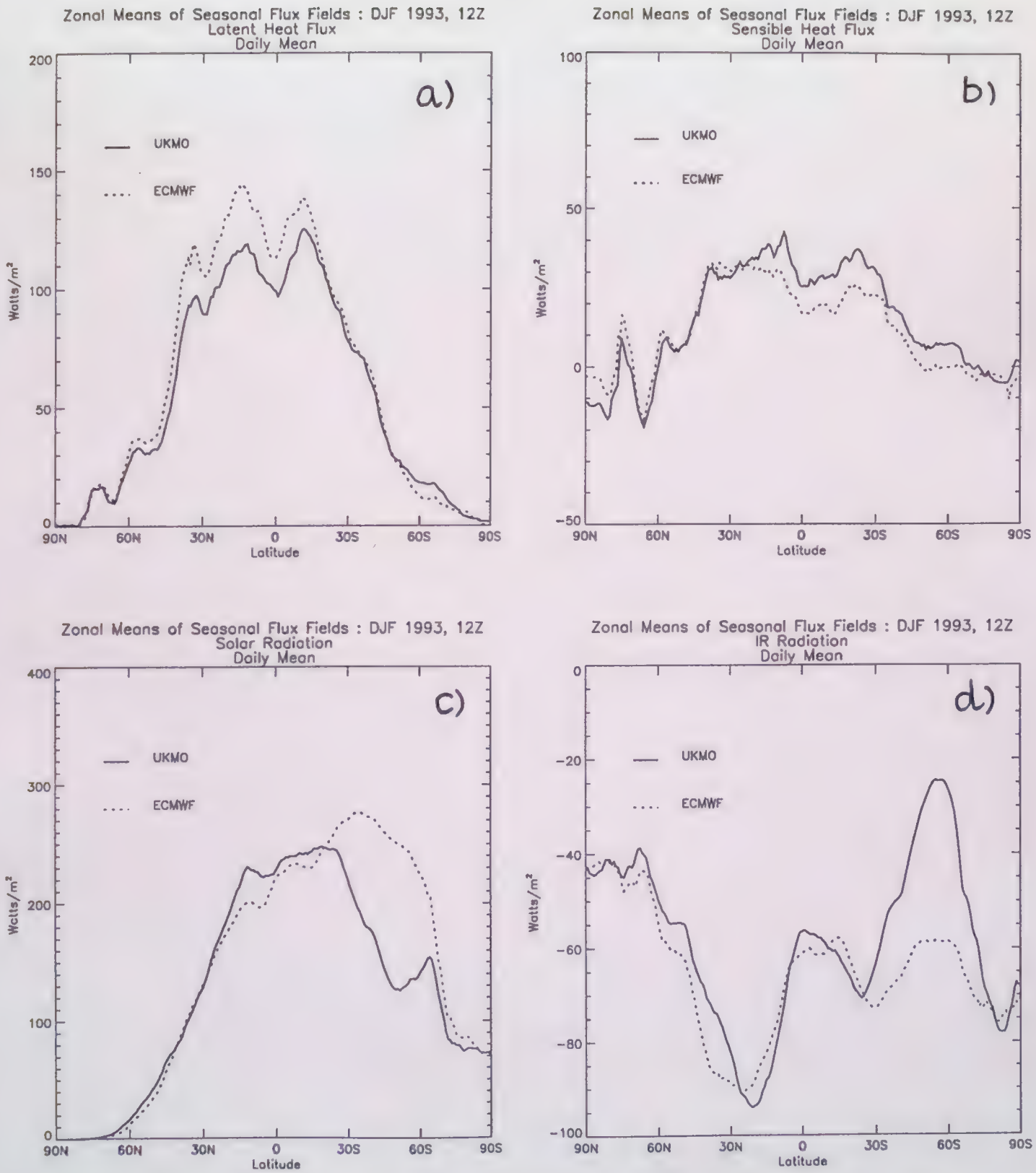

Figure 30: Zonally averaged surface fluxes for Decemeber, January and February 1992/93 for Unified Model (solid) and ECMWF(dashed). a) Latent heat, b) sensible heat, c) Net SW radiation at surface d) Net LW radiation at surface. Upward fluxes are positive for turbulent fluxes but negative for the radiative fluxes.

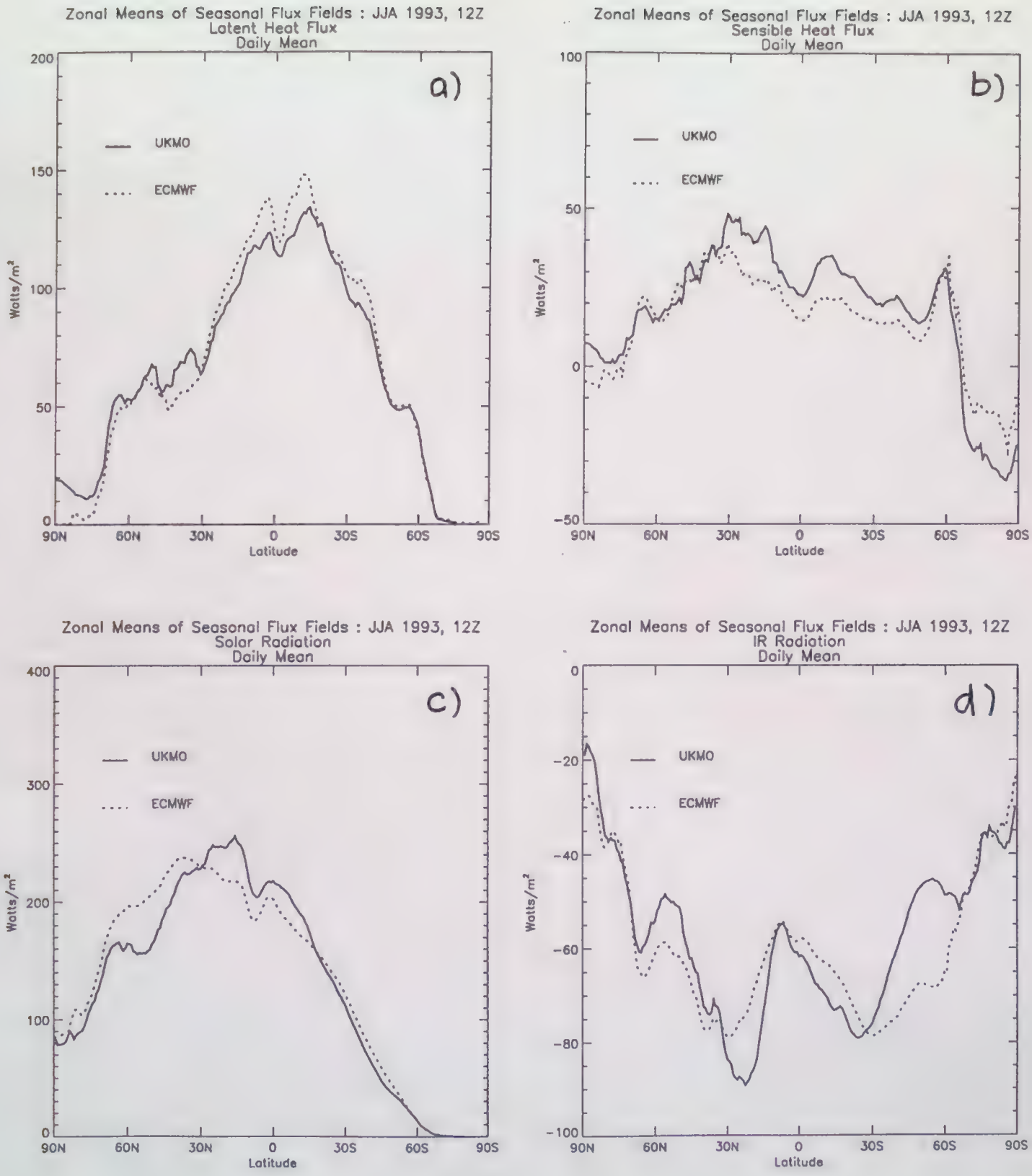

Figure 31: As Figure 30 but for June,July and August 1993.

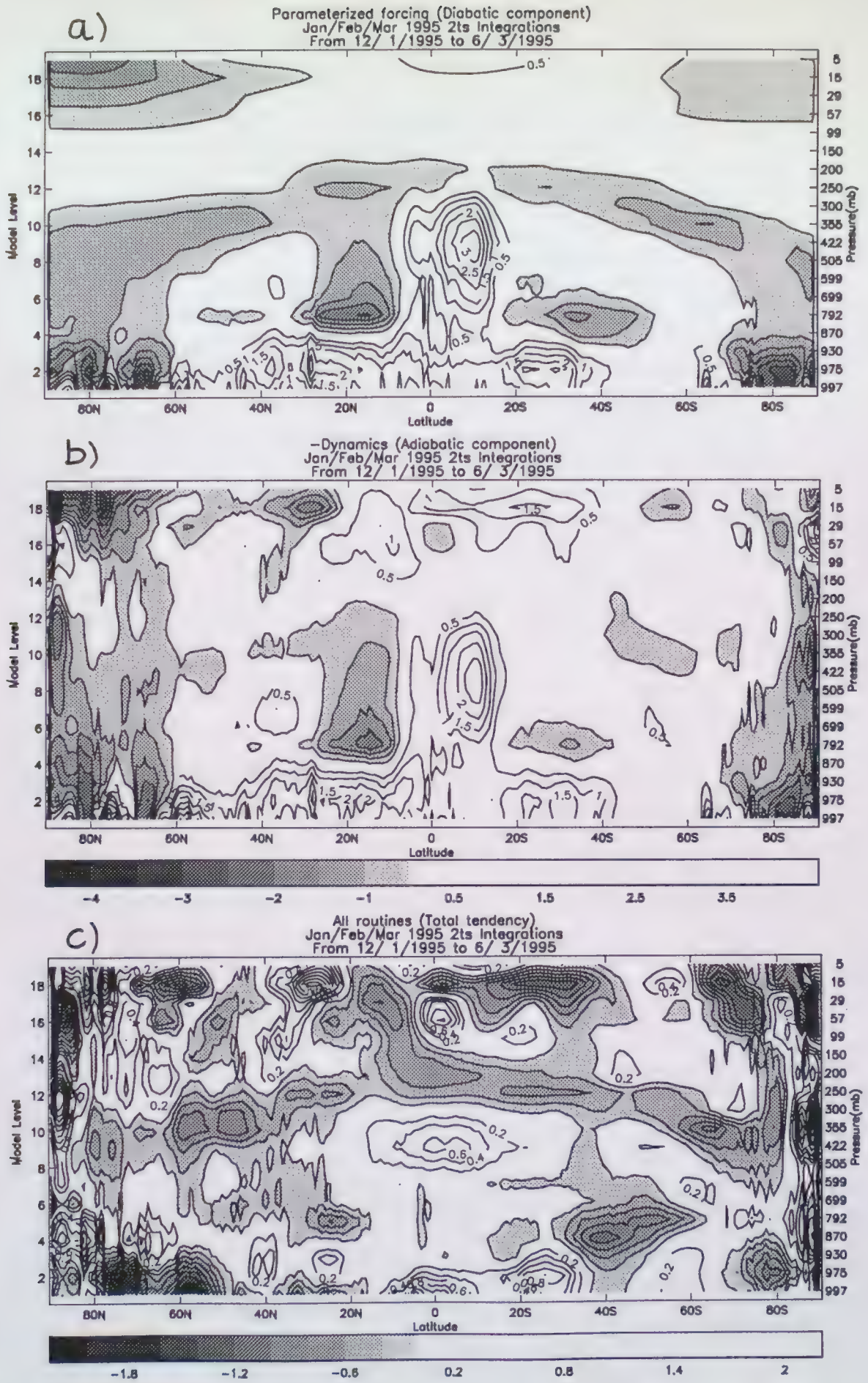

Figure 32: Monthly mean and zonally averaged thermal balance in the Unified Model for January/February/March1995. a) Parametrized heating rates (K/day) - Diabatic component, b) Dynamical heating rates (adiabatic component) with sign reversed, c) Total (residual) tendency = Parametrizations + Dynamics. Zero contour omitted and negative values shaded.

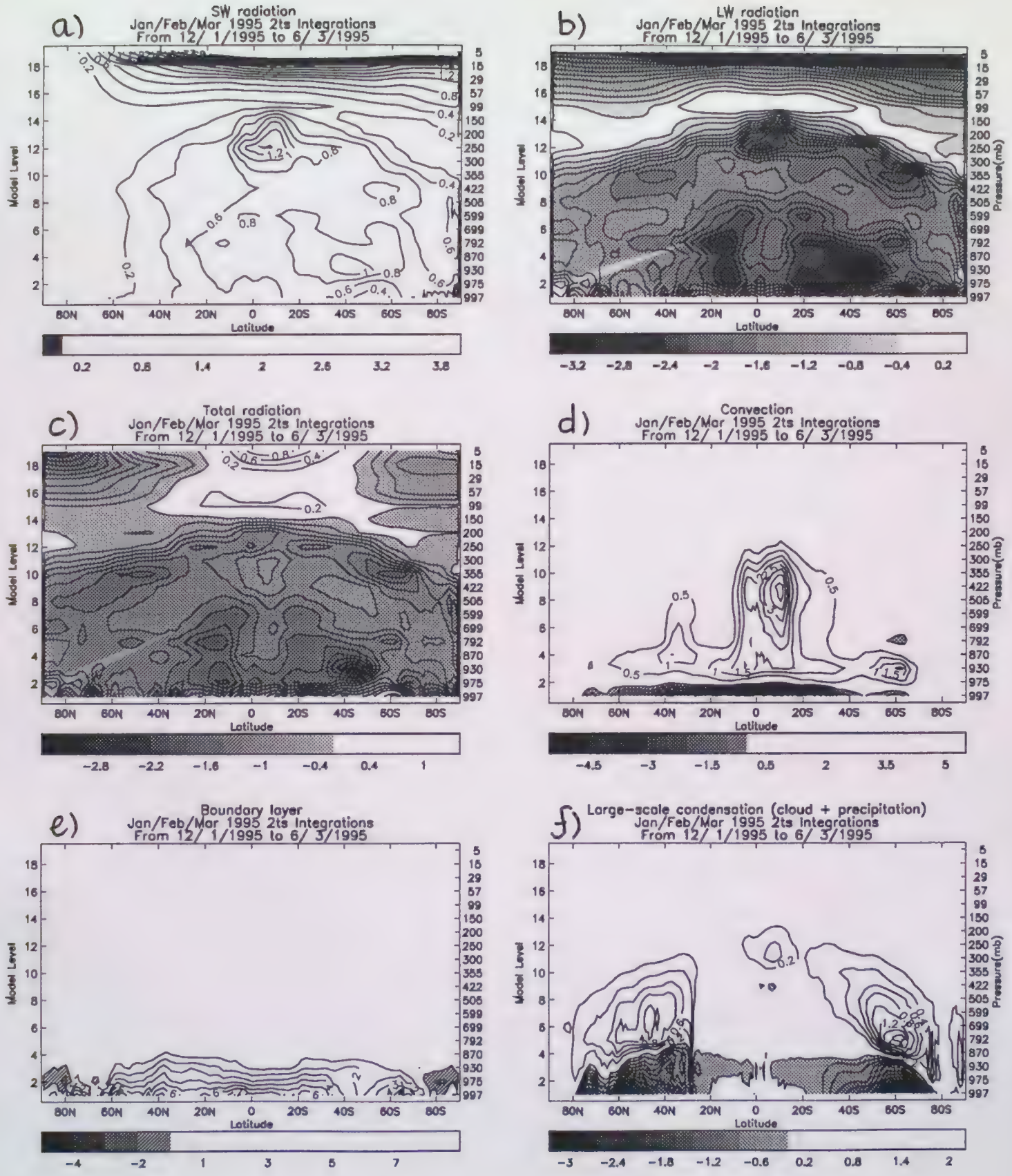

Figure 33: Contributions to monthly mean thermal balance for January/February/March 1995 from the individual parametrized terms a) SW radiation, b) LW radiation, c) Total radiation, d) Convection, e) Boundary layer turbulent mixing, f) Large scale condensation (Clouds and precipitation). Units are K/day. Zero contour omitted and negative values shaded.

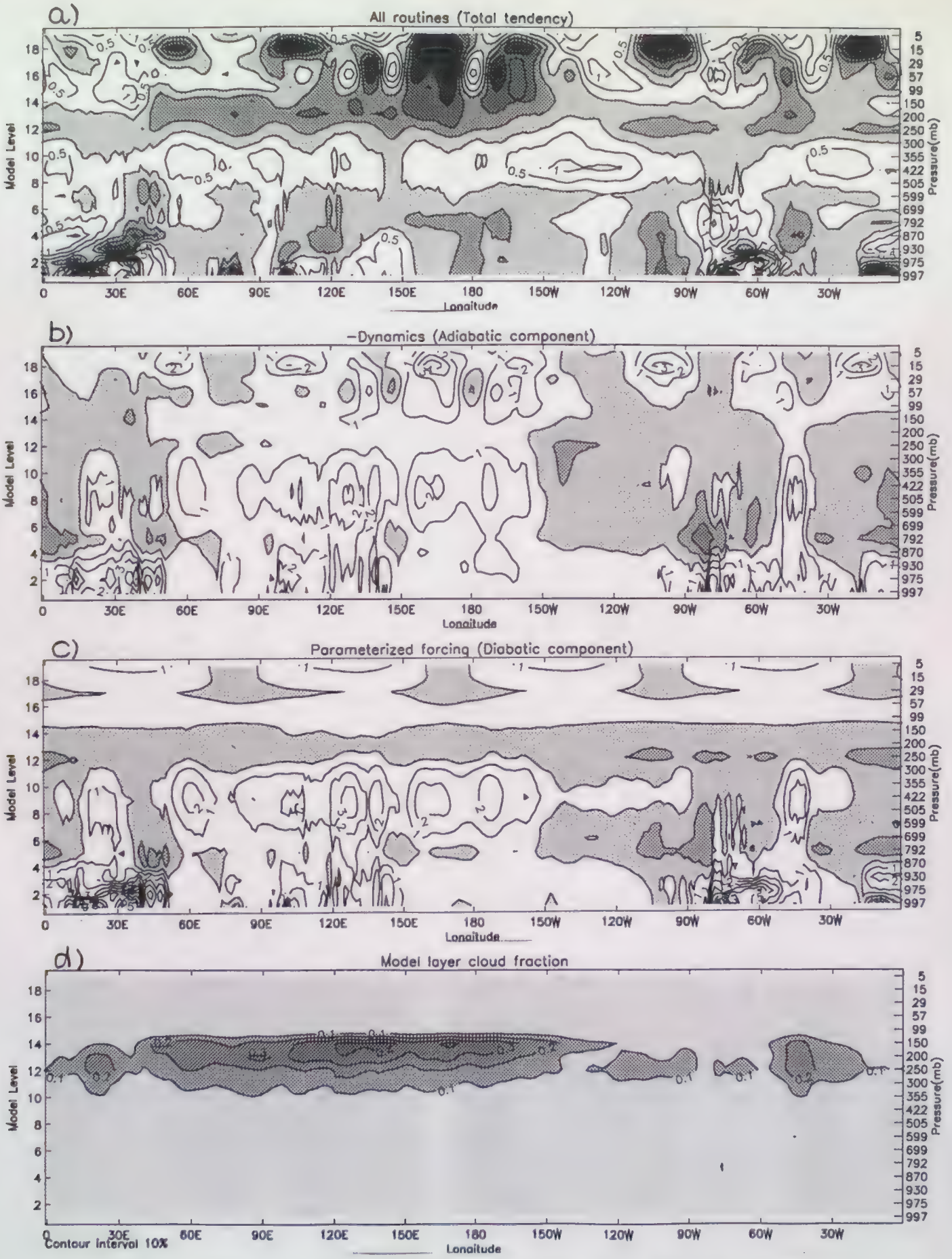

Figure 34: Height-longitude plot of thermal balance for the Tropics (20N-20S) during Jan/Feb/Mar 1995. a) Total (residual) tendency (0.5 K/day) , b) Dynamical heating rates (sign reversed - 1.0K/day), c) Parametrized tendencies (1.0K/day), d) Layer cloud fraction (10%), e) LW Radiation (1.0K/day), f) SW Radiation (1.0 K/day), g) Convection (1.0 K/day), h) Boundary layer (1.0 K/day).

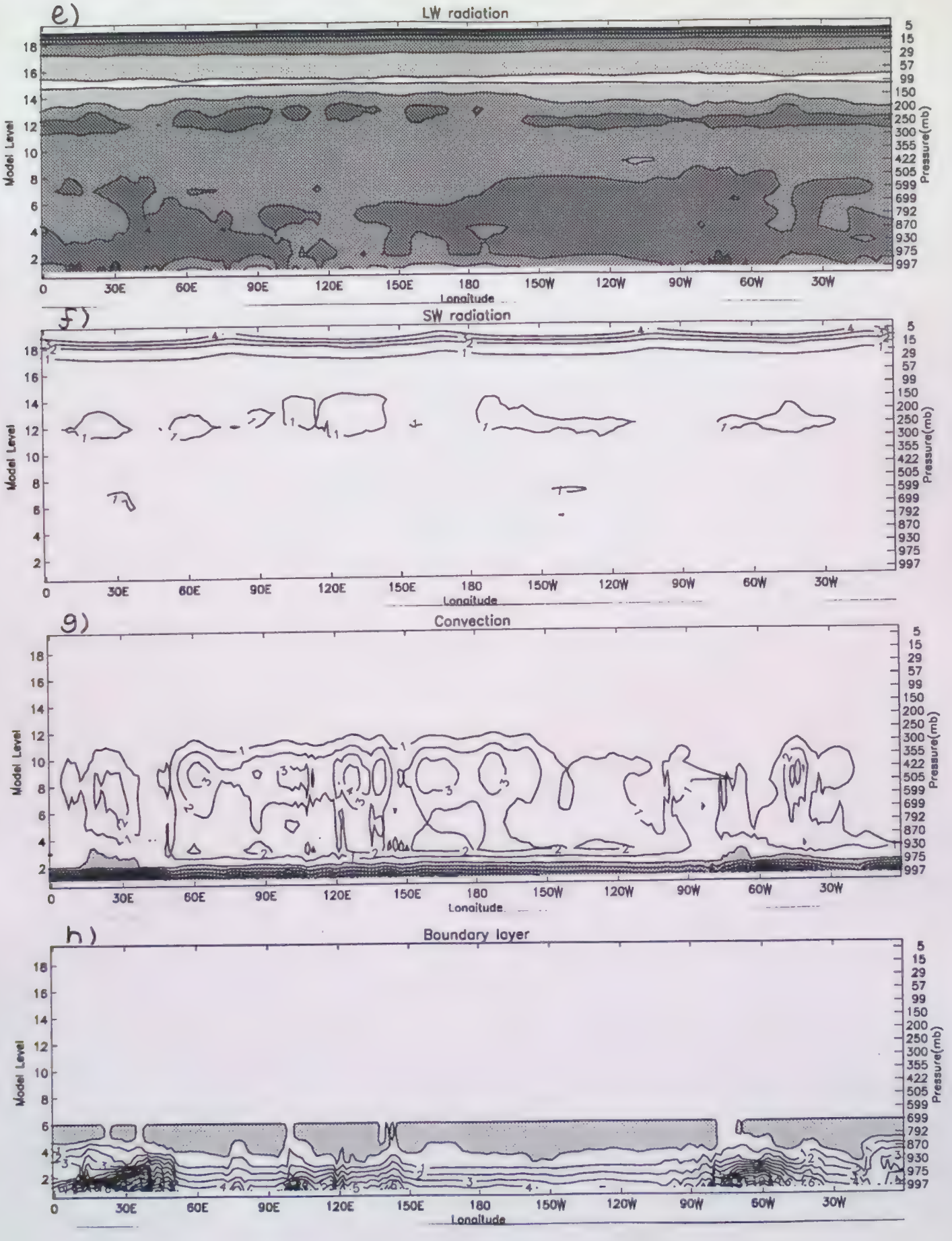

Figure 34: (Continued)

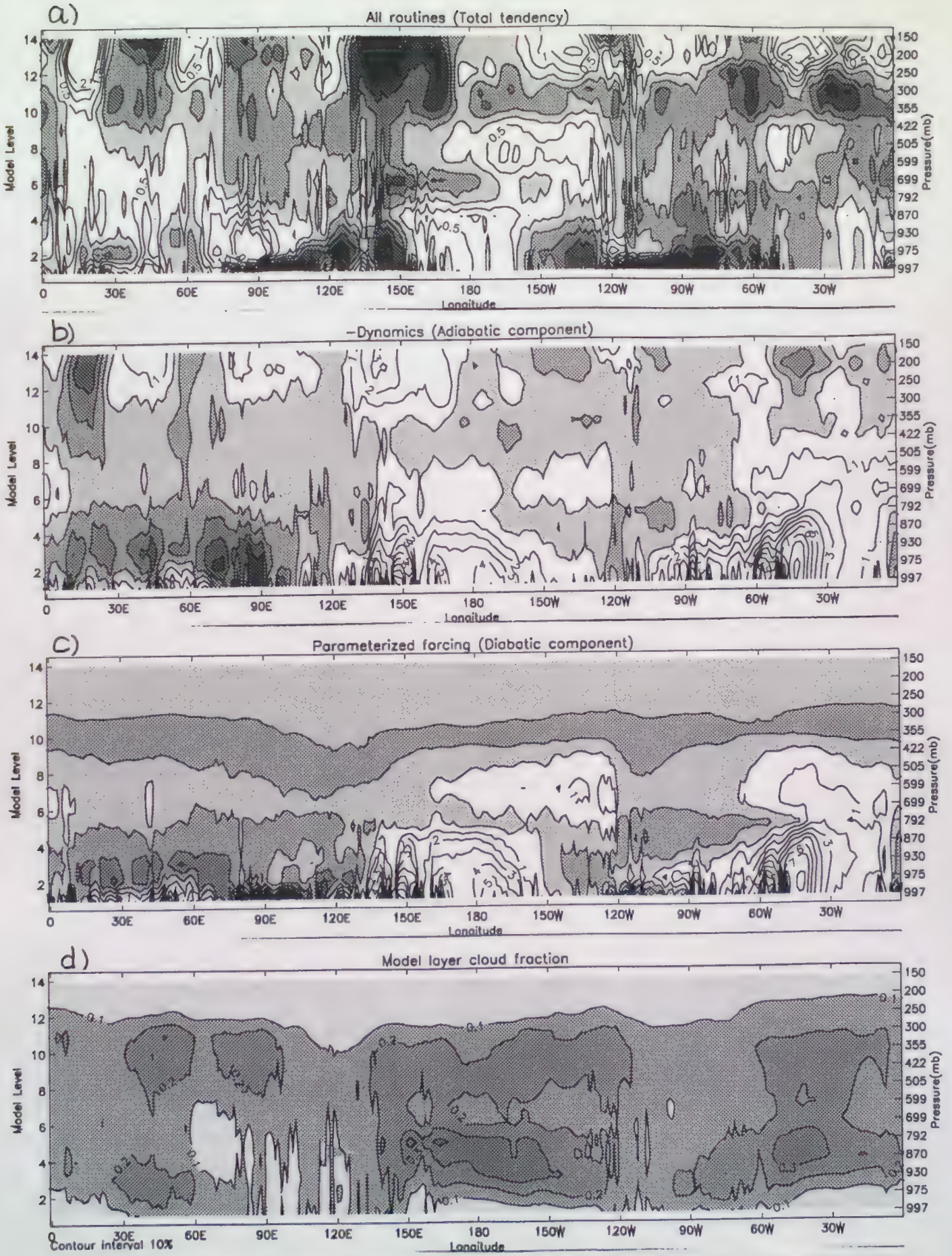

Figure 35: Height-longitude plot of thermal balance for mid-latitudes(60N-40N) during Jan/Feb/Mar 1995. a) Total (residual) tendency (0.5 K/day) , b) Dynamical heating rates (sign reversed - 1.0K/day), c) Parametrized tendencies (1.0K/day), d) Layer cloud fraction (10%), e) LW Radiation (1.0K/day), f) Large scale condensation (1.0 K/day), g) Convection (1.0 K/day), h) Boundary layer (1.0 K/day).

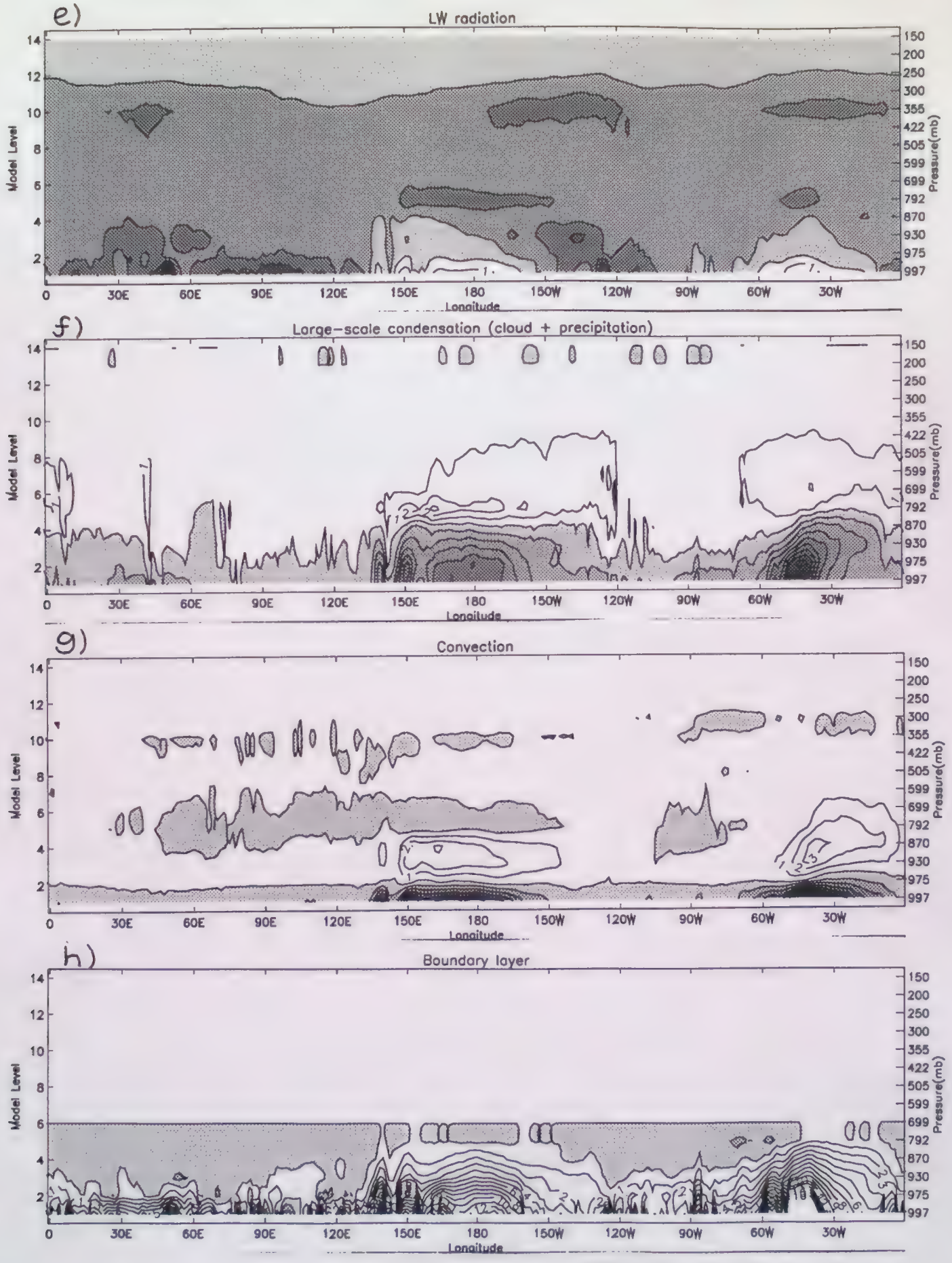

Figure 35: (Continued)

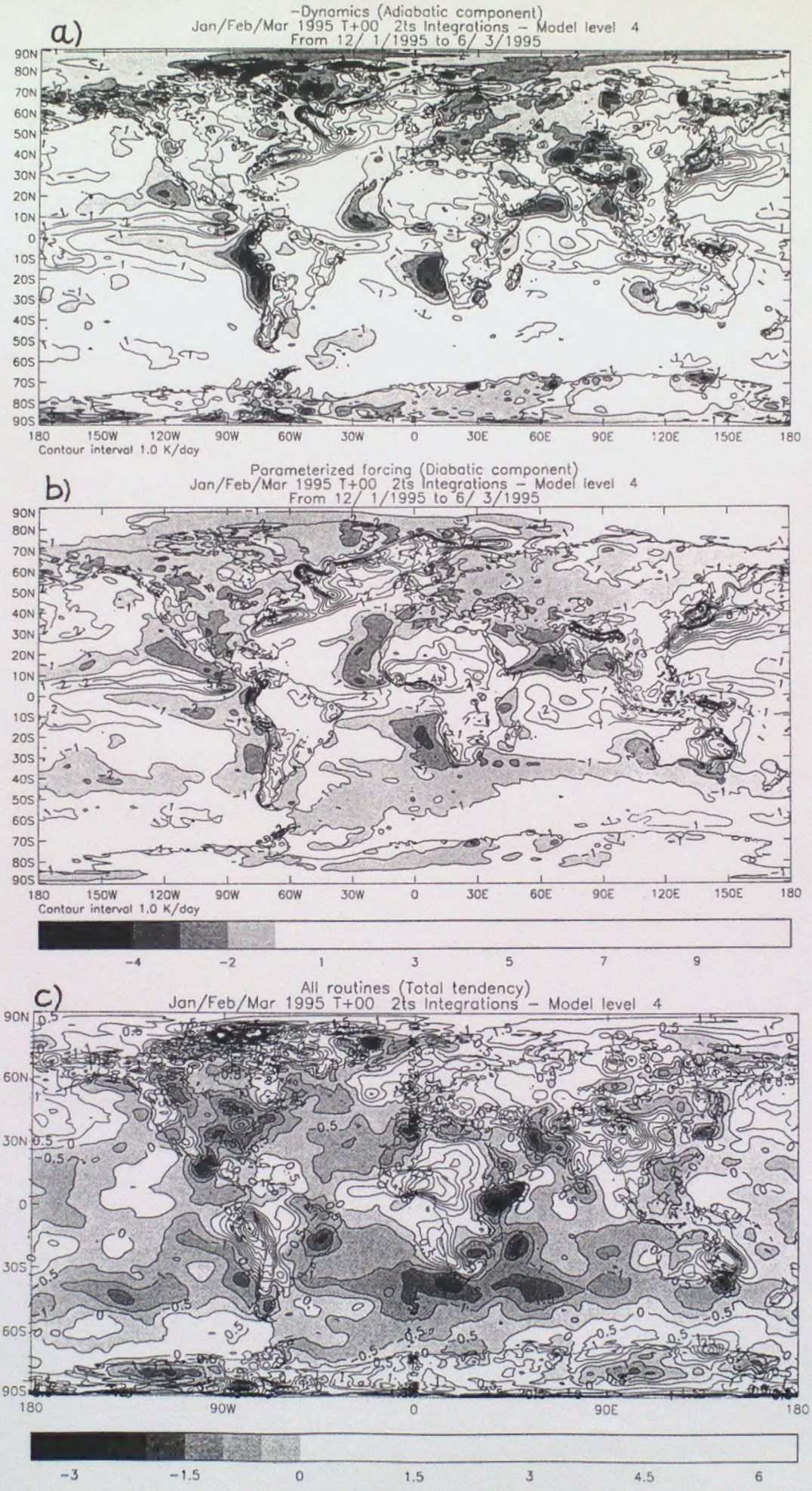

Figure 36: Thermal balance at model level 4 ~ 870hPa during Jan/Feb/Mar 95. a) Dynamical tendencies (sign reversed), b) Parametrized tendencies, c) Total (residual) tendencies. Units are K/Day. Zero contour is omitted in a) and b). Negative values are shaded.

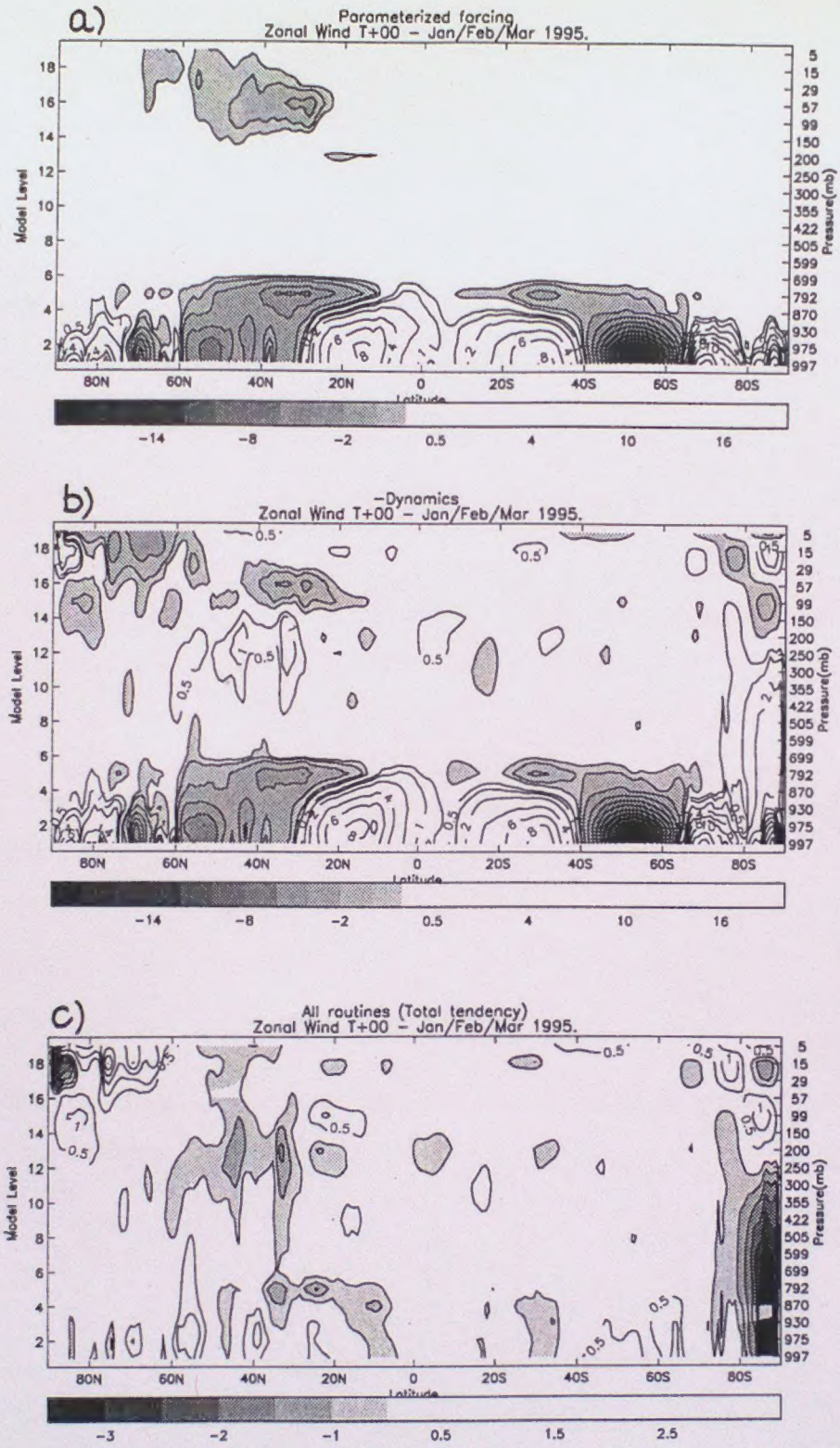

Figure 37: Monthly mean, zonally averaged zonal momentum balance in the Unified Model for January/February/March 1995. a) Parametrized drag , b) Dynamical tendencies (sign reversed), c) Total (residual) tendency . Contour interval for a) and b) is ±0.5,1,2,4,6,8...18 m/s/day and for c) is 0.5 m/s/day. Zero contour omitted and negative values shaded.

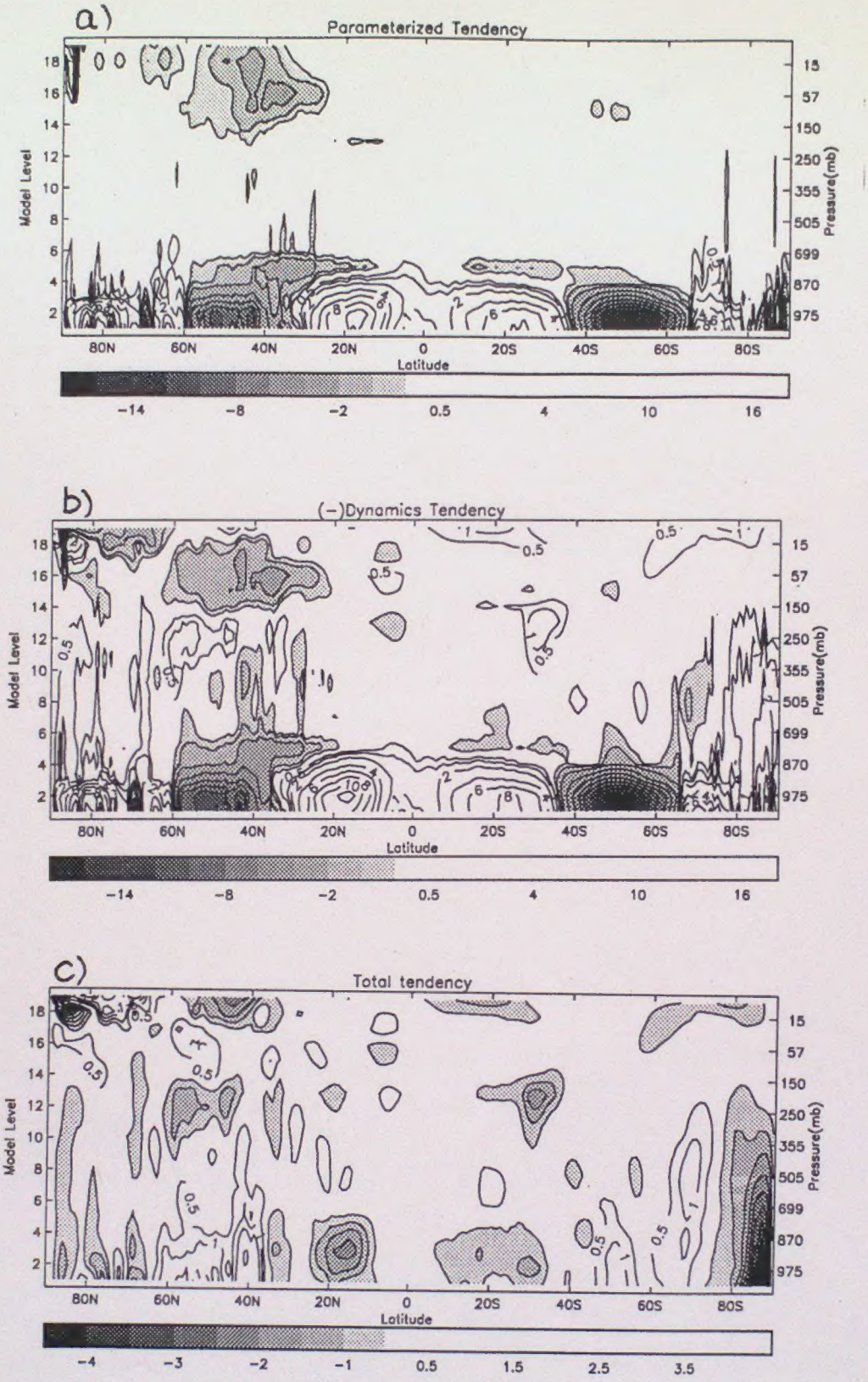

Figure 38: As figure 37 but for December 1993.

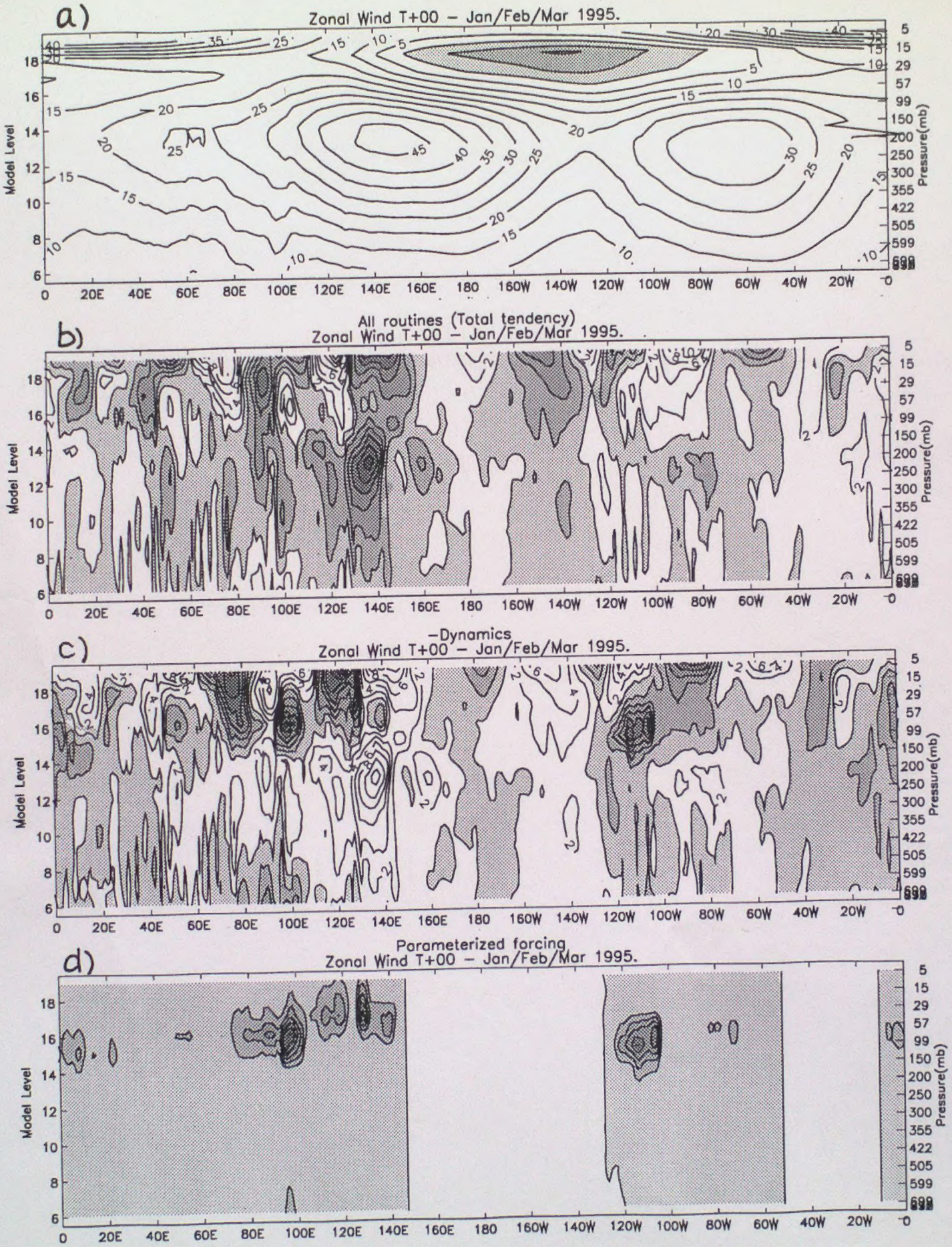

Figure 39: Height-longitude plot of zonal momentum balance for mid-latitudes (50N-30N) and the free troposphere (model level 6-19) during Jan/Feb/Mar 1995. a) T+00 Zonal wind, b) Total tendency (2.0 m/s/day), c) Dynamical tendecies (sign reversed -"implied drag"), d) Parametrized drag (2.0 m/s/day).